AEROSOL OBSERVATIONS FROM SPACE, AIRCRAFT AND SURFACE ANALYZED WITH A GLOBAL MODEL

by

Aaron van Donkelaar

Submitted in partial fulfillment of the requirements
for the degree of Doctor of Philosophy

at

Dalhousie University
Halifax, Nova Scotia
August 2011

DALHOUSIE UNIVERSITY

DEPARTMENT OF PHYSICS AND ATMOSPHERIC SCIENCE

The undersigned hereby certify that they have read and recommend to the Faculty of Graduate Studies for acceptance a thesis entitled "AEROSOL OBSERVATIONS FROM SPACE, AIRCRAFT AND SURFACE ANALYZED WITH A GLOBAL MODEL" by Aaron van Donkelaar in partial fulfillment of the requirements for the degree of Doctor of Philosophy.

Dated: August 4, 2011

External Examiner: _____

Research Supervisor: _____

Examining Committee: _____

_____

Departmental Representative _____

DALHOUSIE UNIVERISTY

Date: August 4, 2011

AUTHOR: Aaron van Donkelaar

TITLE: AEROSOL OBSERVATIONS FROM SPACE, AIRCRAFT AND SURFACE ANALYZED WITH A GLOBAL MODEL

DEPARTMENT: Department of Physics and Atmospheric Science

DEGREE: Ph. D. CONVOCATION: October YEAR: 2011

_____

Signature of Author

I.H.S.

TABLE OF CONTENTS

LIST OF TABLES

LIST OF FIGURES

ABSTRACT

We interpret satellite, aircraft, and ground-based measurements using the GEOS-Chem Chemical Transport Model (CTM) to better understand the global transport and distribution of fine aerosol ($PM_{2.5}$). Using satellite retrievals of Aerosol Optical Depth (AOD) from the Moderate Resolution Imaging Spectroradiometer (MODIS) and the Multiangle Imaging Spectroradiometer (MISR), we estimate an annual growth in Chinese sulfur emissions of 6.2-9.6% between 2000-2006, in agreement with bottom-up inventories. Using aircraft measurements from the Intercontinental Chemical Transport Experiment (INTEX-B) with a CTM, we calculate that 56% of measured sulfate between 500-900 hPa over British Columbia is due to East Asian sources. We find evidence of a 72-85% increase in the relative contribution of East Asian sulfate to the total burden in spring off the northwest coast of the United States since 1985.

We interpret retrievals AOD from MODIS and MISR using GEOS-Chem to estimate global long-term (2001-2006) mean $PM_{2.5}$ concentrations at a resolution of 0.1° x 0.1°. Evaluation of the satellite-derived estimate with ground-based in-situ measurements indicates significant spatial agreement with North American measurements (r = 0.77, slope = 1.07, n = 1057) and with non-coincident measurements elsewhere (r = 0.83, slope = 0.86, n = 244). The one standard deviation uncertainty in the satellite-derived $PM_{2.5}$ is 25%, inferred from the AOD retrieval and aerosol vertical profiles errors and sampling. The global population-weighted mean uncertainty is 6.7 $\mu g/m^3$. We find a global population-weighted geometric mean $PM_{2.5}$ concentration of 20 $\mu g/m^3$. The World Health Organization Air Quality $PM_{2.5}$ Interim Target-1 (35 $\mu g/m^3$ annual average) is exceeded over central and eastern Asia for 38% and 50% of the population, respectively. Annual mean $PM_{2.5}$ concentrations exceed 80 $\mu g/m^3$ over Eastern China.

We test the capability of remotely-sensed $PM_{2.5}$ to capture extreme short-term events by examining the major biomass burning event around Moscow in summer 2010. We find good agreement (r^2=0.85, slope=1.06) between daily estimates of $PM_{2.5}$ from in-situ and satellite-derived sources in the Moscow region during the fires. Both satellite-derived and in-situ values have peak daily mean concentrations of approximately 600 $\mu g/m^3$ on August 7, 2010 in the Moscow region.

LIST OF ABBREVIATIONS AND SYMBOLS USED

Symbol	Units	Description
A	m^{-2}	Area
ACE-Asia		Aerosol Characterization Experiment - Asia
AERONET		Aerosol Robotic Network
AMS		Aerosol Mass Spectrometer
AOD	-	Aerosol Optical Depth
b_{ext}	m^{-1}	Extinction coefficient
BRAVO		Big Bend Regional Aerosol and Visibility Observational Inventory
CALIPSO		Cloud-Aerosol Lidar and Infrared Pathfinder Satellite Observations
CE		Collection Efficiency
CI		Confidence Interval
CTM		Chemical Transport Model
D_p	m	Particle diameter
EDGAR		Emission Database for Global Atmospheric Research
EMEP		European Monitoring and Evaluation Programme
F	W m^{-2}	Intensity
F_0	W m^{-2}	Incident intensity
$\tilde{F}_{abs}$	W m^{-2}	Absorbed intensity
$\tilde{F}_{scat}$	W m^{-2}	Scattered intensity
FRM		Federal Reference Method
GEOS		Goddard Earth Observing System
GEIA		Global Emissions Inventory Activity
GFED		Global Fire Emissions Database
GMAO		Global Modeling Assimilation Office
HR-ToF-AMS		High-resolution time-of-flight aerosol mass spectrometer
INTEX-B		Intercontinental Chemical Transport Experiment
N	-	Total number concentration
MISR		Multiangle Imaging Spectroradiometer
MODIS		Moderate Resolution Imaging Spectroradiometer
MOUDI		Micro-Orifice Uniform Deposit Impactor
NASA		National Aeronautics and Space Administration
NEI		National Emissions Inventory
NSF		National Science Foundation
OC		Organic Carbon
PILS		Particle-Into-Liquid Sampler
PM	$\mu g/m^3$	Particulate Matter
PM_1	$\mu g/m^3$	Fine particulate matter of aerodynamic diameter less than 1 µm
$PM_{2.5}$	$\mu g/m^3$	Fine particulate matter of aerodynamic diameter less than 2.5 µm
PM_{10}	$\mu g/m^3$	Particulate matter of aerodynamic diameter less than 10 µm
Q_{abs}	$molecule^{-1}$	Absorption efficiency
Q_{ext}	$molecule^{-1}$	Extinction efficiency
Q_{scat}	$molecule^{-1}$	Scattering efficiency

Q-AMS		Quadrupole aerosol mass spectrometer
QFED		Quick Fire Emissions Database
r_{eff}		Effective radius
RGB		Red-Green-Blue
RMSD		Root mean square difference
RR		Relative Risk
RR_d		Relative Risk of Death
SO_x		$SO_2 + SO_4^{=}$
TOA		Top of Atmosphere
TEOM		Tapered Element Oscillating Monitors
TRACE-P		Transport and Chemical Evolution of the Pacific
WHO		World Health Organization
z	m	Path length

Greek Symbols

Symbol	Units	Description
α	-	Size parameter
η		The ratio of surface $PM_{2.5}$ to total column AOD
θ	°	Viewing angle
λ_0	nm	Incident wavelength
μ		$cos(\theta)$
π	-	Approximately 3.1415926535
σ_{abs}	m^2 $molecule^{-1}$	single-particle absorption cross section
σ_{ext}	m^2 $molecule^{-1}$	single-particle extinction cross section
σ_{scat}	m^2 $molecule^{-1}$	single-particle scattering cross section
τ	-	Aerosol optical depth
Ω	kg	Column aerosol mass

ACKNOWLEDGEMENTS

This work would not have been possible without the guidance and insight of Randall Martin, my supervising professor. I've also very much valued the contributions provided by the coauthors listed throughout this work. For INTEX-B, the first section of this thesis, this includes: Richard Leaitch, Anne Marie Macdonald, Thomas Walker, David Streets, Qiang Zhang, Edward Dunlea, Jose Jimenez, Jack Dibb, Greg Huey, Rodney Weber and Meinrat Andreae as well as the countless others who helped with the success of INTEX-B. For the second part of this thesis, my thanks go out to Michael Brauer, Ralph Kahn, Robert Levy, Carolyn Verduzco and Paul Villeneuve. Finally, the third section of benefited greatly from the contributions of Robert Levy, Arlindo da Silva, Michal Krzyzanowski, Natalia Chubarova, Eugenia Semutnikova and Aaron Cohen.

The two published sections of my thesis benefited from the comments of several anonymous reviewers. I would also like the acknowledge the Principal Investigators and the staff of the AERONET network which has proved invaluable for the validation of satellite retrievals of aerosol optical depth. Similarly, I would like the thank the MODIS and MISR teams for the availability of both their expertise and their data.

I am also extremely grateful for the financial support offered during my studies by Randall Martin and from the Killam Trust, the National Science and Engineering Research Council (NSERC) and the Sumner Trust.

Chapter 1. INTRODUCTION

1.1 AEROSOL

Aerosol have a large impact on the earth's atmosphere. The effects of these small, suspended particles and droplets are varied. They enhance cloud formation (e.g. Lohmann and Feichter, 2005). They can transport microbes around the world (e.g. Price et al., 2009). In some cases, they are the nutrients that sustain rainforests (e.g. Herrmann et al., 2010), in others, they are the cause of destructive acid rain (e.g. Huo et al., 2011). A clear understanding of aerosol sources, their transport and concentration, provides insight into both our health and climate.

The composition of atmospheric aerosol has changed significantly since the start of the industrial revolution (Tsigaridis et al., 2006) and anthropogenic aerosol presently exceeds natural concentrations in many populated regions (e.g. Waheed et al., 2011; Weijers et al., 2011). While human proximity and the size, composition and radiometric properties of anthropogenic aerosol make them of great interest, natural sources still dominate globally by mass (see Table 1-1). Natural aerosol are directly produced through processes such as volcanic eruptions, forest fires, breaking waves and wind-lifted desert dust.

Globally, combustion dominates anthropogenic aerosol sources, although the contribution from agricultural practices (Ying and Kleeman, 2006) and road dust from vehicles (Karanasiou et al., 2011) can be locally significant. Aerosol can also be produced indirectly, through photochemical reactions of natural and anthropogenic gases in the atmosphere.

Aerosol have a typical atmospheric lifetime of about a week. They are removed from the atmosphere by either wet or dry deposition. Dry deposition is the settling of aerosol in the absence of precipitation. Wet deposition refers to the scavenging of particles by hydrological

Table 1-1: Global emission estimates for major aerosol species and their precursors

Source	Estimated Flux, Tg yr^{-1}	Reference
Mineral dust		Fairlie et al. (2007)
0.1-1.0 µm	178	
1.0-1.8 µm	368	
1.8-3.0 µm	469	
3.0-6.0 µm	439	
Seasalt	5,370	Alexander et al. (2005)
Black carbon		
Fossil fuels	3[a]	Bond et al. (2004)
Biomass	3.4[a]	Bond et al. (2004)
Biofuel	1.6[a]	Bond et al. (2004)
Organic carbon		
Fossil fuels	2.4[a]	Bond et al. (2004)
Biomass	25.1[a]	Bond et al. (2004)
Biofuel	6.4[a]	Bond et al. (2004)
biogenic VOC	150	Heald et al. (2010)
Sulfur ($SO_4^=$ and SO_2)		
DMS	15	Park et al. (2004)
Biomass	1.3	Park et al. (2004)
volcanic SO_2	13	Andres and Kasgnoc (1998)
Anthropogenic activity	57[b]	Park et al. (2004)

[a]Tg C.
[b]Tg S.

processes, involving rain, cloud or snow. The relative effectiveness of dry deposition relates to local turbulence, precipitation rates and surface properties, as well as particle size and density.

Wet deposition of aerosol takes many forms, one of which is the washout of particles by falling raindrops. As a raindrop falls, it collides with large particles (>1 µm) in its path and transports them to the ground. Smaller particles can be swept away without collision by the air current that surrounds a falling raindrop. These particles may still make contact with the raindrop, however, due to the random movements of Brownian motion. The effect of Brownian motion diminishes rapidly with size, making this effect most prominent on the smallest of particles (<0.1 µm). Between 0.1 to 1 µm neither direct collision nor Brownian motion allow for effective washout. This size range is known as the Greenfield gap (Seinfeld and Pandis, 2006).

A second form of wet deposition occurs when particles act as nucleation sites for cloud formation, and are ultimately rained out. The ability of aerosol to act as cloud condensation nuclei and affect cloud growth/lifetimes is the dominant cause of their net cooling of the earth's climate and is referred to as the aerosol indirect effect. The aerosol direct effect, which refers to the scattering and absorption of radiation is also significant. Both are subject to high uncertainties, resulting from the complexity of these interactions and uncertainties in the total aerosol burden (IPCC, 2008).

Chronic exposure to aerosol, particularly that with aerodynamic diameter less than 2.5 μm ($PM_{2.5}$) is associated with deleterious health impacts such as morbidity and mortality (e.g. Dockery et al., 1993; McDonnell et al., 2000). Pope et al. (2009) estimated that an increase of 10 $\mu g/m^3$ in long-term exposure to $PM_{2.5}$ results in a 0.61 ± 0.30 year loss in life expectance over the United States. Due to these effects, the World Health Organisation (WHO) recommends a maximum annual mean exposure not exceeding 10 $\mu g/m^3$ (See Table 1-2).

Table 1-2: Air quality guideline and interim targets for PM: annual mean (from WHO, 2005)

Annual mean level	PM_{10} ($\mu g/m^3$)	$PM_{2.5}$ ($\mu g/m^3$)	Basis for the selection
WHO interim target 1 (IT-1)	70	35	These levels are estimated to be associated with about 15% higher long-term mortality than at ADG levels
WHO interim target 2 (IT-2)	50	25	In addition to other health benefits, these levels lower risk of premature mortality by approximately 6% (2-11%) compared to IT-1 levels
WHO interim target 3 (IT-3)	30	15	In addition to other health benefits, these levels reduce mortality risk by approximately another 6% (2-11%) compared to IT-2 levels.
WHO air quality guidelines (AQG)	20	10	These are the lowest levels at which total cardiopulmonary and lung cancer mortality have been shown to increase with more than 95% confidence in response to $PM_{2.5}$ in the ACS study. The use of the $PM_{2.5}$ guideline is preferred.

1.2 Monitoring of Atmospheric Aerosol

The health and climatic effects of aerosol have motivated the creation of national and international monitoring networks and campaigns. In-situ gravimetric, filter-based measurements, known as dichotomous samplers or the Federal Reference Method (FRM), remain the most robust and reliable of methods. In this approach, air flow causes aerosol to be collected on a filter which can be subsequently analysed for its mass and composition (Winberry, 1999). FRM measurements are typically limited to no more than daily frequency due to their manual nature. Tapered Element Oscillating Monitors (TEOMs) are also common. Though less reliable, these automated instruments provide continuous, unattended aerosol measurement by monitoring the change in resonance frequency caused by the addition of aerosol mass to an internal oscillating member (Allen, 2010).

1.3 Scattering of Radiation by Atmospheric Aerosol and Aerosol Optical Depth

Aerosol can interact with incoming radiation in a variety of ways. An understanding of these interactions allows for the monitoring of aerosol remotely. Radiation can be absorbed by particles or scattered via reflection, refraction or diffraction.

The scattering and absorption of light by a particle is proportional to the amount of incident intensity, F_0, and is defined by the single-particle scattering cross section, σ_{scat} (m^2 $particle^{-1}$), and the single-particle absorption cross section, σ_{abs} (m^2 $particle^{-1}$):

$$\tilde{F}_{scat} = \sigma_{scat} F_0 \quad 1\text{-}1$$

$$\tilde{F}_{abs} = \sigma_{abs} F_0 \quad 1\text{-}2$$

The combined effect of scattering and absorption is referred to as extinction:

$$\sigma_{ext} = \sigma_{scat} + \sigma_{abs} \quad 1\text{-}3$$

and the scattering, absorption and extinction efficiencies are defined as their respective cross-sections per unit area (e.g. $Q_{ext} = \frac{\sigma_{ext}}{A}$), such that:

$$Q_{ext} = Q_{scat} + Q_{abs} \quad 1\text{-}4$$

The extinction coefficient, b_{ext}, gives the combined extinction for a group of particles per inverse length (m^{-1}):

$$b_{ext} = \sigma_{ext} N \quad 1\text{-}5$$

or,

$$b_{ext} = \frac{\pi D_p^2}{4} N Q_{ext} \quad 1\text{-}6$$

where N is the total number concentration (particles per m^{-3}) and D_p is the particle diameter and can be related to the loss of radiation over a path length, z, via the Beer-Lambert Law:

$$\frac{dF}{dz} = -b_{ext} F_0 \quad 1\text{-}7$$

The aerosol optical depth (AOD), τ, is a dimensionless parameter defined as:

$$\tau = \int_z^{z_{TOA}} b_{ext} dz \quad 1\text{-}8$$

Therefore the loss of light passing through the atmosphere can be described as,

$$\frac{F}{F_0} = exp(-\tau) \quad 1\text{-}9$$

Determination of scattering properties can be complex. Mie theory describes the scattering and absorption of light by spherical particles. According to this theory, these effects are dominated by the wavelength, λ, of the incident radiation and the size of the particle (D_p). This parameters are usually combined into the dimensionless size parameter, α:

$$\alpha = \frac{\pi D_p}{\lambda} \qquad 1\text{-}10$$

Figure 1-1 demonstrates the extinction efficiency for a water droplet of varying size with constant radiation of wavelength 500 nm. When the particle is small compared to wavelength ($\alpha << 1$), Mie theory can be greatly simplified and approximated as Rayleigh scattering in which scattering is proportional to λ^{-4} and absorption to λ^{-1}. When a particle is large compared to wavelength ($\alpha >> 1$) geometric optics can describe its interaction with radiation.

AOD is one of the most prominent remotely sensed metric of aerosol. By monitoring incoming solar radiation at multiple angles, ground-based sun photometers can measure AOD with minimal assumption and high accuracy (Holben et al., 1998). Modifying equation 1-9 above to account for an off-zenith viewing angle gives:

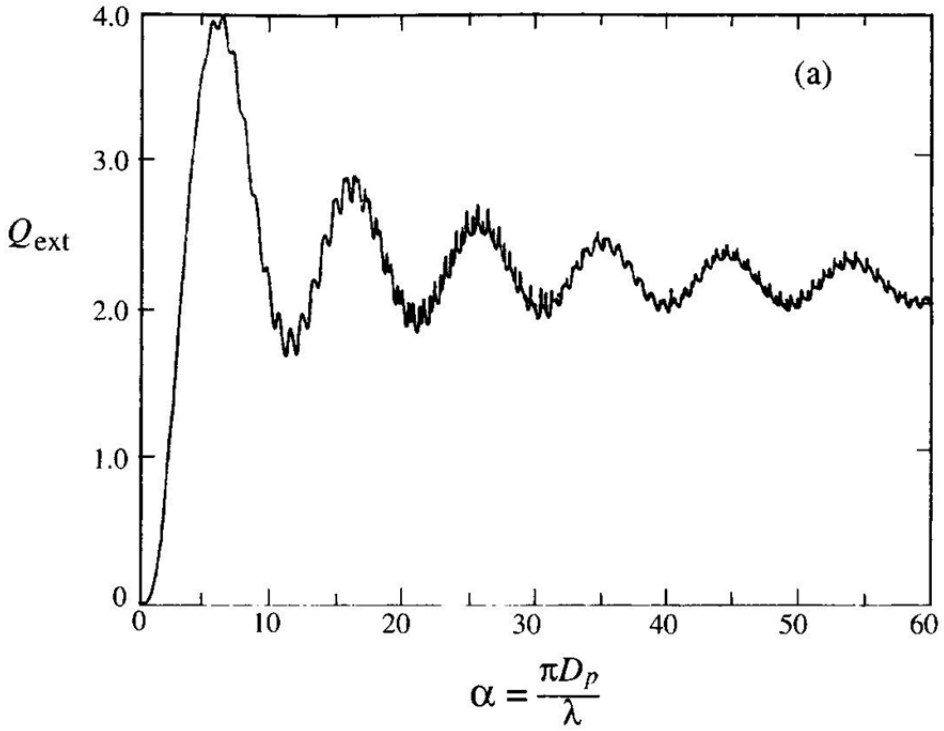

Figure 1-1: Extinction efficiency, Q_{ext}, for a water droplet at $\lambda = 0.5$ µm (adapted from Seinfeld and Pandis, 2006).

$$F = F_0 exp\left(\frac{-\tau}{\mu}\right) \quad 1\text{-}11$$

where $\mu = cos(\theta)$, and θ is the viewing angle. By taking the ratio of two observations at separate viewing angles, θ_1 and θ_2, it can then be shown that:

$$\tau = ln\left(\frac{F_1}{F_2}\right)\left(\frac{1}{cos(\theta_2)} - \frac{1}{cos(\theta_1)}\right) \quad 1\text{-}12$$

AOD can also be directly related to column aerosol mass, Ω:

$$\Omega = \frac{4}{3}\frac{\rho r_{eff}\tau}{Q_{ext}} \quad 1\text{-}13$$

Where r_{eff} is the effective radius and ρ is the density of the aerosol. It is possible to relate AOD to near-surface $PM_{2.5}$ given a knowledge of the near-surface AOD contribution and hygroscopic effects (van Donkelaar et al., 2006):

1.4 Satellite Retrievals of Aerosol Optical Depth

Satellite retrievals have allowed unprecedented observational coverage of our planet. Under cloud-free conditions, instruments such as the Moderate Resolution Imaging Spectroradiometer (MODIS) can provide daily global AOD retrievals at a resolution of 10 km × 10 km. Unlike ground-based observations, however, space-borne retrievals must account for the contribution of surface-reflected solar radiation to the observed radiance from their position looking down from the top of the atmosphere. At visible wavelengths over the ocean this contribution is typically small in the absence of sun-glint or heavy sediment (Remer et al., 2005). Over land, however, surface-reflected radiation can be both large and uncertain, requiring assumptions that can reduce AOD retrieval quality (Levy et al., 2007) or more complex instrument design, such as the Multiangle Imaging Spectroradiometer (MISR; Diner et al., 2005) which capture views of each scene at multiple angles during each overpass. Despite these

challenges, satellite-based AOD have opened up new possibilities in air quality monitoring, providing observationally-based estimates of aerosol around the world.

1.5 Chemical Transport Models

Concentrations of aerosol (and other atmospheric constituents) can also be estimated without the direct use of observations through modelling. Chemical Transport Models (CTMs) solve for the temporal and spatial evolution of aerosol and gaseous compounds using meteorological data sets, emission inventories, and equations that represent the physics and chemistry of atmospheric constituents. The concentrations calculated by these models have proven to be a valuable source of information for atmospheric monitoring, providing complete horizontal and vertical global coverage at high temporal resolution, albeit at a relatively coarse resolution.

1.6 Goals of this Present Work

In-situ, remote sensed and modelled aerosol monitoring have each provided important insight into the state of the atmosphere. This work brings together these sources, drawing on their individual strengths, to globally investigate aerosol transport and concentrations.

Anthropogenic emissions in China have grown rapidly over the past decade (Streets et al., 2009). Such changes affect not only local air quality, but have the potential to affect North America through long-range transport. The first part of this thesis investigates both this recent growth in emissions and the impact of aerosol transport from eastern Asia within the context of the Intercontinental Chemical Transport Experiment (INTEX-B; Singh et al., 2009), which took place during spring 2006. We interpret in-situ aerosol measurements from the INTEX-B aircraft and ground-based monitors with satellite retrievals of AOD and the GEOS-Chem chemical

transport model (Bey et al., 2001) to better understand the impact of east Asian aerosol on western Canada. This work was published in Atmospheric Chemistry and Physics in 2008.

There remains much uncertainty about global exposure to $PM_{2.5}$, whether from local or transported sources. Even the reliable, relatively dense networks of Canada and the United States, have gaps of hundreds of kilometers without monitoring stations. Globally, sparse available measurements suggest the highest concentrations of $PM_{2.5}$ occur in developing countries where the in-situ monitoring is least (e.g. Gupta et al., 2006a). The second part of this thesis interprets the high resolution, column-integrated AOD retrievals from the MODIS and MISR instruments using a chemical transport model to globally estimate long term mean $PM_{2.5}$ concentrations at 0.1° x 0.1°. This work was published in Environmental Health Perspectives in 2010.

Both acute and chronic exposure to aerosol are of interest to epidemiologists who study the impacts of $PM_{2.5}$ on human health. Extreme events, such as the major fires that occurred near Moscow during summer 2010, challenge both in-situ and remotely sensed monitoring. In this final section, the ability of remote sensing to monitor air quality daily during major biomass burning events is explored by investigating the fires that occurred near Moscow in the summer of 2010. This section builds on the previous chapter, employing a chemical transport model to relate MODIS-retrieved AOD to surface $PM_{2.5}$, but at a higher temporal resolution and in more detail than feasible with a global analysis. The effects of cloud-screening and emission accuracy is explored. This work has been submitted to Atmospheric Environment.

Chapter 2. Analysis of Aircraft and Satellite Measurements from the Intercontinental Chemical Transport Experiment (INTEX-B) to Quantify Long-Range Transport of East Asian Sulfur to Canada

Authors: Aaron van Donkelaar[1], Randall V. Martin[1,2], W. Richard Leaitch[3], Anne Marie Macdonald[3], Thomas W. Walker[1,4], David G. Streets[5], Qiang Zhang[5], Edward J. Dunlea[6], Jose L. Jimenez[6], Jack E. Dibb[7], L. Greg Huey[8], Rodney Weber[8], Meinrat O. Andreae[9]

[1]Dept. of Physics and Atmospheric Science, Dalhousie University

[2]Harvard-Smithsonian Center for Astrophysics

[3]Science and Technology Branch, Environment Canada

[4]Dept. of Physics, University of Toronto

[5]Decision and Information Sciences Division, Argonne National Laboratory

[6]Department of Chemistry and Biochemistry, and Cooperative Institute for Research in the Environmental Sciences (CIRES), University of Colorado

[7]Climate Change Research Center/EOS, University of New Hampshire

[8]School of Earth & Atmospheric Sciences, Georgia Institute of Technology

[9]Biogeochemistry Department, Max Plank Institute for Chemistry

Article published in Atmospheric Chemistry and Physics, 8, 2999-3014, 2008. All text, figures, and presented results were contributed by the first author.

2.1 ABSTRACT

We interpret a suite of satellite, aircraft, and ground-based measurements over the North Pacific Ocean and western North America during April-May 2006 as part of the Intercontinental Chemical Transport Experiment Phase B (INTEX-B) campaign to understand the implications of long-range transport of East Asian emissions to North America. The Canadian component of INTEX-B included 33 vertical profiles from a Cessna 207 aircraft equipped with an aerosol mass spectrometer. Long-range transport of organic aerosols was insignificant, contrary to expectations. Measured sulfate plumes in the free troposphere over British Columbia exceeded 2 $\mu g/m^3$. We update the global anthropogenic emission inventory in a chemical transport model (GEOS-Chem) and use it to interpret the observations. Aerosol Optical Depth (AOD) retrieved from two satellite instruments (MISR and MODIS) for 2000-2006 are analyzed with GEOS-Chem to estimate an annual growth in Chinese sulfur emissions of 6.2% and 9.6%, respectively. Analysis of aircraft sulfate measurements from the NASA DC-8 over the central Pacific, the NSF C-130 over the east Pacific and the Cessna over British Columbia indicates most Asian sulfate over the ocean is in the lower free troposphere (800-600 hPa), with a decrease in pressure toward land due to orographic effects. We calculate that 56% of the measured sulfate between 500-900 hPa over British Columbia is due to East Asian sources. We find evidence of a 72-85% increase in the relative contribution of East Asian sulfate to the total burden in spring off the northwest coast of the United States since 1985. Campaign-average simulations indicate anthropogenic East Asian sulfur emissions increase mean springtime sulfate in Western Canada at the surface by 0.31 $\mu g/m^3$ (~30%) and account for 50% of the overall regional sulfate burden between 1 and 5 km. Mean measured daily surface sulfate concentrations taken in the Vancouver area increase by 0.32 $\mu g/m^3$ per 10% increase in the simulated fraction of Asian

sulfate, and suggest current East Asian emissions episodically degrade local air quality by more than 1.5 $\mu g/m^3$.

2.2 INTRODUCTION

The transport of Asian emissions to North America has been well documented (e.g. Bertschi et al., 2004; Jaffe et al., 1999; Liang et al., 2004; Park et al., 2004; Parrish et al., 1992). *Andreae et al.* (1988) measured sulfate ($SO_4^=$) concentrations off the northwest coast of the United States in May 1985, and attributed enhancements in the free troposphere to Asian sources. Asian emissions of sulfur oxides ($SO_x \equiv SO_2 + SO_4^=$) are dominated by SO_2 and have grown substantially over the last two decades (Streets and Waldhoff, 2000). They increasingly impact North America, affecting both regional air quality (Heald et al., 2006; Park et al., 2004) and climate (Liu et al., 2008). Additional analysis of in-situ and remote-sensed observations are needed to quantify this long-range transport and its implications.

A growing body of evidence exists for long-range transport to Canada. During the Polar Sunrise Experiment in 1992 at Alert concentrations of SO_x were well correlated with long-range transport of fine anthropogenic aerosol (Barrie et al., 1994). Sirois and Barrie (1999) analyzed aerosol composition between 1980 and 1995 to infer the presence of Eurasian $SO_4^=$ in the Canadian Arctic. Asian pesticides have been observed in the Yukon Territory as a result of transpacific flow (Bailey et al., 2000). The influence of long-range transport to Canada is not limited to remote regions, and is especially relevant in populated areas. Asian pesticides have been transported to the Fraser Valley, British Columbia (Harner et al., 2005). Chinese dust has been observed in British Columbia's Lower Fraser Valley (McKendry et al., 2001) and can be linked to $SO_4^=$ transport through the uptake of sulfur dioxide (SO_2) on dust (Jordan et al., 2003; Song et al., 2007). Dust transport to western Canada has also been observed from as far as the

Sahara Desert (McKendry et al., 2007). Although aerosol in the Asian boundary layer may be readily scavenged near its source by wet deposition, SO_2 emissions can escape to the free troposphere prior to $SO_4^=$ conversion and be subsequently transported across the Pacific Ocean (Brock et al., 2004; Dunlea et al., 2009). Elevated aerosol concentrations, attributed to East Asian combustion sources, have been observed reaching North America near the Canadian border at Cheeka Peak (Jaffe et al., 1999).

Satellite observations offer a top-down constraint on emissions. Previous work includes absolute emissions of nitrogen oxides (Jaegle et al., 2005; Leue et al., 2001; Martin et al., 2003a; Muller and Stavrakou, 2005), volatile organic compounds (*Palmer et al.*, 2003; *Fu et al.*, 2007), and carbon monoxide (Arellano et al., 2004; Heald et al., 2004; Petron et al., 2004), as well as trends in nitrogen oxide (Richter et al., 2005; van der A et al., 2006; Zhang et al., 2007) emissions. The clearest signals in current SO_2 retrievals are of volcanic activity (Khokhar et al., 2005), although anthropogenic activity has also been detected (Carn et al., 2007; Eisinger and Burrows, 1998; Krotkov et al., 2006). In some regions satellite-retrieved Aerosol Optical Depth (AOD) is closely related to SO_2 emissions through production of $SO_4^=$ (Dubovik et al., 2007; Massie et al., 2004).

Springtime weather patterns generally produce the strongest seasonal outflow from Asia (Jacob et al., 2003; Liu et al., 2005a), and can result in a pronounced influence of Asian emissions upon the North American continent. During April and May 2006, the Intercontinental Chemical Transport Experiment, Phase B (INTEX-B) set out to assess this influence using a combination of aircraft and satellite measurements throughout the northeastern Pacific (Singh et al., 2009). This NASA-driven initiative constituted the second half of the INTEX project, and was designed to improve the understanding of gas and aerosol transformation and transport on transcontinental and intercontinental scales.

In this paper we investigate the long-range transport of East Asian $SO_4^=$ to Canada. Section 2 presents the aircraft component of the Canadian contribution to INTEX-B and outlines the other instruments, platforms and the model used in this study. In section 3, we estimate the recent growth in East Asian SO_x emissions based upon remote sensing measurements. Section 4 combines data from a chemical transport model with in-situ measurements to characterize the Asian sulfur transport to Canada during INTEX-B. This section goes on to assess the development of East Asian $SO_4^=$ influx to North America between 1985 and INTEX-B using aircraft data from both periods. A case study of an Asian plume is presented in section 5, along with the implications for Canadian air quality. Conclusions are in section 6.

2.3 INTEX-B PLATFORMS

Here we introduce the aircraft, surface and satellite measurements, and the model used for interpretation.

2.3.1 IN-SITU MEASUREMENTS

Figure 2-1 provides an overview of the measurement platforms and regions examined throughout this manuscript. Several aircraft participated in INTEX-B, including the NASA DC-8, the NSF C-130 and a Canadian Cessna 207 described below. Throughout this manuscript, we limit the DC-8 and C-130 measurements to within the boxed regions of Figure 2-1 to focus on long-range transport of Asian aerosol to Canada. The DC-8 aircraft utilized both a mist chamber (Cofer et al., 1985) and bulk aerosol filters to characterize the $SO_4^=$ aerosol load, during 10 flights between April 17, 2006 and May 15, 2006. The size cutoff of the onboard mist chamber system is ~1 μm (based on estimated particle transmission efficiency through the inlet and sampler) while that of the bulk aerosol filters has been empirically determined to be ~4.5 μm (McNaughton et al., 2007). Mist chamber sampling periods are less than two minutes and

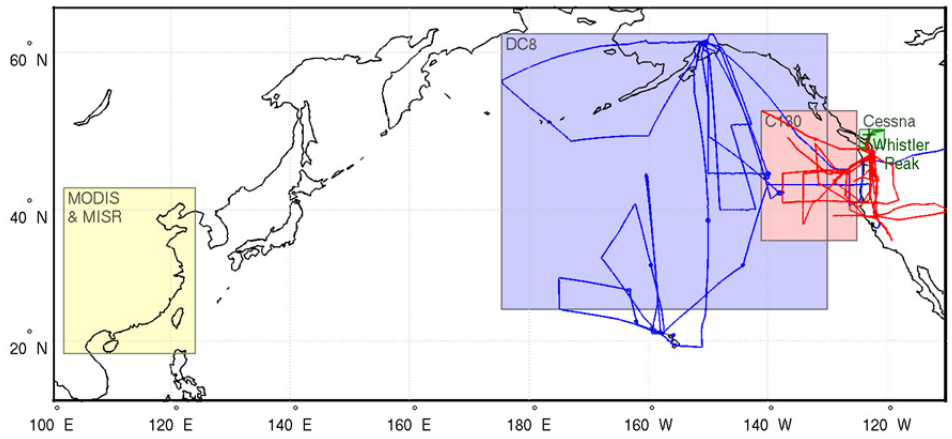

Figure 2-1: Spatial domain of observations used to characterize Asian SO_2 emissions and their impact. The domains and flightpaths of the DC-8, C-130 and Cessna aircraft are shown in blue, red and green, respectively. The domain of the MODIS and MISR satellite observations used to estimate emissions is shown in yellow. Figure 2-2 shows a detailed plot of the Cessna flight tracks.

aerosol filters are not exposed longer than 10 to 20 minutes, depending upon altitude. Uncertainties in the reported $SO_4^=$ mixing ratios are ~20% from the mist chamber and ~25 pptv (~110 ng/m^3) from the filters. A chemical ionization mass spectrometer (CIMS) instrument (Huey et al., 2004; Kim et al., 2007) was also onboard the DC-8 and used for the measurement of SO_2 with a sampling frequency of approximately 3 seconds.

The C-130 platform included a high-resolution time-of-flight aerosol mass spectrometer (HR-ToF-AMS) (Canagaratna et al., 2007; DeCarlo et al., 2006; Dunlea et al., 2009) with ~12 second sampling frequency and a particle-into-liquid sampler (PILS) (Peltier et al., 2008; Weber et al., 2001) of one minute sampling frequency during its 11 flights between April 21, 2006 and May 15, 2006. AMS particle transmission is approximately PM_1 in vacuum aerodynamic diameter (Jayne et al., 2000) with particle transmission efficiency rapidly decreasing for aerosols larger than 0.7 µm (e.g. Liu et al., 2007a; Rupakheti et al., 2005). A collection efficiency (CE) of 0.5 is used for the AMS on the C-130 and is based on many previous intercomparisons (Canagaratna

et al., 2007, and references therein), with a correction for increased CE under high acidity conditions (Quinn et al., 2006) as discussed by Dunlea et al. (2009). PILS measurements were restricted to particles less than 1 µm (at 1 atm. pressure) aerodynamic diameter via a single-stage micro-orifice impactor (Model 100, MSP Corp.). AMS and PILS sulfate measurement uncertainties are estimated at 25% and 10%, respectively.

Whistler Peak Station (50.1° N, 122.9° W, 2182 m) is operated by Environment Canada and has provided continuous measurements of meteorological data, CO and O_3 since its establishment in 2002 (Macdonald et al., 2006). Inorganic filter packs of $SO_4^{=}$, NO_3^{-} and Ca^{+} are also routinely collected and analyzed. In addition to these regular measurements, a HR-ToF-AMS (Sun et al., 2009) and a Micro-Orifice Uniform Deposit Impactor (MOUDI) were operated at the site for the duration of INTEX-B. The MOUDI was operated with three stages to isolate particles into three nominal size bins of < 1 µm, 1-3 µm and > 3 µm.

A Cessna 207 aircraft, supplied by Environment Canada during INTEX-B, contained a suite of instruments designed to capture both trace gases and aerosol pollutants (Leaitch et al., 2009). Aerosol instrumentation included number concentrations of ultra-fine aerosol (PMS7610), aerosol size distribution (FSSP300: <18 µm and PCASP: <2.5 µm) and aerosol composition by way of a quadrupole aerosol mass spectrometer (Q-AMS) (Jayne et al., 2000; Jimenez et al., 2003; Rupakheti et al., 2005). The Q-AMS detection limits are 40 ng/m^3 for $SO_4^{=}$ and nitrate, and 600 ng/m^3 for organic aerosol for each one-minute average measurement. The CE used with the Cessna AMS is discussed by (Leaitch et al., 2009). Walker et al. (2010) describe and interpret O_3 and CO measurements on the Cessna.

All Cessna 207 flights, shown in Figure 2, originated outside Pemberton, B.C., 35 km north of Whistler, with the exception of one inter-comparison flight with the C-130, conducted on May 9,

2006 along the Canada-US border and related transit. Most Cessna flight tracks consisted of an ascent and descent near Whistler Peak Station before returning to the takeoff site. Thirty-three flights occurred between April 22, 2006 and May 17, 2006, with most extending from the surface to approximately 5 km (550 hPa) altitude and those with valid Q-AMS data occurring mid-late morning to late afternoon. Q-AMS data from the May 9 inter-comparison and several other flights were lost due to radio frequency interference, resulting in a total of 21 flights with successful Q-AMS measurements.

The right panel of Figure 2-2 shows the flight paths for the May 3 inter-comparison flight between the Cessna and the C-130. The inter-comparison zone is outlined in grey. The Cessna descent was not completed within the comparison region until approximately 50 minutes after

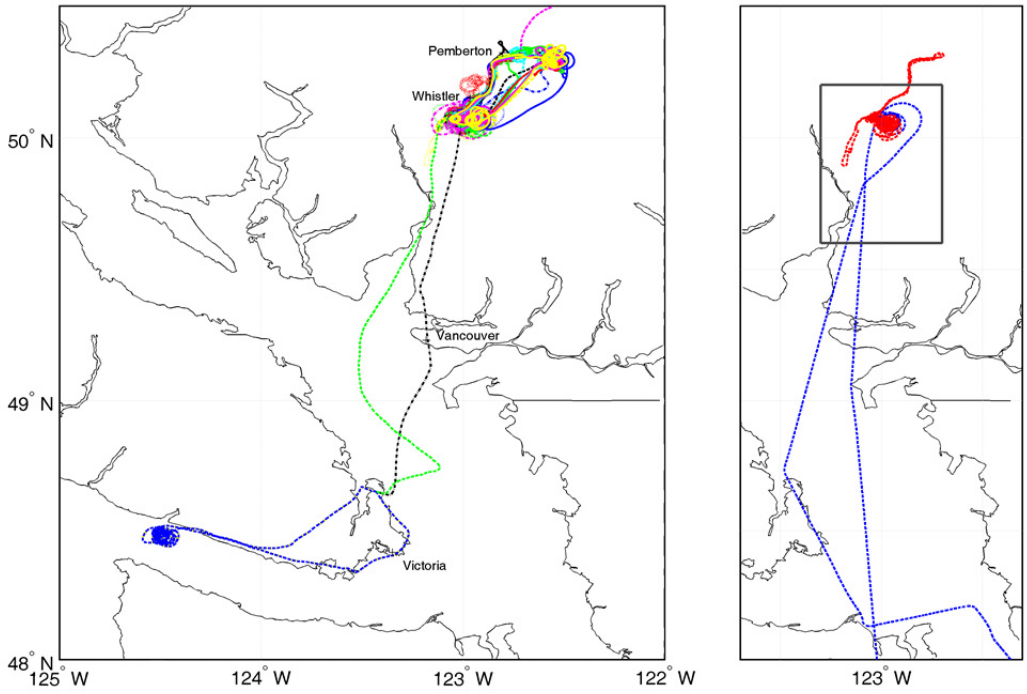

Figure 2-2: Flight paths of the Cessna 207 aircraft during the INTEX-B campaign over April 22, 2006 to May 17, 2006. The left panel shows all Cessna 207 flights, with colors representing individual flights. The right panel highlights the May 3, 2006 inter-comparison flight between the Cessna and C-130 aircraft. The flight track of the Cessna is shown in red, and of the C-130 in blue. The grey box defines the inter-comparison region.

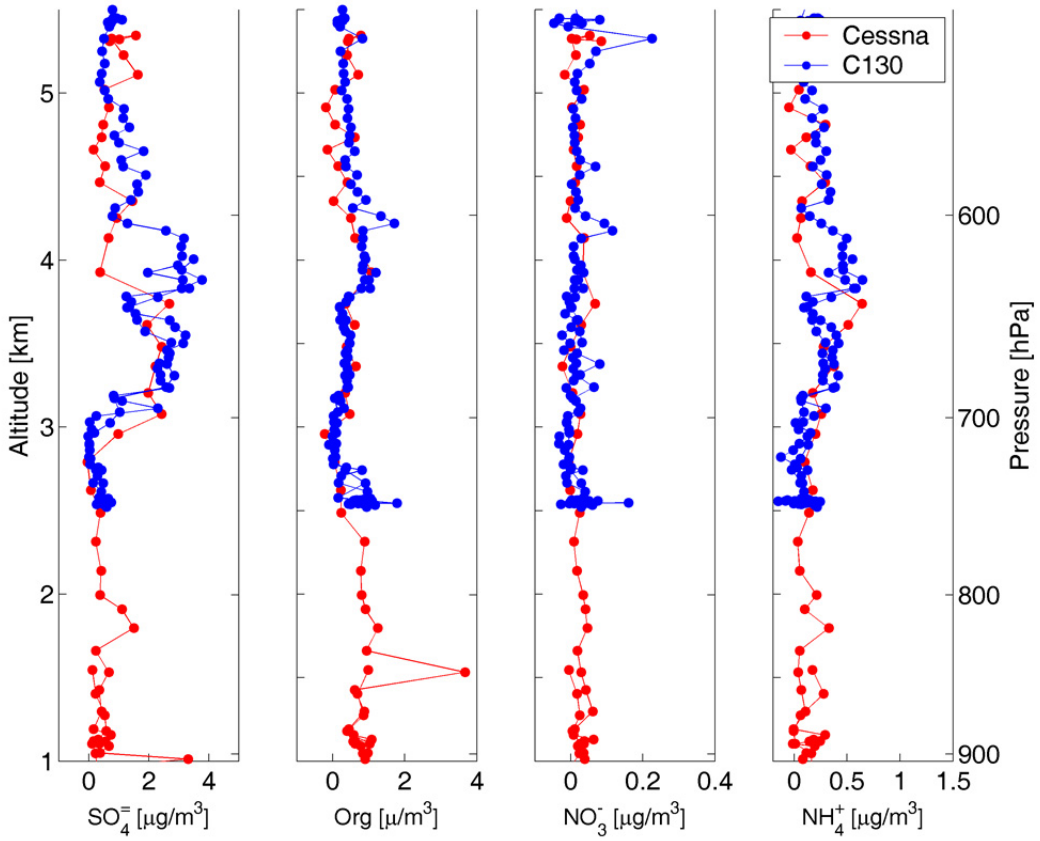

Figure 2-3: Aerosol Mass Spectrometer (AMS) measurements from the May 3, 2006 inter-comparison flight over Whistler Peak Station (50.1° N, 122.9° W). Cessna data are shown in red. C-130 data are shown in blue. All data at STP. No scaling for the upper size cut of the AMS has been applied to these data.

the C-130 had left the inter-comparison zone. To minimize the effect of sampling time differences, we compare only measurements taken during the Cessna upward spiral against those from the C-130.

Figure 2-3 shows the speciated aerosol profiles from both aircraft during this intercomparison. All measurements are converted to concentrations at standard temperature and pressure of 1013 hPa and 0 °C. Significant agreement is found between the AMS measurements, with respective Root Mean Square Differences (RMSD) and mean bias of, 0.9 and 0.3 µg/m^3 for $SO_4^=$, 0.3 and 0.2 µg/m^3 for organics, 0.03 and 0.003 µg/m^3 for nitrate, and 0.2

and -0.0007 μg/m^3 for ammonium. The largest disagreement is found in $SO_4^=$ at approximately 625 hPa, likely representative of a change in air mass, as indicated by significant and abnormal disagreement (~30%) between the relative humidity measurements on the two aircraft. Measurements at this particular pressure were sampled ~35 minutes apart. Removal of points between 600 and 650 hPa, decreases the RMSD and bias in $SO_4^=$ to 0.6 and -0.01 μg/m^3 respectively, leaving other species largely unchanged. This is considered good agreement for these sampling conditions.

MOUDI measurements of the $SO_4^=$ size distribution at Whistler Peak during INTEX-B indicate a mean ratio of total $SO_4^=$ aerosol to $SO_4^=$ below 1 μm in aerodynamic diameter of 1.4. This value is likely more appropriate for lower tropospheric $SO_4^=$, which is the focus of this study, than for upper tropospheric $SO_4^=$. We scale the submicron $SO_4^=$ measurements by this correction factor, which is further justified in section 4, to better represent total $SO_4^=$ mass. Airborne measurements off the west coast of Washington State and Oregon in May 1985 found that up to half of the non-seasalt $SO_4^=$ mass was above 1.5 μm (Andreae et al., 1988) suggesting either the use of a larger scale factor may be appropriate, or that a change in the $SO_4^=$ size distribution has occurred between these flight periods. MOUDI measurements of the NO_3^- size distribution indicate that total NO_3^- aerosol is eight times larger than submicron NO_3^-. However, we do not apply a correction factor to nitrate measurements due to concerns about such a large scale factor.

Figure 2-4 shows average vertical profiles of Cessna Q-AMS and water (H_2O) concentration data obtained during four separate enhancement periods. $SO_4^=$ concentrations of 1-3 μg/m^3 dominate in the free troposphere and tend to increase with altitude, implying long-range transport. In contrast, organic concentrations typically decrease with altitude and dominate at the surface, implying a local source. These opposing trends suggest that the amount of organics

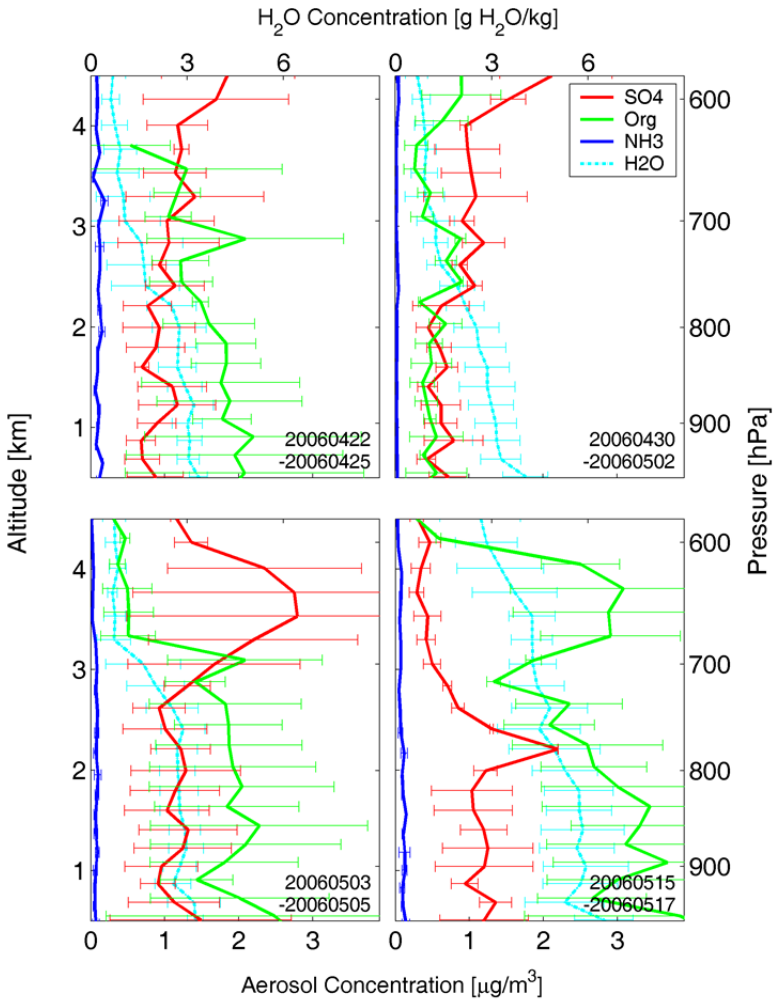

Figure 2-4: Cessna Q-AMS vertical profiles of sulfate, organics and nitrate during four enhancement periods. Sulfate ($SO_4^=$) data have been scaled by multiplying with a factor of 1.4 to account for particle size restrictions as inferred from MOUDI measurements at Whistler summit. Aerosol data are at STP. Water (H_2O) concentration profiles are in cyan. Date ranges are indicated in the bottom right of each plot. Error bars represent one standard deviation of the data.

transported with $SO_4^=$ is small and that long-range transport of organic aerosols is not a significant contributor to the organic concentration in the region studied. Leaitch et al. (2009) find a high level of mass closure with Cessna Q-AMS measurements, suggesting that the relatively high Q-AMS detection limit for organics (0.4 - 0.6 µg/m^3) has not impacted this conclusion. They also show that the occurrence of increased sulfate usually accompanies an increase in the number and mass concentrations of coarse particles. Dunlea et al. (2009) find

that $SO_4^=$ concentrations exceed those of organics for all Asian plume intercepts in the C-130, with older air masses being characterized by a larger $SO_4^=$/organics ratio than younger ones having undergone more rapid transport, presumably due to additional production of $SO_4^=$ during their extended transport time. The organic enhancement over May 15 - May 17 is likely fuelled by an unusually high mixed layer depth, as indicated by the water concentration profile, and can be attributed to local sources. This period is further examined by Sun et al. (2009) and McKendry et al. (2008). The contribution of nitrate to particulate mass is relatively insignificant, in part reflecting AMS size restrictions. We focus on long-range transport of $SO_4^=$ for the remainder of the manuscript.

2.3.2 MODEL DESCRIPTION

We use the GEOS-Chem chemical transport model v7-04-09 (Bey et al., 2001) (http://www-as.harvard.edu/chemistry/trop/geos/index.html) to interpret the aforementioned measurements. GEOS-Chem is driven by assimilated meteorological data from the Goddard Earth Observing System (GEOS-4) at the NASA Global Modeling Assimilation Office (GMAO), with 30 vertical levels and degraded to the model's horizontal resolution of 2° latitude by 2.5° longitude.

The aerosol simulation in GEOS-Chem includes the sulfate-nitrate-ammonium system (Park et al., 2004; Park et al., 2006), carbonaceous aerosols (Liao et al., 2007; Park et al., 2003), mineral dust (Fairlie et al., 2007) and sea-salt (Alexander et al., 2005). The aerosol and oxidant simulations are coupled through formation of sulfate and nitrate (Park et al., 2004), heterogeneous chemistry (Jacob, 2000) and aerosol effects on photolysis rates (Martin et al., 2003b). Wet and dry deposition are based upon Liu et al. (2001), including both washout and rainout. GEOS-Chem captures both the timing and distribution of Asian dust outbreaks during

TRACE-P and ACE-Asia (Fairlie et al., 2007). It exhibits no significant bias in Asian SO_x (SO_2 + $SO_4^=$) outflow during spring 2001 as part of the TRACE-P campaign (Park et al., 2005), although modeled $SO_4^=$ concentrations were 50% high during ACE-Asia, which may suggest an error in SO_2 oxidation rates (Heald et al., 2005).

The global emission inventory in the standard GEOS-Chem model is based on GEIA (Benkovitz et al., 1996) for the base year of 1985 with scale factors to 1998. We implement here the EDGAR 3.2FT2000 emission inventory based upon the year 2000 (Olivier et al., 2002) to provide a more current estimate of global emissions of NO_x, SO_x and CO. The global inventory is replaced by regional inventories from NEI99 (http://www.epa.gov/ttn/chief/net/1999inventory.html) over the United States for 1999, BRAVO (Kuhns et al., 2005) over Mexico for 1999 and Streets et al. (2003; 2006) for 2000 (NO_x and SO_x) and 2001 (CO) for eastern Asia. EMEP emissions (http://www.emep.int) of NO_x and CO are used over Europe for up to 2000. We update the eastern Asia emissions to 2006 from Zhang et al. (Zhang et al., 2009) and implement CAC emissions (http://www.ec.gc.ca/pdb/cac/) over Canada for 2005 and EMEP SO_x emissions (Vestreng et al., 2007) over Europe for the year 2004.

We scale all regional and global inventories from their respective base year to 2003, the last year of available statistics, unless its base year is after 2003. Our approach follows Bey et al. (2001) and Park et al. (2004). Emissions are scaled according to estimates provided by individual countries, where available. These countries/regions include the United States, Canada, Japan and Europe. NO_x emissions of remaining countries are scaled proportional to changes in total CO_2 emissions. SO_x emissions are similarly scaled to solid fuel CO_2 emissions and CO emissions to liquid fuel CO_2 emissions. A scale factor of 4.1% per year is used for ship emissions (Corbett et al., 2007). CO_2 emission data are obtained from the Carbon Dioxide Information Analysis Center (CDIAC).

In addition to annual scale factors, diurnal scale factors are also applied to NO_x emissions. Here, the intra-day variation of each grid cell is based upon the diurnal variation of each source type, as provided with the EDGAR inventory, and its relative contribution to total NO_x emissions within that cell.

2.3.3 SATELLITE INSTRUMENTATION

Aerosol Optical Depth (AOD), a measure of light extinction, has been retrieved since 2000 from the Moderate Resolution Imaging Spectroradiometer (MODIS) and Multi-angle Imaging Spectroradiometer (MISR), onboard the NASA satellite Terra. The MODIS retrieval of AOD is based on scene brightness over dark surfaces, using empirical relationships in the spectral variation in surface reflectivity (Kaufman et al., 1997; Remer et al., 2005). We use the MODIS collection 5 dataset (Levy et al., 2007). The MISR algorithm uses observed differences in the spatial variation of backscattered radiation with changing viewing angle to self-consistently retrieve surface reflectivity and AOD (Kahn et al., 2005; Martonchik et al., 2002). Global coverage in the absence of clouds is achieved daily from MODIS and in 6 to 9 days from MISR.

2.4 ESTIMATE OF SULFUR EMISSION GROWTH FROM CHINA

Significant increases in AOD retrieved from the Total Ozone Mapping Spectrometer (TOMS) over China between 1979-2000 and the Advanced Very High Resolution Radiometer (AVHRR) off the east coast of China between the periods 1988-1991 and 2002-2005 are attributed to increased aerosol sources (Massie et al., 2004; Mishchenko and Geogdzhayev, 2007). Here we investigate recent retrievals of AOD from MODIS and MISR and assess their relationship with Chinese sulfur emissions growth. We first use GEOS-Chem, with East Asian anthropogenic emissions held at year 2000 levels, to investigate meteorologically induced changes to AOD.

The top row of Figure 2-5 shows mean AOD for 2000-2006 over East Asia from MODIS, MISR and GEOS-Chem. Simulated AOD includes all major aerosol types (mineral dust, sulfate-nitrate-ammonium, carbonaceous, and sea-salt). A region of pronounced enhancement, designated as Region 1, is apparent in all three datasets. MODIS AOD exceeds MISR AOD by 12% over this region, consistent with comparisons by Abdou et al. (2005). Simulated AOD exceeds MISR AOD by 22% and exhibits a smoother distribution than both retrievals, with a more centralized maximum that reflects the temporally static emissions used. The middle panel of Figure 2-5 presents monthly average AOD within the Region 1. All three datasets contain a distinct seasonal variation with a spring maximum and a fall minimum that reflects the seasonal variation in dust as noted by Prospero et al. (2002). Simulated AOD generally captures the retrieved monthly variation and magnitude as compared to both instruments (MODIS: $r^2 = 0.46$, RMSD = 0.09; MISR: $r^2 = 0.36$, RMSD = 0.12), although the simulation tends to overestimate springtime AOD. Simulated AOD contributions from dust (green) and $SO_4^=$ (magenta) indicate that dust comprises the largest fraction of springtime AOD, whereas $SO_4^=$ dominates during other periods. We focus on the periods between July and December, as indicated by yellow bars, when an average 56% of total AOD results from the presence of $SO_4^=$, compared to 17% from dust.

The bottom left panel of Figure 2-5 shows the annual mean difference over July - December between simulated and retrieved AOD for Region 1, expressed as a percentage of the mean retrieved AOD from each instrument over the six-year, low-dust period. We find a significant trend in the satellite-model AOD difference for both MODIS (+4.1%/year, $r^2 = 0.72$) and MISR (+3.4%/year, $r^2 = 0.54$). We associate this trend with increased SO_x emissions, as $SO_4^=$ dominates simulated AOD in this comparison, simulated SO_x emissions are held at 2000 levels and interannual changes of non-anthropogenic aerosols, such as dust and sea salt, are accounted for

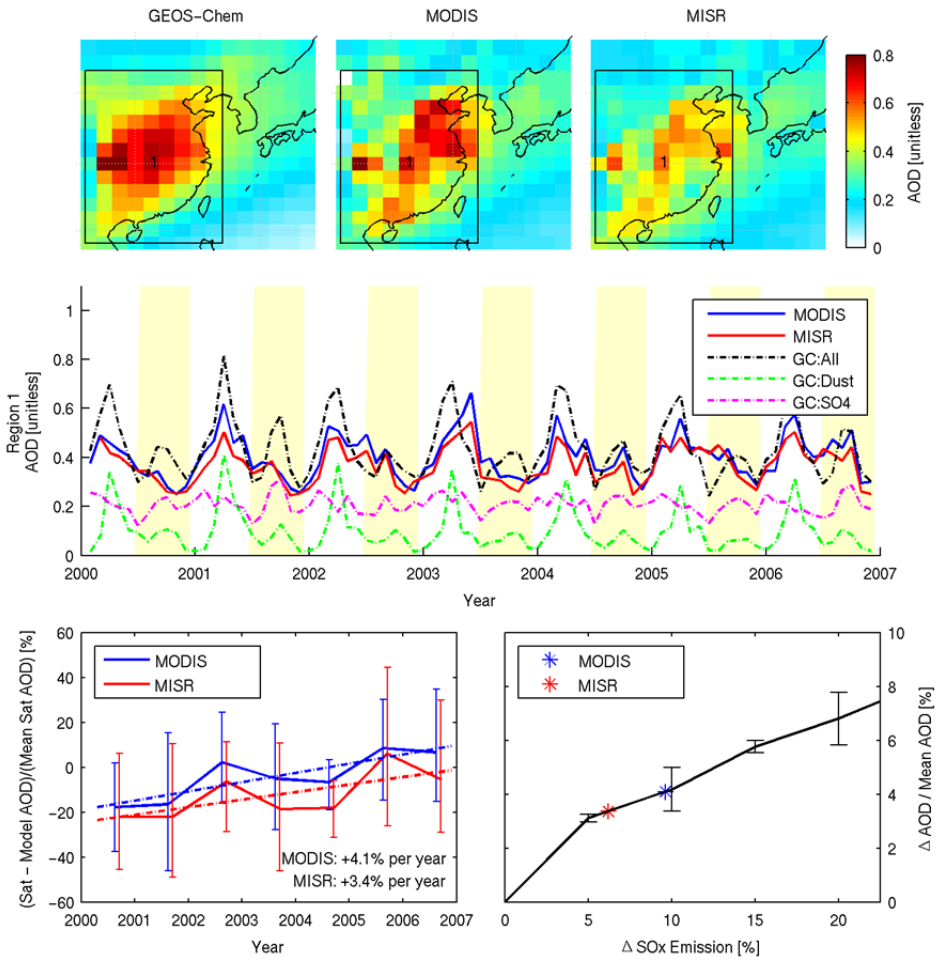

Figure 2-5: Aerosol Optical Depth (AOD) from the MODIS and MISR satellite instruments and a GEOS-Chem simulation. The top row shows mean AOD over 2000-2006 and defines Region 1 as used in the lower panels. The middle panel shows monthly mean for Region 1 retrieved and simulated AOD with simulated SO_x emissions held at 2000 levels. Simulated contributions of dust and $SO_4^=$ to total AOD are also shown. Highlighted areas indicate time periods used in the lower panels. The bottom left panel shows the Region 1 difference between retrieved and simulated AOD averaged between July and December of each year expressed as a percentage of mean retrieved AOD. Dashed line indicates best linear fit, error bars represent the 20th and 80th percentile. The bottom right panel shows the simulated relationship in Region 1 between total AOD and SO_x emissions over July-December 2000-2006 as calculated with 5 simulations with SO_x emissions increased by 0%, 5%, 10%, 15% and 20%. The red and blue stars respectively indicate the observed change in difference of simulated AOD between MISR and MODIS. Error bars denote one standard deviation of the data.

in the simulation. Trends in other aerosols could play a role, but would be less apparent due to their smaller AOD over this region during July - December.

The quantitative relationship between AOD and SO_2 emissions depends on a number of factors including SO_2 oxidation rates, dynamics and aerosol deposition (Dubovik et al., 2008). We quantify the relationship by conducting sensitivity simulations with increased SO_x emissions, and examining the change in simulated AOD. The bottom right panel of Figure 2-5 shows the calculated relationship between SO_x emissions and AOD over Region 1. The calculated ratio of $\Delta AOD(\%) / \Delta SO_x$ emissions (%) is nearly linear over this region during July to December. The annual trends in the difference between simulated and retrieved AOD correspond to simulations with an annual growth in SO_x emissions of 6.2 %/yr for MISR and 9.6 %/yr for MODIS. In general agreement, a comparison of the two bottom-up SO_x emission inventories for 2000 (Streets et al., 2003) and 2006 (Zhang et al., 2009) over Region 1 yields an annual growth of 9.9%. Beyond actual emission growth, changes between the 2000 and 2006 inventories include the addition of local inventories not present in, and improvement and corrections made to, the original 2000 inventory. These factors may account for the slight discrepancy between the growth estimates. We adopt the 2006 bottom-up inventory for our standard simulation, as it provides additional information on the spatial distribution of these SO_x emissions.

2.5 Campaign Average Analysis of Transpacific Transport

The top row of Figure 2-6 shows campaign average SO_x concentrations for the DC-8 over the domain in Figure 2-1. Filter pack and mist chamber measurements of $SO_4^=$ have been combined with corresponding CIMS SO_2 measurements. Both filter pack and mist chamber based measurements show a maximum around 700 hPa. Heald et al. (2006) attribute the $SO_4^=$ maximum in the lower free troposphere to preferential scavenging during transport either in the boundary layer or during lifting to the upper troposphere. Our standard simulation of total SO_x captures the relative vertical profile of filter pack based measurements over the domain of the

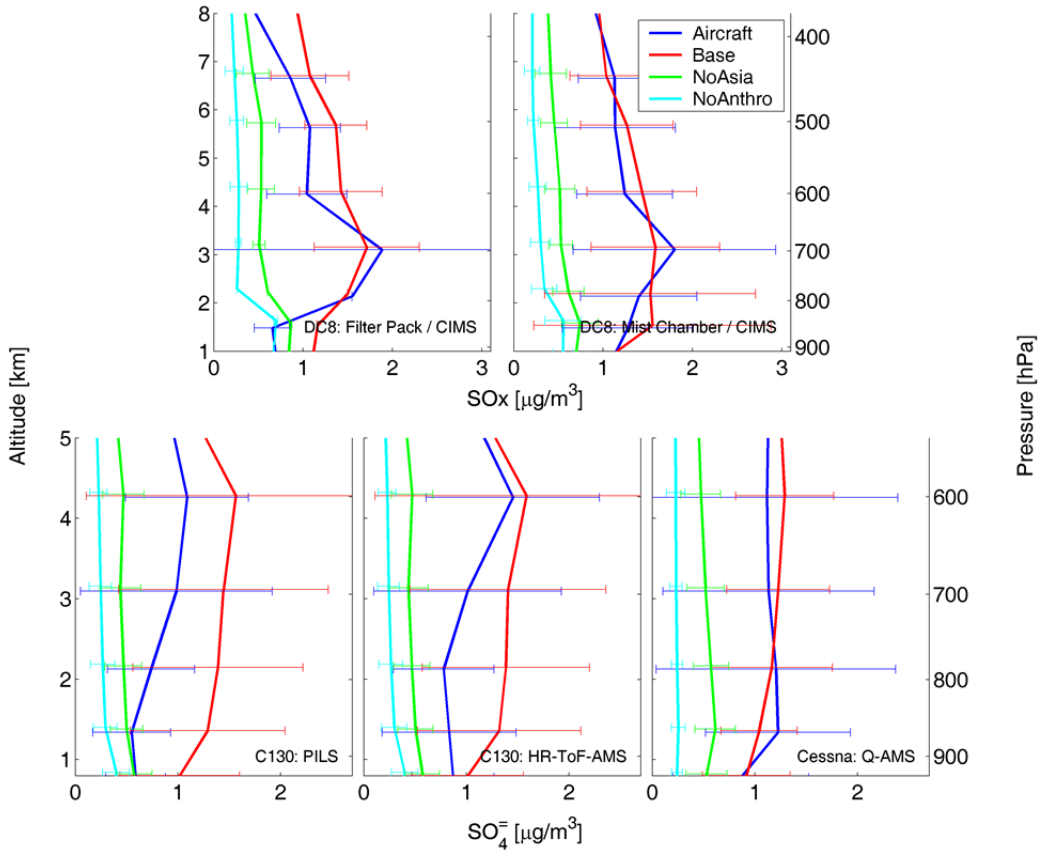

Figure 2-6: Campaign average aircraft measurements of SO_x and $SO_4^=$ during INTEX-B, within the boundaries shown in Figure 2-1. Simulated cases include our standard simulation, no East Asian emissions, and no global anthropogenic emissions. All measured and modeled data are at STP. Mist Chamber, AMS and PILS $SO_4^=$ data are increased by a factor of 1.4 to account for particle size restrictions. Error bars denote one standard deviation. A small vertical offset is included between datasets for visibility.

DC-8, but overestimates their magnitude between 500-900 hPa with a RMSD of 0.32 μg/m^3 (mean bias = 15%). Mist chamber $SO_4^=$ measurements are scaled by 1.4 to account for supermicron aerosol as described in Section 2.1. Over 500-900 hPa, the campaign average filter pack measurements are 33% higher than the unscaled mist chamber measurements, lending support to this scale factor. Mist chamber based SO_x measurements are well captured over the same range (RMSD = 0.20 μg/m^3, mean bias = 7.5%). Direct comparison of filter pack and mist chamber $SO_4^=$ with simulated values show weaker agreement (Filter Pack: RMSD = 0.47 μg/m^3, mean bias = 42%; Mist Chamber: RMSD = 0.42 μg/m^3, mean bias = 42%) than for SO_x, likely

reflecting an overestimate in the SO_2 oxidation rate (Heald et al., 2005). However, the bias in $SO_4^=$ found here for the East Pacific is lower than found by Heald et al. (2005) for the West Pacific, suggesting a decrease with air mass age as continued $SO_4^=$ production during transport decreases the ratio of SO_2 to SO_x.

The bottom panels of Figure 2-6 show campaign average $SO_4^=$ measurements on the C-130 and Cessna, sampled coincidently in time and space with simulated concentrations. Campaign average $SO_4^=$ concentrations for the C-130 measurements generally increase with altitude, reaching a maximum at 600 hPa. The C-130 HR-ToF-AMS measurements consistently exceed the PILS measurements, indicative of current uncertainties in aerosol measurement technologies. During a blind intercomparison conducted May 15, 2006 during a period of DC-8 and C-130 formation flying, the DC-8 Mist Chamber and C-130 PILS sulfate were in close agreement (slope = 1.00, 1 sigma = 0.03 μg/m^3, range 0.15 to 1.15 μg/m^3, r^2 = 0.95). The C-130 had considerable freedom to chase individual events. Despite this, simulated total $SO_4^=$ between 500-900 hPa has an RMSD of 0.40 μg/m^3 (mean bias = 34%) versus C-130 HR-ToF-AMS measurements and an RMSD of 0.54 μg/m^3 (mean bias = 59%) versus C-130 PILS measurements. The simulation exhibits the weak enhancement at 600 hPa, although fails to represent the lower concentrations at lower altitudes.

The sampling strategy for the Cessna was to conduct frequent profiles over Whistler Peak. Such a sampling strategy facilitated comparison with simulated results, provided context for the measurements at Whistler summit, and accommodated the range and duration of the Cessna. Cessna measurements indicate a fairly uniform vertical profile, with a large standard deviation in the free troposphere that reflects an oscillation between clean conditions and plumes. The simulation agrees significantly with size-correction scaled measured $SO_4^=$ (RMSD = 0.13 μg/m^3, mean bias = 2.5%). While recognizing the potential influence of both measurement uncertainty

and the limitation of applying a constant size-correction factor across both altitude and aircrafts, the eastward decrease in the bias between the DC-8 and Cessna aircraft may indicate an increasing $SO_4^=/SO_x$ ratio in the measurements.

Figure 2-6 also shows simulations without anthropogenic East Asian and all anthropogenic sources for all three aircraft flight tracks. Anthropogenic East Asian SO_x dominates throughout the DC-8 profiles, comprising 60% of the simulated mass between 500-900 hPa, with the largest contribution in the lower free troposphere. Other anthropogenic SO_x sources comprise an additional 17%. For the C-130 flight track, closer to North America, the sensitivity simulation attributes 67% of $SO_4^=$ to be of Asian origin, with a peak at 600 hPa. For the Cessna profiles over Whistler, local sources are most significant below 850 hPa, with the influence of East Asian anthropogenic emissions increasing with altitude. We calculate that 56% of the measured $SO_4^=$ between 500-900 hPa is from East Asia. Model analysis indicates the influence of East Asian sources at higher altitudes in both C-130 and Cessna versus the DC-8 measurements. This orographic effect is induced by rising air masses on approach to North American mountain ranges.

Of interest is the evolution of Asian sulfate over the last two decades. Figure 2-7 shows the mean non-seasalt sulfate profile observed by Andreae et al. (1988) during 4 flights in May 1985 using the NCAR King Air, covering a part of the C-130 INTEX-B flight domain. $SO_4^=$ concentrations (adjusted to STP at 273 K, sum of coarse and fine fractions) increased with altitude below 5 km, from 0.3-0.6 $\mu g/m^3$ in the marine boundary layer to 0.6-0.8 $\mu g/m^3$ in the cloud convection layer and free troposphere. The 1985 measurements thus showed lower concentrations, but a similar trend with increased altitude as was seen in the C-130 measurements. Mean C-130 measurements between 500-900 hPa are higher than the 1985 data by 60% from the PILS and by 90% from HR-ToF-AMS.

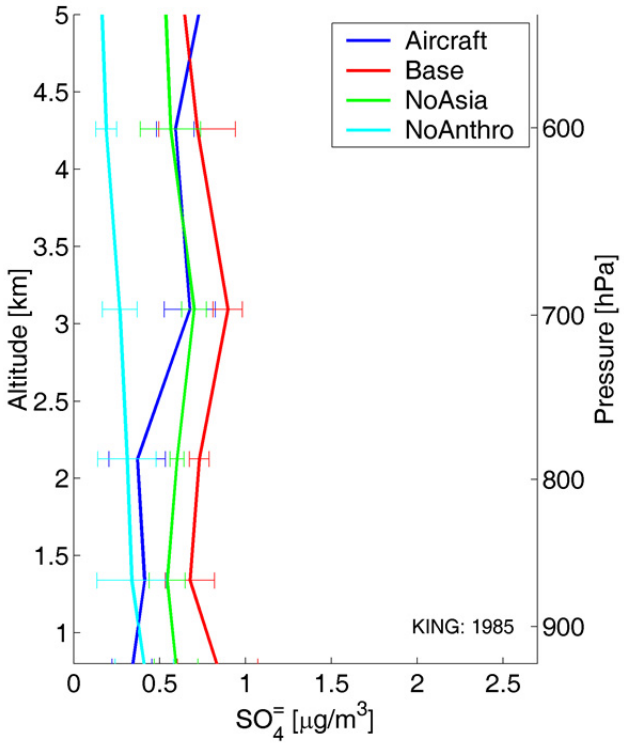

Figure 2-7: Average aircraft measurements of $SO_4^=$ during 1985 King Air flights, within the boundary shown in Figure 2-1. Simulated cases of total $SO_4^=$ include our standard simulation, no East Asian emissions, and no global anthropogenic emissions. All measured and modeled data are at STP. Error bars denote one standard deviation. A small vertical offset is included between datasets for visibility.

Differences in measurement techniques, flight tracks and meteorology could contribute to the apparent trend. Therefore we further interpret these observations by conducting a GEOS-Chem simulation using 1985 emissions and meteorology and sampling along the 1985 flights tracks. Global emissions for 1985 are taken from GEIA (Benkovitz et al., 1996), except for East Asia which are based on Streets et al. (2003; 2006) and scaled following Streets et al. (2000; 2006). The simulation reproduces the measurements with an RMSD of 0.25 μg/m^3 (mean bias = 21%) over 500-900 hPa. A sensitivity simulation without anthropogenic East Asian emissions reveals that this source contributes 0.14 μg/m^3 (20%) to the measured values in 1985, significantly reduced compared to the 67% along the C-130 flights in 2006.

To account for meteorological variation between 1985 and 2006, we also simulate the 2006 INTEX-B period using 1985 emissions. The relative contribution of East Asian $SO_4^=$ to the C-130 area (April-May, 34-55° N, 123.75-141.25° W, 500-900 hPa) between 1985 and 2006 increased 72% under identical meteorological conditions. The relative contribution in the King Air (April-May, 45-49° N, 123.75-126.25° W, 500-900 hPa) and Cessna (April-May, 49-51° N, 123.75-121.23° W, 500-900 hPa) flight regions increase similarly by 74% and 85%, respectively.

2.6 Asian Plume Development and Influence

Figure 2-8 examines the development of an Asian plume from April 18, 2006 to April 25, 2006. MODIS AOD retrievals from both the Aqua (1:30 overpass) and Terra (10:30 overpass)

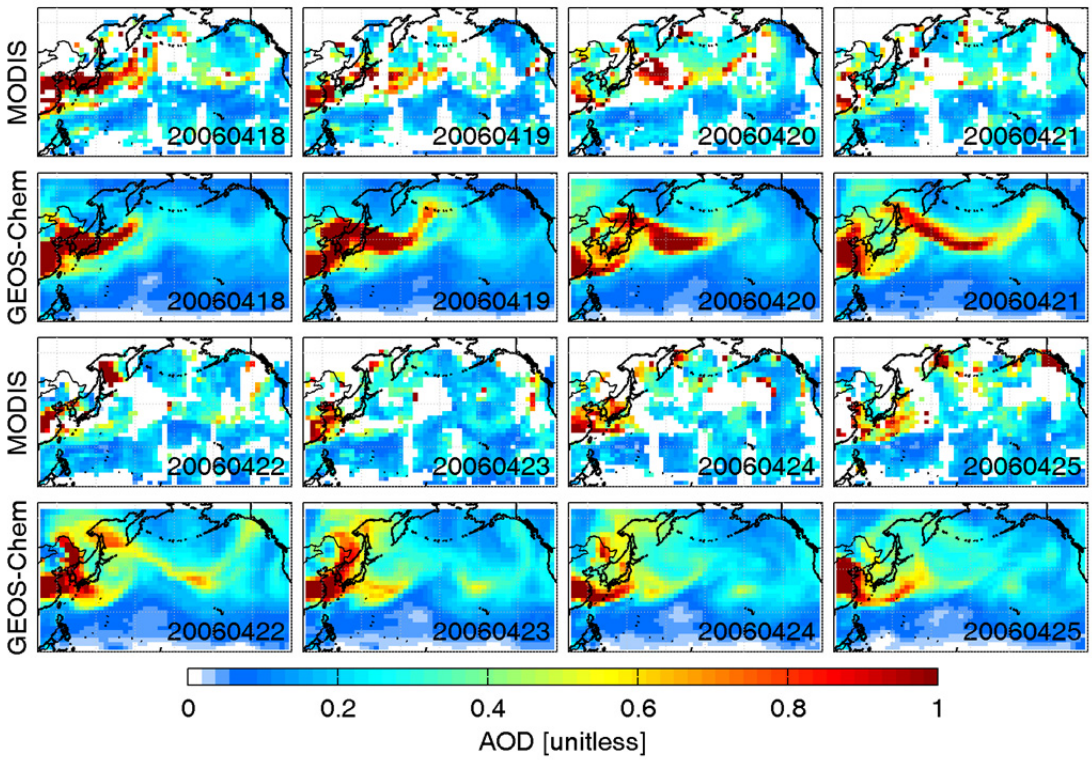

Figure 2-8: The development of an Asian plume between April 18-25, 2006 as retrieved from MODIS and as simulated by GEOS-Chem. White spaces indicate regions of less than 10 cloud free scenes within a 2° x 2.5° area.

satellites are plotted with simulation results from the same period. The GEOS-Chem simulation successfully captures many of the features associated with the influx event, which is dominated by dust, and also carries $SO_4^=$. Both retrieval and simulation show this plume beginning from China on April 18 and stretching across the Pacific Ocean through April 21, and finally sweeping down from the north while moving eastward over the North American coast. This event is further discussed by McKendry et al. (2008).

Figure 2-9 shows individual Cessna and GEOS-Chem $SO_4^=$ profiles taken between April 22 and 25, during the arrival of this Asian plume. The accuracy of individual simulated profiles, shown in the left panel cluster, varies with RMSD ranging between 0.39-0.87 μg/m^3. Simulations

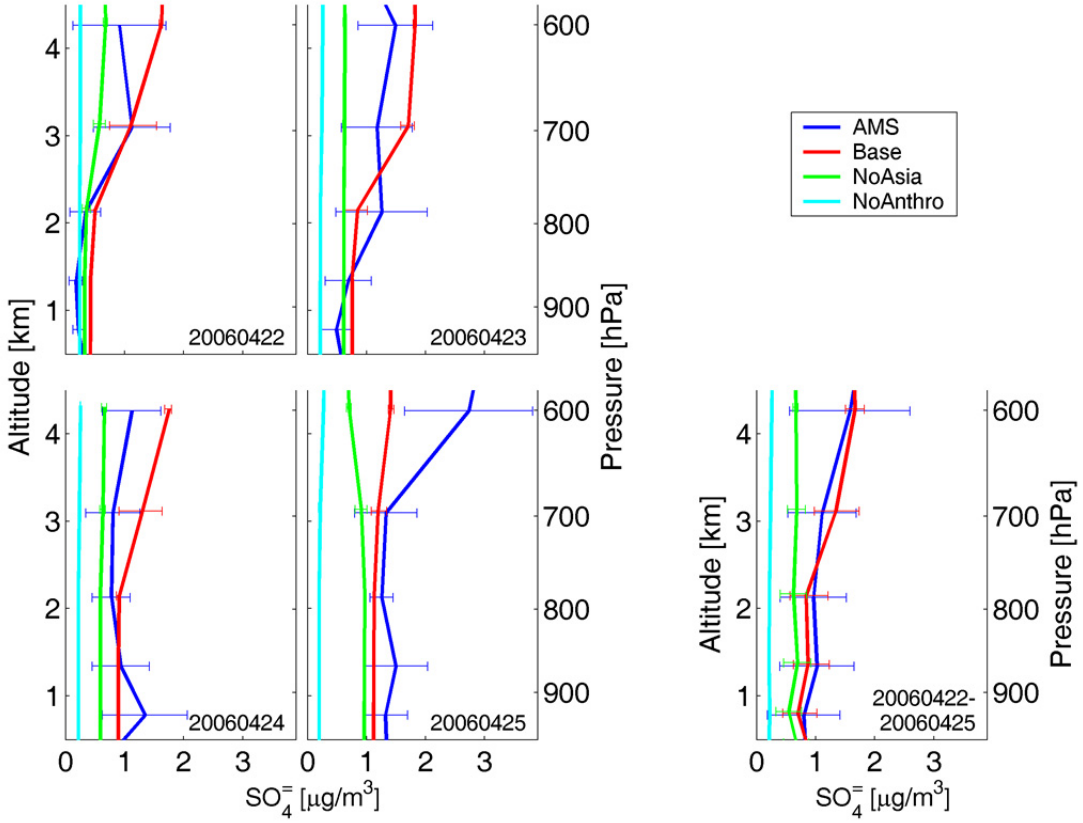

Figure 2-9: Cessna Q-AMS $SO_4^=$ profiles taken April 22-25, 2006. The left-hand panels show individual flight profiles. The right panel shows a mean profile of the same data. Error bars represent one standard deviation of the data. Q-AMS data are at STP and scaled a factor of 1.4 to account for particle size restrictions.

can fail to produce accurate plumes (e.g. Dunlea et al., 2009), but in this case the simulated plume has been transported too quickly, with simulated concentrations exceeding measurements on April 24, but the opposite on April 25. During long range transport events, small errors in the meteorological fields used by chemical transport models can compound to create offsets in time and space, making individual model profiles less representative than average comparisons. The right panel shows a mean profile comparison during this period. Significant agreement (RMSD = 0.25 $\mu g/m^3$) suggests this event was well represented, despite the weaker agreement of individual profiles.

Figure 2-10 shows simulated average conditions during April and May 2006. The top panel shows mean concentrations at 2 km, where DC-8 $SO_4^=$ enhancements were observed. Simulated $SO_4^=$ along the North American Pacific coast show increased concentrations relative to western continental regions. Major regional anthropogenic sources produce a large increase in $SO_4^=$ concentrations over eastern United States and Canada. The middle and bottom panels show vertical cross-sections of $SO_4^=$ and percentage of $SO_4^=$ originating from East Asia, respectively, averaged between the blue lines of the top panel. The highest overall magnitude (>1 $\mu g/m^3$) is again simulated in eastern North America and is predominately from regional emissions. Nonetheless, a narrow band of Asian influence in excess of 40% prevails over the continent at 4.5 km, where overall concentrations are ~0.3 $\mu g/m^3$. Along coastal regions, the largest East Asian influence is found between 1 and 5 km, where 40% of the overall $SO_4^=$ burden originated in East Asia. Interaction with the planetary boundary layer is facilitated by a combination of plume subsidence and mountain-induced mixing processes typical of southern British Columbia (McKendry et al., 2001). We calculate that surface concentrations of $SO_4^=$ along the southern Pacific Canadian coast are increased by 0.31 $\mu g/m^3$ (~30%) as a result of Asian emissions in spring. We take the mean model bias as compared to the C-130 and Cessna aircraft to estimate

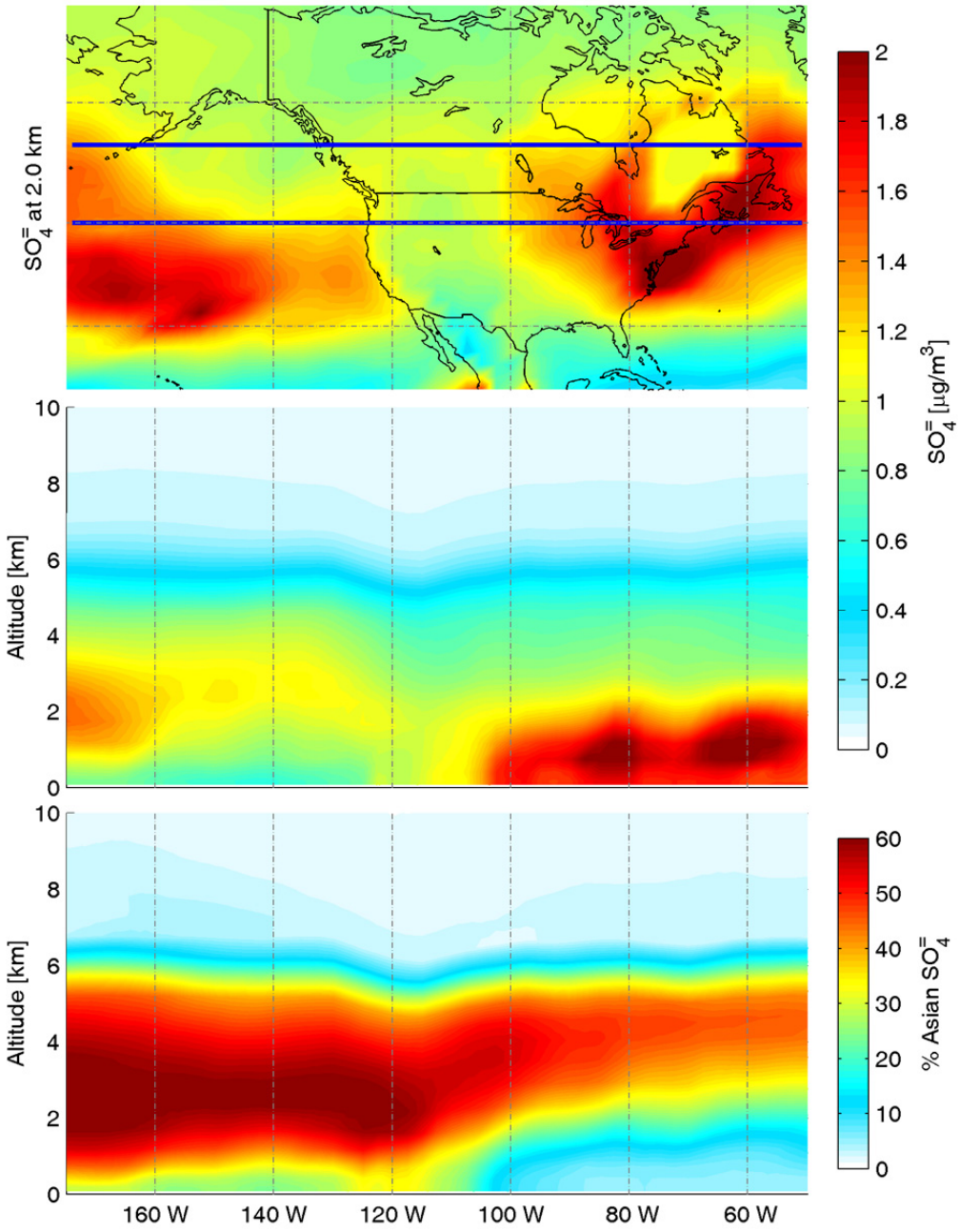

Figure 2-10: Average simulated conditions for April and May 2006. The top panel shows total $SO_4^=$ concentrations at ~2 km altitude. Middle and bottom panels display the mean cross-sectional total concentration and East Asian influence, respectively, between the blue lines in the top panel.

an error of approximately 25% in this calculation. Heald et al. (2006) found a 0.16 µg/m^3 enhancement in $SO_4^=$ over the northwest United States during periods of Asian influence. Yu et

al. (2008) used MODIS observations to access the seasonal variation in transpacific pollution aerosol and conclude that springtime transport is about twice as large as during other seasons.

We go on to explore the surface $SO_4^=$ measurements from the National Air Pollution Surveillance (NAPS) Network in the Vancouver area for evidence of Asian influence. Figure 2-11 shows surface $SO_4^=$ concentrations between April and May 2006 in the Vancouver area as a function of the modeled percent $SO_4^=$ originating in Asia. The two measurement sites in the Vancouver area, Abbotsford and Vancouver, reside in the same model grid box. Black circles correspond to measurement averages, binned at intervals of 5% simulated East Asian influence.

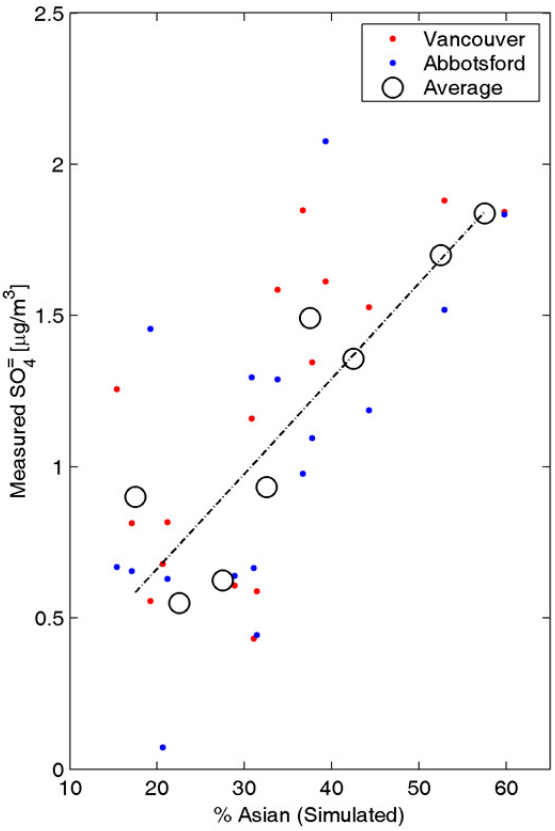

Figure 2-11: The influence of Asian $SO_4^=$ on coastal western Canadian surface concentrations during April-May 2006. Black circles denote mean filter pack sulfate measurements from Canada's National Air Pollution Network sites in Vancouver and Abbotsford as averaged at 5% intervals of percent Asian $SO_4^=$. Dashed line shows linear best fit. Percent Asian sulfate is simulated using the GEOS-Chem model.

Individual measurements show substantial scatter, but linear regression of the binned measurements show a significant correlation (r^2 = 0.82). Binned measurements indicate that an additional 0.32 μg/m^3 reaches the surface with each 10% increase in modeled Asian $SO_4^=$, corroborating that current levels of Asian sulfur emissions are impacting surface $SO_4^=$ concentrations in Canada. Aerosol transport events are episodic and the daily influence of East Asian $SO_4^=$ varies dramatically. Figure 2-11 suggests that during plumes East Asian $SO_4^=$ can contribute more than 1.5 μg/m^3 to coastal western Canadian concentrations. This is of similar magnitude to enhancements observed by the Cessna Q-AMS during plume events shown in Figure 2-4.

2.7 CONCLUSIONS

We interpreted a suite of satellite (MODIS and MISR), aircraft (DC-8, C-130 and Cessna 207) and ground-based measurements (Whistler Peak, NAPS) over the North Pacific Ocean and western North America in April-May 2006 as part of the INTEX-B campaign to understand the implications of long-range transport of Asian aerosol to Canada.

The Canadian component of INTEX-B included 33 flights from a Cessna 207 aircraft. We compare the Cessna quadrupole Aerodyne Mass Spectrometer (Q-AMS) measurements with a high resolution time of flight AMS (HR-ToF-AMS) onboard the C-130 during an intercomparison flight, yielding an overall bias of -0.01 μg/m^3 with appreciable scatter (RMSD = 0.6 μg/m^3) for sulfate ($SO_4^=$) and similar agreement for organics (bias = 0.2 μg/m^3, RMSD = 0.3 μg/m^3). However, there was a small systematic difference (<20%) between the C-130 HR-ToF-AMS sulfate and a co-located PILS measurement of $SO_4^=$ (Dunlea et al., 2009). We use ground-based measurements (MOUDI) of the $SO_4^=$ size distribution at Whistler Peak to estimate the mass in the super-micron range and use a factor of 1.4 to compensate for this loss. Cessna profiles over

Whistler, B.C. show $SO_4^=$ enhancements of 1-2 μg/m^3 over 600-700 hPa, indicative of long-range transport, whereas organic enhancements are largest near the surface, suggesting a local emission source. We did not detect long-range transport of significant organic aerosol from the Cessna data, contrary to expectations.

We interpret these observations with a global chemical transport model, GEOS-Chem, to simulate the implications of anthropogenic activity. We implement a more recent global bottom-up inventory (EDGAR) and develop updated scale factors, bringing global anthropogenic emissions from 1998 to at least the year 2003. We also implement current bottom-up inventories for East Asia for 2006 (Zhang et al., 2009), Canada for 2005 and Europe for 2004.

Retrieved Aerosol Optical Depth (AOD) from MISR and MODIS during low dust periods (July-Dec) are used to evaluate the growth of SO_x emissions between 2000-2006. We find a growth in the difference between simulated and retrieved AOD of 3.4%/yr (MISR) and 4.1%/yr (MODIS) using constant anthropogenic emissions sources as represented by GEOS-Chem. GEOS-Chem calculations of the change in AOD for a change in SO_x emissions indicate a near-linear relationship with a ratio of approximately 0.4 over East Asia. We estimate the average annual growth in East Asian SO_x emissions to be between 6.2% using MISR and 9.6% using MODIS, supporting the bottom-up estimate of an annual increase of 9.9% from 2000 (Streets et al., 2003) to 2006.

We use this simulation to understand the characteristics of East Asian outflow as measured by the INTEX-B aircraft. Over the Pacific Ocean, Asian outflow of SO_x is strongest in the lower troposphere, with enhanced $SO_4^=$concentrations of 1-1.5 μg/m^3 observed by the DC-8 between 700-800 hPa. The mean C-130 and Cessna aircraft $SO_4^=$ measurements of 1-1.5 μg/m^3 over 600-800 hPa indicate that Asian plumes are often elevated by orographic effects along coastal North

America. The simulation generally captures the campaign mean profile shape of DC-8 SO_x, and C-130/Cessna $SO_4^=$ measurements, with RMSD of 0.13-0.54 μg/m^3 (mean bias of 2.5-59%). Bias in simulated SO_2 oxidation likely contribute to the lower agreement found with respect to the C-130 measurements. Simulations without Asian emissions reveal that long-range transport of $SO_4^=$ dominates campaign-mean aircraft measurements in the free troposphere.

We compare the INTEX-B measurements with aircraft measurements in May 1985 over a similar domain as the C-130. Measured free tropospheric $SO_4^=$ concentrations increase by 60-90% from 1985 to 2006. Sensitivity simulations for 1985 and without East Asian emissions indicate that their relative contribution to $SO_4^=$ concentrations during April and May between 500-900 hPa increased by 72-85% due to emission changes as compared to 1985 depending on the specific region.

Comparison of individual plumes with aircraft profiles and MODIS AOD reveals a general consistency, but offsets in time and space. Campaign-mean simulations show that 50% of the $SO_4^=$ burden between 1 and 5 km over Whistler is of anthropogenic Asian origin. These emissions increase surface concentrations along the western Canadian coast by an average 0.31 μg/m^3 (~30%) in spring. This effect is corroborated with surface measurements, where we find an increase of 0.32 μg/m^3 with each 10% increase in simulated fraction of Asian $SO_4^=$ during INTEX-B, with episodic enhancements of more than 1.5 μg/m^3.

A better understanding of SO_2 oxidation is still needed. Previous work (Heald et al., 2006) and our analysis indicate an overestimate in the simulated SO_2 oxidation rate. Development of size-resolved aerosol simulations and $SO_4^=$ instruments that sample larger particles with high time resolution would facilitate model-measurement comparison. Improved understanding of inter-instrument $SO_4^=$ measurements would be valuable.

2.8 Acknowledgements

We thank David Parrish for his helpful suggestions. Rob Buchanan provided professional and tireless piloting of the Cessna during the study. Tragically, Rob lost his life in the crash of the Cessna following the conclusion of the study. Mohammed Wasey, Armand Gaudenzi, Dave Halpin and John Deary provided technical and logistical support. Special thanks to Juniper Buller, Anton Horvath, the Whistler Ski Patrol and Whistler Blackcomb for their support. This work is supported by the Natural Sciences and Engineering Research Council of Canada Special Research Opportunity Program and Environment Canada. Edward J. Dunlea and Jose L. Jimenez were supported by NASA grants NNG04GA67G and NNG06GB03G and NSF grants ATM-0449815 and ATM-0513116. Rodney Weber was funded through NASA grant NNG06GA68G. We thank the MODIS and MISR teams for their level 3 aerosol products and Environment Canada for their NAPS data.

Chapter 3. GLOBAL ESTIMATES OF AMBIENT FINE PARTICULATE MATTER CONCENTRATIONS FROM SATELLITE-BASED AEROSOL OPTICAL DEPTH: DEVELOPMENT AND APPLICATION

Authors: Aaron van Donkelaar[1], Randall V. Martin[1,2], Michael Brauer[3], Ralph Kahn[4], Robert Levy[4], Carolyn Verduzco[1] and Paul J. Villeneuve[5,6]

[1]Department of Physics and Atmospheric Science, Dalhousie University, 6300 Coburg Rd., Halifax, Nova Scotia, Canada, B3H 3J5

[2]Harvard-Smithsonian Center for Astrophysics, Cambridge, Massachusetts, USA.

[3]School of Environmental Health, University of British Columbia, British Columbia, Canada.

[4]NASA Goddard Space Flight Center, Greenbelt, MD 20771 USA

[5]Dalla Lana School of Public Health, University of Toronto, Toronto, Ontario, Canada.

[6]Population Studies Division, Health Canada, Ottawa, Ontario, Canada.

Article published in Environmental Health Perspectives, 118(6), June 2010. All text, figures, tables and presented results were contributed by the first author.

3.1 ABSTRACT

Background: Epidemiologic and health impact studies of fine particulate matter ($PM_{2.5}$) are limited by the lack of monitoring data, especially in developing countries. Satellite-observations offer valuable global information about $PM_{2.5}$ concentrations.

Methods: Global ground-level $PM_{2.5}$ concentrations were mapped using total column aerosol optical depth (AOD) from the MODIS and MISR satellite instruments and coincident aerosol vertical profiles from the GEOS-Chem global chemical transport model.

Results: Global estimates of long-term average (2001-2006) $PM_{2.5}$ concentrations at ~10 km × 10 km resolution indicate a global population-weighted geometric mean $PM_{2.5}$ concentration of 20 $\mu g/m^3$. The World Health Organization Air Quality $PM_{2.5}$ Interim Target-1 (35 $\mu g/m^3$ annual average) is exceeded over central and eastern Asia for 38% and 50% of the population, respectively. Annual mean $PM_{2.5}$ concentrations exceed 80 $\mu g/m^3$ over Eastern China.

Evaluation of the satellite-derived estimate with ground-based in-situ measurements indicates significant spatial agreement with North American measurements ($r = 0.77$, slope = 1.07, $n = 1057$) and with non-coincident measurements elsewhere ($r = 0.83$, slope = 0.86, $n = 244$). The one standard deviation uncertainty in the satellite-derived $PM_{2.5}$ is 25%, inferred from the AOD retrieval and aerosol vertical profiles errors and sampling. The global population-weighted mean uncertainty is 6.7 $\mu g/m^3$.

Conclusions: Satellite-derived total-column AOD, when combined with an aerosol transport model, provides estimates of global long-term average $PM_{2.5}$ concentrations.

3.2 INTRODUCTION

Chronic exposure to airborne fine particulate matter with diameter less than 2.5 μm ($PM_{2.5}$) is associated with adverse human health impacts including morbidity and mortality (e.g. Dockery et al., 1993; McDonnell et al., 2000; Pope et al., 2009). Several national environmental agencies in North America and Europe monitor $PM_{2.5}$ concentrations at numerous sites throughout their jurisdictions, but even these relatively dense networks have limited geographical coverage. Few long-term measurement sites exist elsewhere in the world, particularly in rapidly developing countries where concentrations and estimated health impacts are greatest (Cohen et al., 2003). Point measurements collected at monitoring sites are not necessarily representative of regional concentration, and regional variability is difficult to assess from point measurements alone.

Application of satellite observation to surface air quality has advanced considerably in recent years (Hoff and Christopher, 2009; Martin, 2008). Global aerosol observations from satellite could substantially improve estimates of population exposure to $PM_{2.5}$.

The Moderate Resolution Imaging Spectroradiometer (MODIS) and Multiangle Imaging Spectroradiometer (MISR) instruments onboard the Terra satellite have provided since mid-2000 global observations of aerosol optical depth (AOD), a measure of light extinction by aerosol in the atmospheric column above the Earth's surface. Terra's Sun-synchronous orbit encircles the Earth approximately 15 times each day, with each pass crossing the Equator at approximately 10:30, local time. Observations of AOD from Terra provide daily insight into the global distribution of column-integrated aerosol. However, the applicability of AOD to surface air quality depends upon several factors, including the vertical structure, composition, size distribution and water content of atmospheric aerosol.

Many studies have investigated the relationship between total-column AOD and surface $PM_{2.5}$ measurements. Most have developed simple empirical relationships between these two variables (e.g. Engel-Cox et al., 2004a; Wang and Christopher, 2003), while more recent works often used local meteorological information to improve agreement (e.g. Koelemeijer et al., 2006; Liu et al., 2005b) or to filter the data (e.g. Gupta et al., 2006b). Some studies have employed LIDAR instruments to capture the vertical aerosol distribution at specific locations (e.g. Engel-Cox et al., 2006; Schaap et al., 2008). As noted by Schaap et al. (2008), locally derived AOD-$PM_{2.5}$ relationships cannot be easily extended to other regions due to variation in meteorology and aerosol composition. Unique, local, time-dependent AOD-$PM_{2.5}$ relationships are necessary to infer global estimates of $PM_{2.5}$. Ground-based measurements of aerosol vertical profiles and properties have insufficient coverage to estimate global AOD-$PM_{2.5}$ relationships.

Global chemical transport models (CTMs) resolve atmospheric composition at a resolution of hundreds of kilometres horizontally by hundreds of meters vertically, with a temporal frequency of tens of minutes. Liu et al. (2004) first estimated surface-level $PM_{2.5}$ from MISR observations by using CTM output to represent local AOD-$PM_{2.5}$ conversion factors over the contiguous United States. Van Donkelaar et al. (2006) extended the approach of Liu et al. (2004) to estimate $PM_{2.5}$ from both MODIS and MISR observations and investigated the factors affecting the agreement between AOD and surface-level $PM_{2.5}$. Statistical models have also been used to relate AOD to $PM_{2.5}$, using MISR-retrieved spherical vs. non-spherical particle fraction, in addition to model-derived vertical distribution, to separate mineral dust from other aerosol species (Liu et al., 2007b). Some recent work also probed the limitations of using AOD without accounting for vertical distribution or speciation, and concluded that agreement with ground-based monitors based on this approach might depend on factors other than satellite observations (Paciorek and Liu, 2009).

In this paper, we develop a global satellite-based estimate of surface $PM_{2.5}$ at a spatial resolution of 0.1° × 0.1°, or approximately 10 km × 10 km at mid-latitudes. The methods section develops an approach for combining MODIS and MISR AOD into a single, improved estimate of AOD. AOD-$PM_{2.5}$ conversion factors, calculated with a global chemical transport model, are produced and applied to these AOD in the results section. We present a global estimate of $PM_{2.5}$ concentrations and validate this with ground-based (*in-situ*) observations. We estimate global exposure to outdoor ambient $PM_{2.5}$ using our satellite-derived product to demonstrate potential application for global health studies. We then examine sources of error.

3.3 METHODS

3.3.1 SATELLITE OBSERVATIONS

The MODIS instrument measures a wide range of spatial and spectral information from its orbit aboard the Terra satellite. The near-daily global coverage from the MODIS AOD retrieval (Levy et al., 2007) is advantageous. The MISR instrument, also aboard Terra, offers smaller spatial and spectral ranges, but views each scene on the Earth from nine different angles. This additional angular information allows the MISR AOD retrieval (Diner et al., 2005; Martonchik et al., 2009) to reduce algorithmic assumptions and retrieval bias, as well as obtain information about microphysical properties, and plume heights in aerosol source regions (Kahn et al., 2007). Neither instrument can retrieve AOD in cloudy conditions.

We use the MODIS BRDF/Albedo product (MOD43, Collection 5) to distinguish surface types and, in conjunction with ground-based retrievals of AOD, to identify regions of high bias in both MODIS and MISR AOD. We define these surface types for each month according to the ratio of surface albedo for different wavelengths, similar to assumptions inherent in the MODIS AOD retrieval. We remove AOD retrieved from either instrument with an anticipated bias greater than the larger of ±(0.1 or 20%), based on comparison with AERONET sun photometer measurements of AOD. Remaining MODIS and MISR AOD are averaged to produce a single value at a given grid cell. The supplemental material describes in detail the satellite retrievals, and this bias filtration. We restrict our subsequent analysis to locations with at least 50 successful satellite retrievals over 2001-2006, to yield near-complete (95%) global geographic coverage.

3.3.2 ESTIMATING $PM_{2.5}$ FROM AEROSOL OPTICAL DEPTH

Estimating ground-level concentrations of dry 24-h $PM_{2.5}$ (in $\mu g/m^3$) from satellite observations of total-column AOD (unitless) requires a conversion factor that ccounts for their spatially and temporally varying relationship.

$$PM2.5 = \eta \cdot AOD \qquad 3\text{-}1$$

η is a function of the factors that relate 24-h dry aerosol mass to satellite observations of ambient AOD: aerosol size, aerosol type, diurnal variation, relative humidity and the vertical structure of aerosol extinction (van Donkelaar et al., 2006). Following Liu et al. (2007b; 2004) and van Donkelaar et al. (2006), we use a global 3-D chemical transport model (GEOS-Chem; Supplemental Material) to calculate the daily global distribution of η.

The GEOS-Chem model solves for the temporal and spatial evolution of aerosol (sulfate, nitrate, ammonium, carbonaceous, mineral dust and sea salt) and gaseous compounds using meteorological data sets, emission inventories, and equations that represent the physics and chemistry of atmospheric constituents. The model calculates the global 3-D distribution of aerosol mass and AOD with a transport timestep of 15 minutes. We apply the modelled relationship between aerosol mass and relative humidity for each aerosol type to calculate $PM_{2.5}$ for relative humidity values that correspond to surface-measurement standards (35% for U.S. and Canada; 50% for Europe) We calculate daily values of η as the ratio of 24-h ground-level $PM_{2.5}$ for a relative humidity of 35% (U.S. and Canadian surface-measurement gravimetric analysis standard), and at 50% (European surface-measurement standard), to total-column AOD at ambient relative humidity. The AOD is averaged between 10 a.m. and 12 p.m. local time, corresponding to the Terra overpass period. We interpolate values of η from 2° × 2.5°, the resolution of the GEOS-Chem simulation, to 0.1° × 0.1° for application to satellite AOD values.

We compare the original MODIS and MISR total-column AOD with coincident ground-based measurements of daily mean $PM_{2.5}$. Canadian sites are part of the NAPS Network, maintained by Environment Canada (http://www.etc.cte.ec.gc.ca/NAPS/index_e.html). U.S. data are from the IMPROVE network (http://vista.cira.colostate.edu/improve/Data/data.htm) and the U.S. Environmental Protection Agency Air Quality System Federal Reference Method sites (http://www.epa.gov/air/data/index.html). Validation of global satellite-derived $PM_{2.5}$ estimates is hindered by the lack of available surface-measurement networks in many parts of the world. We collect 244 annually representative, ground-based $PM_{2.5}$ data from both published and unpublished field measurements outside the United States and Canada, as described in the supplemental material.

3.4 RESULTS

The top and middle panels of Figure 3-1 show mean AOD for 2001-2006 over North America from MODIS and MISR. Both datasets exhibit similar AOD values of 0.15-0.25 over the eastern United States, reflecting a combination of anthropogenic and biogenic sources. Several individual cities can be clearly identified in mean MODIS AOD for the Great Lakes region. A large AOD enhancement over the southwestern United States appears in the MODIS retrievals, but is absent from the MISR retrievals. The bottom panel of Figure 3-1 shows the mean combined

Table 3-1: Comparison of coincidently sampled six-year mean measurements[a] of daily 24h average $PM_{2.5}$ with AOD and satellite-derived $PM_{2.5}$.

	slope[b]	intercept	r	n
MODIS AOD	0.020	0.10	0.39	1218
MISR AOD	0.010	0.11	0.39	353
Average AOD	0.015	0.06	0.44	1236
Combined AOD	0.017	0.10	0.61	1057
Satellite-derived $PM_{2.5}$	1.066	-1.75	0.77	1057

[a] A minimum of 50 measurements are required for each point.
[b] calculated with reduced major-axis linear regression (Hirsh and Gilroy, 1984)

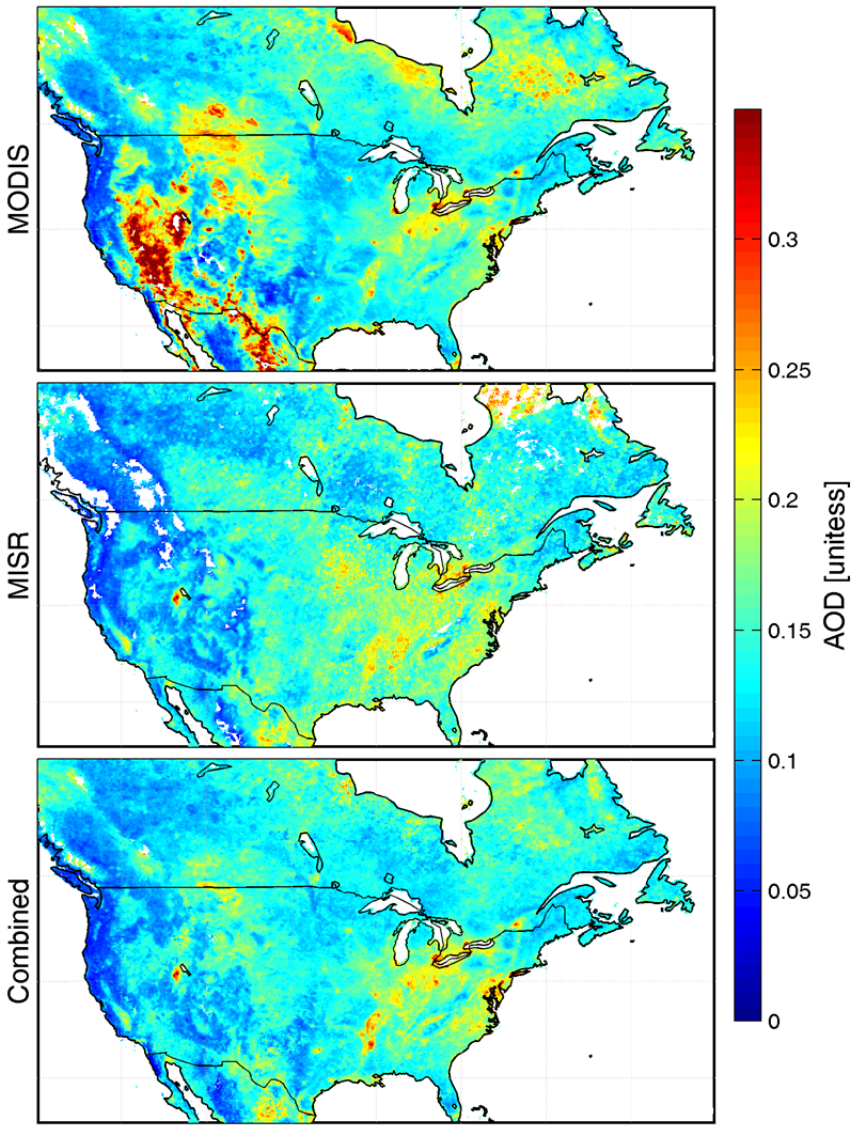

Figure 3-1: Mean aerosol optical depth (AOD) over 2001-2006 from the MODIS and MISR satellite instruments. The bottom panel indicates data from the combined product developed here. White space denotes water or fewer than 50 measurements.

MODIS and MISR AOD over North America. Our combination of these two AOD products removes the biased AOD observed by MODIS over the western United States. The combined product is dominated by MODIS in the east due to finer temporal sampling. MISR dominates in the west due to its accuracy.

Table 3-1 gives statistics comparing the spatial variation in six-year mean AOD retrievals with measurements of daily 24-h average $PM_{2.5}$ sampled on the same days as successful satellite observations. Both the MODIS and MISR instruments indicate some relationship between retrieved total-column AOD and in-situ $PM_{2.5}$, both with spatial correlation coefficients of 0.39. A simple average of the daily AOD from both instruments yields a correlation of 0.44. Combining retrievals from these instruments as described in the methods section increases the correlation to 0.61. Additional information is required to quantitatively estimate $PM_{2.5}$ concentrations from AOD as presented below.

Figure 3-2 shows the annual mean distribution of daily η values used to relate satellite-observed total-column AOD to $PM_{2.5}$ at 35% relative humidity. Average values of η are typically 20-130 μg/m^3. High values of η over regions of large dust concentration (Prospero et al., 2002) reflect in part its low hygroscopicity. Values of η are lower for hygroscopic aerosols as their dry volume is significantly smaller than under ambient conditions. Ground-level aerosol sources in industrial regions lead to vertical profiles that peak near ground, and moderate values of η.

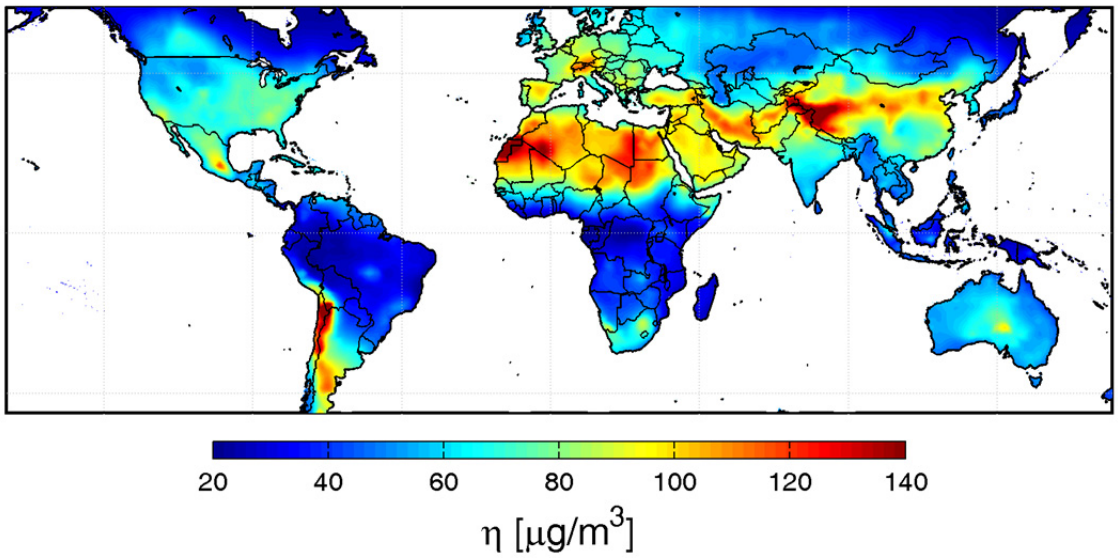

Figure 3-2: Annual mean η (ratio of $PM_{2.5}$ to AOD) for 35% relative humidity. White space indicates water.

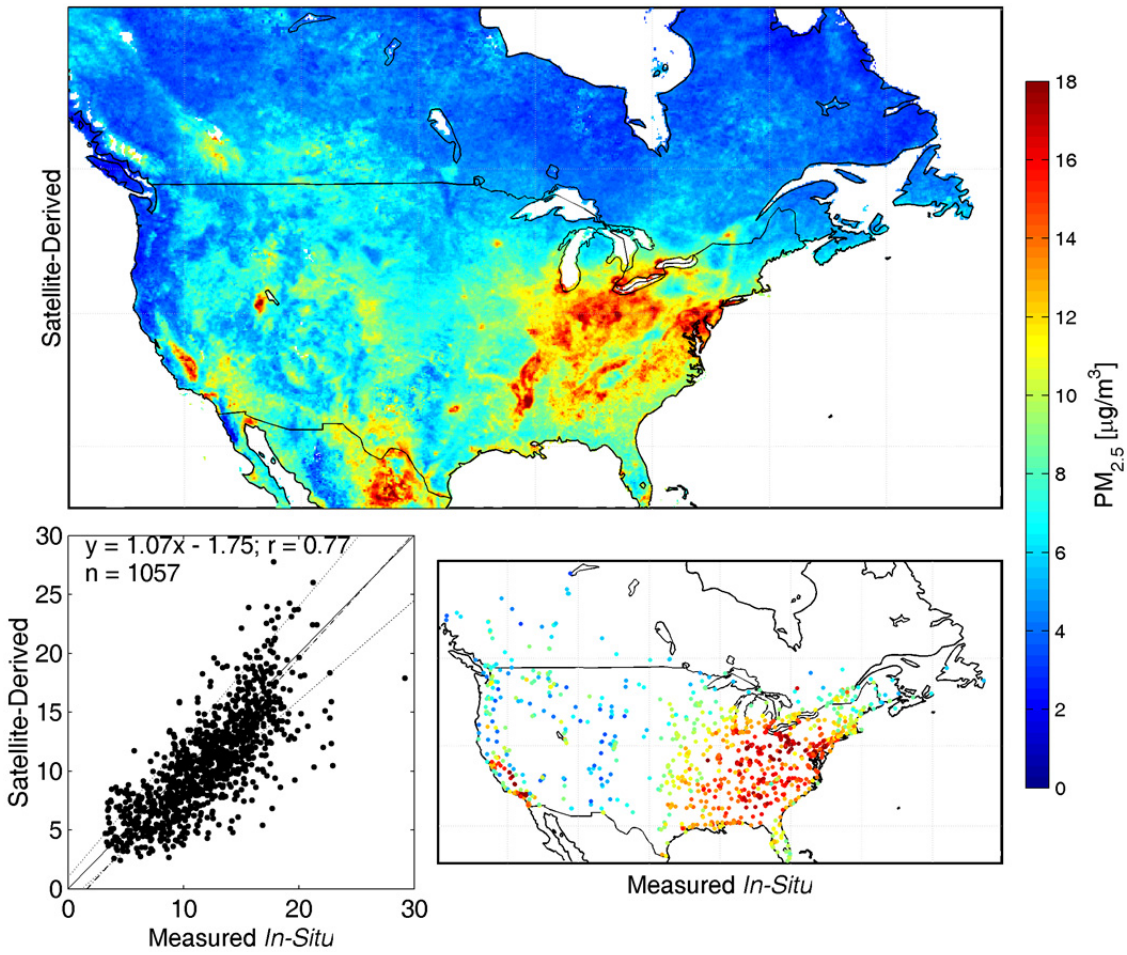

Figure 3-3: Satellite-derived $PM_{2.5}$ and comparison with surface measurements. The top panel shows mean satellite-derived $PM_{2.5}$ between 2001-2006. White space denotes water or fewer than 50 AOD measurements. The bottom right panel shows positions and mean values of coincidently measured surface sites. The bottom left panel compares average coincident values of both measured and satellite-estimated $PM_{2.5}$ in $\mu g/m^3$. The solid black line denotes unity. Thin dotted lines show uncertainty of $\pm(1\ \mu g/m^3 + 15\%)$. The line of best fit (Hirsh and Gilroy, 1984) is dashed.

Western North America is characterized by low η, providing additional insight into the poor AOD-$PM_{2.5}$ correlations (Engel-Cox et al., 2004b; Hu, 2009) associated with this region, and in agreement with Liu et al. (2007b) who found that transported dust aloft affects the western North America AOD-$PM_{2.5}$ relationship. η is related to land types only insomuch as these are typified by particular aerosol types, meteorology and vertical structures. Temporal variation in η is considerable.

The top panel of Figure 3-3 shows the six-year mean of 24-h average satellite-derived surface $PM_{2.5}$ over North America as calculated from equation 3-1 at a daily timescale. A large-scale $PM_{2.5}$ enhancement is apparent over the eastern United States. The western and northern parts of the continent are generally characterized by low concentrations, with a few exceptions. Geographic mean $PM_{2.5}$ concentrations over eastern and western North America are 6.9 $\mu g/m^3$ and 6.2 $\mu g/m^3$, respectively. Application of η (Figure 3-2) increased the spatial contrast relative to Figure 3-1, reflecting ground-level aerosol sources in the east and aerosols aloft in the north and west.

We evaluate the satellite-derived $PM_{2.5}$ with surface monitors. The bottom right panel of Figure 3-3 shows the annual mean of 24-h $PM_{2.5}$ concentrations measured with the surface monitors and sampled on the same days as the satellite-derived $PM_{2.5}$. Ground-level measurements show similar features to our satellite-derived product. The bottom left panel of Figure 3-3 quantitatively compares satellite-derived and ground-level measured $PM_{2.5}$. We find significant cross-sectional correlation between average coincidently sampled satellite-derived and ground-based $PM_{2.5}$ across North America ($r = 0.77$, slope = 1.07, bias = -1.75 $\mu g/m^3$). Many factors contribute to the scatter of points, including differences between what satellite and *in situ* measurements represent that do not necessarily indicate errors in either measurement.

3.5 Global Estimates of $PM_{2.5}$ Concentrations

Figure 3-4 presents the six-year mean of our global satellite-derived $PM_{2.5}$. This figure, and all subsequent, are at 50% RH in agreement with European ground-based measurements. We reject points created with less than 50 values, enabling 95% global geographic coverage. The satellite-derived $PM_{2.5}$ include an adjustment for discontinuous sampling as described in the error analysis. Annual mean $PM_{2.5}$ concentrations vary spatially by more than an order of

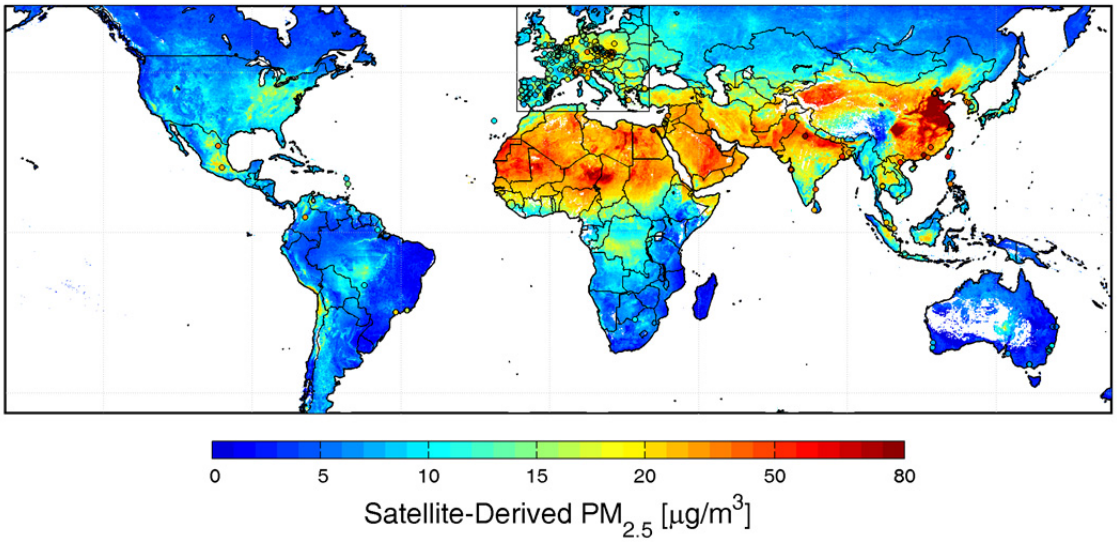

Figure 3-4: Global satellite-derived $PM_{2.5}$ averaged over 2001-2006. White space indicates water or locations containing less than 50 measurements. Circles correspond to values and locations of comparison sites outside Canada and the United States. The black rectangle outlines European sites.

magnitude. Values are less than 10 µg/m^3 for large regions of the earth. In contrast, $PM_{2.5}$ concentrations of 60-90 µg/m^3 are found over eastern China, with values in excess of 100 µg/m^3 for its major industrial regions. The Indo-Gangetic plain, from New Delhi eastward contains the highest $PM_{2.5}$ concentrations in India, with values of 80-100 µg/m^3, especially in winter (e.g. Di Girolamo et al., 2004). Concentrations elsewhere in northern India are 15-60 µg/m^3. Biomass burning effects on $PM_{2.5}$ levels are visible in central South America and central Africa, where concentrations of 10-17 µg/m^3 are estimated. Dust transport in the fine mode is substantial (Jones and Christopher, 2007), contributing to large-scale $PM_{2.5}$ in the Middle East of approximately 20-50 µg/m^3.

Figure 3-4 also shows locations of ground-based measurements and values outside North America that were used for comparison. Despite increased uncertainty due to temporal sampling differences, significant overall agreement exists (r = 0.83, slope = 0.86, intercept = 1.15

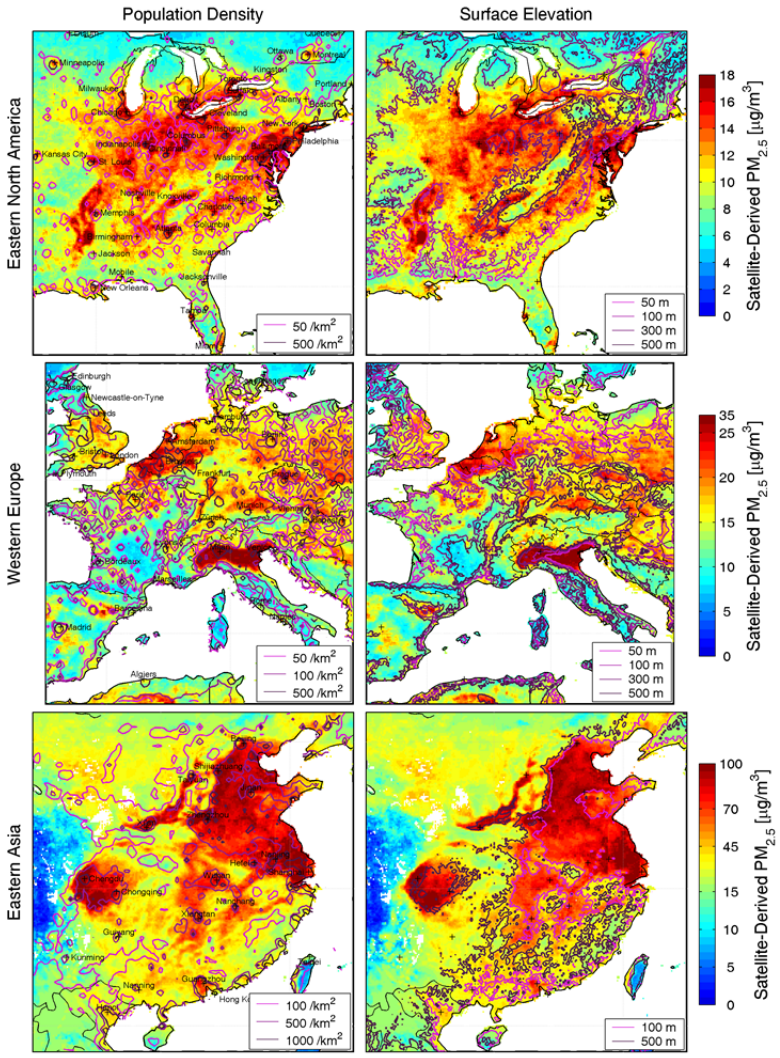

Figure 3-5: Regional satellite-derived $PM_{2.5}$ concentrations. Columns show mean satellite-derived $PM_{2.5}$ for 2001-2006 at locations containing at least 50 measurements. Contours denote population density in the left column and surface elevation in the right. The color scale varies by region. Crosses indicate city centers in both columns. Altitude data are from the United States Geological Survey.

$\mu g/m^3$, n = 244). Similar agreement is obtained when all sites except Europe and North America are considered (r = 0.83, slope = 0.91, intercept = -2.64 $\mu g/m^3$, n = 84).

Figure 3-5 overlays contours of population density and surface elevation onto satellite-derived $PM_{2.5}$ for regions of major anthropogenic sources: eastern North America, western Europe and eastern Asia. Some relationships are apparent between $PM_{2.5}$, topography and

population. Heavily populated and highly polluted, low-lying regions of eastern China and the Po Valley of northern Italy contrast sharply with neighbouring higher altitude regions. The Appalachian Mountains in eastern North America emerge as a relatively clean region. Many $PM_{2.5}$ enhancements are associated with urban or industrial areas, but these relationships are complex.

3.6 Error Analysis

The dominant sources of error in satellite-derived $PM_{2.5}$ arise from uncertainties in both AOD retrieval and aerosol vertical structure (van Donkelaar et al., 2006). The residual AOD bias after data filtering is within the larger of ±(0.1 + 20%), as evaluated with ground-based AERONET measurements. We evaluate the GEOS-Chem simulation of the aerosol vertical profile using observations from the CALIPSO satellite. The GEOS-Chem simulation generally captures to within 5% the fraction of AOD within the boundary layer (Supplemental Material). We estimate the error in satellite-derived $PM_{2.5}$ as the change in $PM_{2.5}$ that occurs when η and AOD are adjusted by their uncertainty, approximated as the GEOS-Chem vertical profile bias and residual

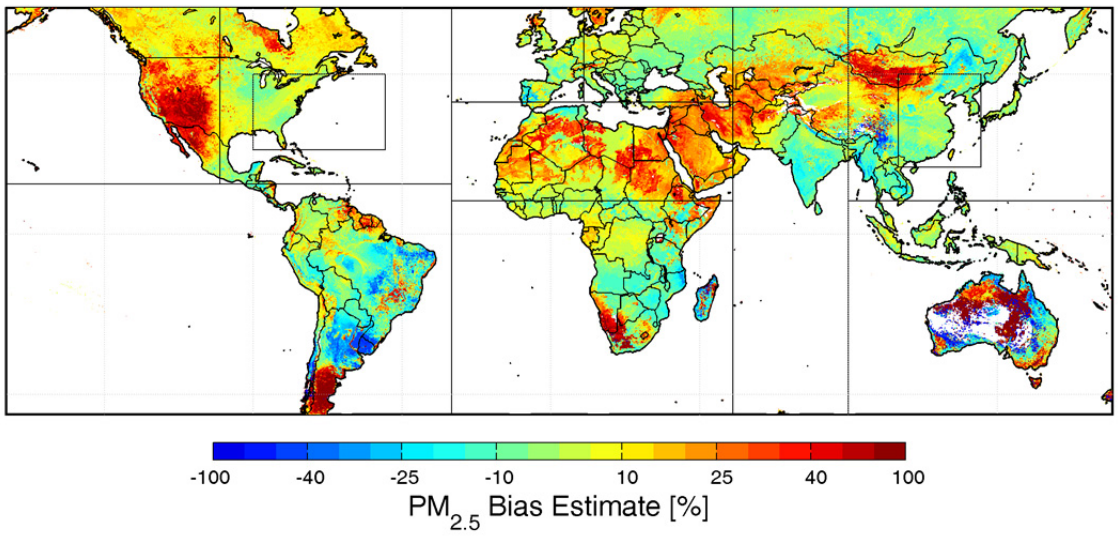

Figure 3-6: Estimate of the satellite-derived $PM_{2.5}$ bias, defined as (satellite-derived $PM_{2.5}$ - truth) / truth. Boxed areas define the regions used in Figure 3-8.

satellite AOD bias, respectively.

Figure 3-6 shows the error distribution of coincidently sampled satellite-derived $PM_{2.5}$. Arid regions are typically over-predicted, and populated regions of East Asia under-predicted. We find that one standard deviation of the global error distribution is within ±15% of the satellite-derived value. We test this uncertainty estimate by comparison with coincident $PM_{2.5}$ observations for North America (Figure 3-2) and find that one standard deviation of the data lies within ±(1 μg/m^3 + 15%). The necessary inclusion of a small absolute term suggests that our uncertainty estimate may be underestimated at low $PM_{2.5}$ values, and supports the presence of a small negative bias, as indicated by the line of best fit, shown in the lower left panel of Figure 3-3.

Non-uniform and incomplete sampling by satellites have the potential to create bias in long-term mean observations (Levy et al., 2009; Paciorek and Liu, 2009). Here we investigate how non-random sampling of AOD by satellite observations affect the representation of annual mean $PM_{2.5}$. The total number of successful satellite retrievals are shown in the top panel of Figure 3-7 and summarized regionally as population-weighted mean in Table 3-2. Lower sampling is

Table 3-2: Regional $PM_{2.5}$ statistics, number of observations and population in excess of WHO Air Quality Guideline (AQG) and Interim Targets (IT)[a]. Regions are defined in Figure 3-6.

Region	Population-weighted statistics [μg/m^3]				Pop.-weighted total obs.	Population (million people)				
	ave	std	geo. ave	geo. std.		Total	AQG (10 μg/m^3)	IT-3 (15 μg/m^3)	IT-2 (25 μg/m^3)	IT-1 (35 μg/m^3)
World	27	23	20	2.3	297	6,400	5,100 (81%)	4,000 (63%)	2,300 (37%)	1,600 (25%)
E. Asia	44	29	34	2.2	270	1,900	1,800 (93%)	1,600 (83%)	1,200 (65%)	940 (50%)
C. Asia	31	16	27	1.8	230	1,500	1,400 (94%)	1,300 (86%)	780 (54%)	560 (38%)
N. Africa	26	10	24	1.5	195	540	530 (98%)	450 (85%)	250 (47%)	8.7 (17%)
S. Africa	11	6	9	1.9	368	540	240 (47%)	110 (21%)	7.7 (1.5%)	0.1 (0.0%)
E. Europe	15	5	14	1.4	437	450	400 (88%)	210 (47%)	14 (3.0%)	1.8 (0.4%)
S. America	7	4	5	2.0	361	400	52 (13%)	18 (4.5%)	5.3 (1.3%)	0.0 (0.0%)
E. North America	13	5	12	1.5	476	350	250 (72%)	110 (32%)	17 (4.7%)	0.0 (0.0%)
S. Asia/ Australia	12	6	10	1.8	304	310	180 (58%)	72 (24%)	13 (4.4%)	1.3 (0.4%)
W. Europe	17	5	16	1.4	311	260	250 (94%)	170 (63%)	15 (5.9%)	3.7 (1.4%)
W. North America	11	5	10	1.6	366	120	56 (46%)	22 (18%)	0.3 (0.2%)	0.0 (0.0%)

[a] (WHO 2005)

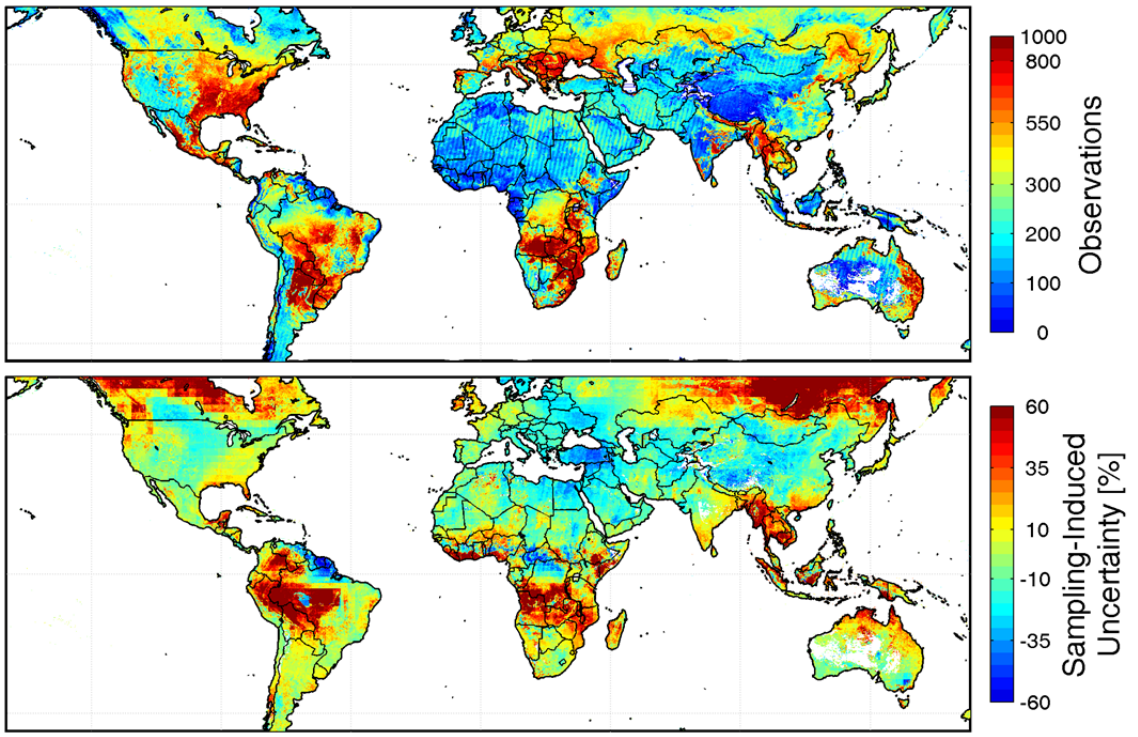

Figure 3-7: Satellite-derived $PM_{2.5}$ sampling and its estimated induced uncertainty. The top panel shows the annual average number of values used from satellite. The bottom panel shows the percent change in average coincidently-sampled simulated $PM_{2.5}$ concentrations relative to a full year average.

fortuitously collocated with lower population. The global population-weighted mean number of observations per 0.1° × 0.1° box is 297. The bottom panel of Figure 3-7 shows the percent difference between a GEOS-Chem simulation of $PM_{2.5}$ sampled coincidently with daily satellite-derived $PM_{2.5}$ versus a complete annual mean of the simulated values. Most regions exhibit a sampling-induced uncertainty (one standard deviation) within ±20% of simulated $PM_{2.5}$. Regions of low sampling do not necessarily demonstrate enhanced uncertainty and vice versa. Sampling error of satellite-derived $PM_{2.5}$ is larger in regions influenced by biomass burning, mineral dust, or persistent cloud due to a combination of large seasonal variability and non-representative sampling. We apply the ratio of complete to coincident mean simulated $PM_{2.5}$ to reduce uncertainty from sampling variability.

Validation of this is inhibited by the lack of in-situ measurements in the regions most significantly affected by intermittent sampling. Statistical comparison over the United States and Canada of non-coincident satellite-derived and *in-situ* $PM_{2.5}$ decreases the agreement relative to a coincident comparison (non-coincident: slope = 1.13, r = 0.70 versus coincident: slope = 1.07, r = 0.77), supporting the need for sampling error correction. Uncertainties derived from both the $PM_{2.5}$ estimate and sampling can vary substantially on the regional scale. Testing the combined uncertainty of ±25% from both sources reveals that approximately one standard deviation of the North American data falls within this overall error envelope. Globally, the population-weighted mean uncertainty in satellite-derived $PM_{2.5}$ is 6.7 $\mu g/m^3$.

3.7 Global Ambient $PM_{2.5}$: Application to Population Exposure

Pope et al. (2009) estimate that a long-term $PM_{2.5}$ exposure decrease of 10 $\mu g/m^3$ increases life expectancy by 0.61 ± 0.30 years for the United States. We estimate global long-term exposure to ambient $PM_{2.5}$ at a spatial resolution of 0.1° using our satellite-derived values for 2001-2006 and the Gridded Population of the World (Tobler et al., 1997) data for 2005 from the Socioeconomic Data and Applications Center (SEDAC; GPW v3; http://sedac.ciesin.columbia.edu/). Figure 3-8 shows the global and regional distributions of long-term ambient $PM_{2.5}$ exposure. Table 3-2 summarizes these results. All regions exhibit non-linear relationships between population and $PM_{2.5}$ concentrations. Eastern and central Asia have the highest levels of $PM_{2.5}$ concentrations with 38-50% of the regional population exceeding the WHO Air Quality Interim Target-1 (WHO, 2005) of 35 $\mu g/m^3$. According to the WHO Guidelines, concentrations at this level and higher are associated with approximately a 15% increased mortality risk, relative to the Air Quality Guideline of 10 $\mu g/m^3$. Globally 80% of the population lives in regions that exceed the Air Quality Guideline. These $PM_{2.5}$ estimates

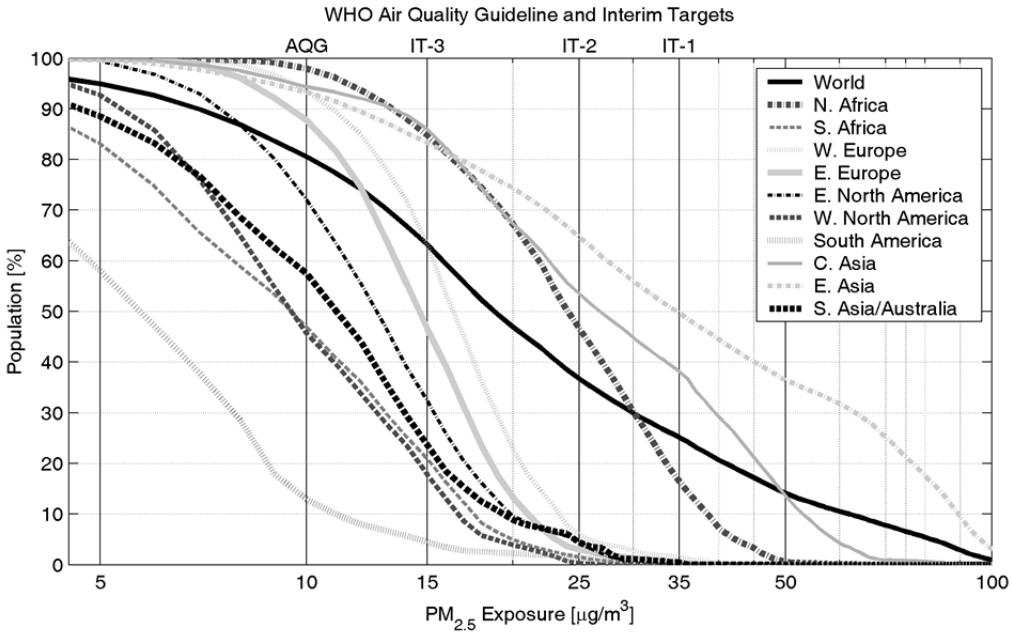

Figure 3-8: Cumulative distribution of regional, annual mean $PM_{2.5}$ estimated from satellite-derived $PM_{2.5}$ at a resolution of 0.1° × 0.1° for 2001-2006 per 0.1° grid box. The top axis identifies WHO Air Quality Guidelines (AQG) and Interim Targets (IT-#) associated with each concentration level. Regions are defined in Figure 3-6.

should be of considerable value for assessing the chronic health impacts of air pollution, especially in regions with sparse ground-based monitoring.

3.8 DISCUSSION

A major challenge for global epidemiological studies and assessments of air pollution health impacts is the lack of representative exposure estimates (Cohen et al., 2003). While extensive ground-based monitoring networks exist in some parts of the world, major portions of the globe are not covered. The situation is especially acute in developing countries with large populations and high pollution levels, but limited monitoring with traditional ground-based sampling techniques. While measurements from ground monitors are currently the "gold-standard" for epidemiological studies, these are not only sparse, but may represent only a small spatial extent in heterogeneous regions (Chen et al., 2006). Satellite observations offer area-integrated values with global coverage, providing valuable additional information for global health studies.

In this work, we produced a satellite-derived climatology of $PM_{2.5}$ concentrations. These estimates should facilitate studies of chronic exposure to particulate matter, similar to those already conducted in Europe and North America (e.g. Beelen et al., 2008; Dockery et al., 1993; Pope et al., 2002; Pope et al., 2009), in regions of the world currently without extensive ground-based monitoring networks. Although there are a growing number of studies of the impacts of short-term exposure to particulate matter have in previously under-represented regions of the world (e.g. Romieu et al., 2009; Wong et al., 2008), studies of long-term exposure also incorporate impacts related to chronic disease and therefore provide a more comprehensive estimate of overall health effects (Kunzli et al., 2001). Our estimates suggest the global population-weighted geometric mean $PM_{2.5}$ concentration is 20 $\mu g/m^3$ and that 80% of the global population resides in locations where ambient concentrations exceed the WHO Air Quality Guideline of 10 $\mu g/m^3$. Application of the satellite-derived $PM_{2.5}$ dataset also identifies global regions and areas of specific concern; half (50%) of the eastern Asian population lives in regions that exceed the WHO Air Quality Interim Target 3 of 35 $\mu g/m^3$, and are therefore at increased risk from air pollution-related health impacts. These results highlight the potential of satellite aerosol observations to contribute to chronic effects studies at regional and global scales.

Several notable developments over previous work were included in these estimates. Combining AOD from two satellite instruments (MODIS and MISR) improved the correlation of AOD versus ground-based $PM_{2.5}$ measurements. Extending the satellite data over six years (2001-2006) reduces sampling issues. The unprecedented global spatial resolution of 0.1° × 0.1° retains variation relevant to population distribution. A chemical transport model (GEOS-Chem) was applied to account for aerosol vertical distribution, a key factor affecting the relationship between satellite-retrieved, total column AOD and near-surface $PM_{2.5}$. We found significant

spatial agreement between mean coincident satellite-derived and ground-based $PM_{2.5}$ for North America (slope = 1.07, r = 0.77, n = 1057), as well as evidence of global agreement with non-coincident measurements from published and unpublished data (slope = 0.86, r = 0.83, n = 244). Notably, this level of agreement with ground-based $PM_{2.5}$ is significantly better than that obtained using a global chemical transport model (GEOS-Chem) without satellite data (Supplemental Material). Detailed spatial structure in the satellite-derived $PM_{2.5}$ concentrations reflect multiple influences.

We assessed the uncertainty in the satellite-derived product through comparison with independent observations and error propagation. We estimated our coincident satellite-derived $PM_{2.5}$ to be accurate at the one standard deviation level to within ±15% of the satellite-derived value using the relative AOD vertical profile measured by the CALIPSO satellite and the total column AOD from ground-based measurements (AERONET). We found evidence that the effect of non-uniform satellite sampling typically biases annual mean satellite-derived $PM_{2.5}$ by less than ±20% of the satellite-derived value. Larger effects are expected over regions influenced by substantial seasonal variation, by persistent cloud, or for individual, severe pollution events. The overall combined $PM_{2.5}$ uncertainty of ±25% indicates a mean global, population-weighted uncertainty in $PM_{2.5}$ concentration of 6.7 $\mu g/m^3$.

Additional developments could continue to reduce error in the satellite-derived $PM_{2.5}$ estimates presented here. Increased satellite coverage would reduce sampling concerns and may allow for satellite-derived $PM_{2.5}$ to be applied to studies of temporal or spatiotemporal variation. Further improvements to the AOD retrieval (e.g. Drury et al., 2008) would improve accuracy and reduce sampling bias by reducing data rejection. Simulating the AOD-$PM_{2.5}$ conversion factors at finer spatial resolution would better capture their variability, which is especially important in regions of sharp topographic or emissions gradients. Further

development of aerosol speciation capability (e.g. Liu et al., 2007b) and satellite-based estimates of additional species, such as NO_2 (Lamsal et al., 2008) would be valuable to more specifically estimate pollutant concentrations.

3.9 Acknowledgments

Funded by Health Canada (contract 4500171909 and 4500220294). A. van Donkelaar was supported by graduate fellowships from the Natural Sciences and Engineering Research of Canada (NSERC) and the Killam Trust.

3.10 *Supplemental Material:* Global Estimates of Ambient Fine Particulate Matter Concentrations from Satellite-based Aerosol Optical Depth: Development and Application

3.10.1 Collection of Global Ground-based $PM_{2.5}$ measurements

Satellite-derived and simulated global $PM_{2.5}$ concentrations require validation against surface measurements. We combine values from numerous sources for the purpose of comparison. We use European data from a combination of the European Monitoring and Evaluation Programme (EMEP; http://www.emep.int/) and the European Air quality dataBase (AIRBASE; http://air-climate.eionet.europa.eu/databases/airbase/). Australian data were collected from the Environment Protection and Heritage Council (http://www.ephc.gov.au/). New Zealand data were collected from the New Zealand Ministry for the Environment website (http://www.mfe.govt.nz/). Mexican data are from the ESCALA project (Gouveia et al., 2008; Romieu et al., 2009). Columbian data were provided by Victor Miranda and Isabelle Romieu and from the Instituto de Hidrologia Meteorologia y Estudios Ambientales (www.ideam.gov.co). Some Brazilian data for Sao Paulo are from the secretary of State for the Environment, Sao Paulo (http://www.cetesb.sp.gov.br/). Chilean data were provided by CENMA, the Chilean National

Environment Center (http://www.cenma.cl/). Additional sources are described in Table 3-3. We exclude sites from all sources that are suspected to be spatially or temporally biased.

We combine measurements onto the same 0.1° × 0.1° grid as the satellite dataset. We average colocated studies/sites, weighted by the product of their temporal range (years) and number of monitors (to a maximum of 5), such that long-term, multi-monitor studies have greater influence on final comparison values. Any surface $PM_{2.5}$ grid cell with an overall weight of less than 1 monitor-year is considered unrepresentative and is not used for evaluation of satellite-derived $PM_{2.5}$.

3.10.2 DESCRIPTION OF THE GEOS-CHEM MODEL

We use v8-01-04 of the GEOS-Chem chemical transport model (http://acmg.seas.harvard.edu/geos/index.html). The GEOS-Chem model is driven by assimilated meteorology from the Goddard Earth Observing System (GEOS-4) at the NASA Global Modeling Assimilation Office (GMAO). Our simulation is run at 2° × 2.5° with 42 vertical levels ranging between the surface and approximately 80 km. The thickness of the lower layer is approximately 100 meters. The model timestep for transport is 15 minutes.

The GEOS-Chem aerosol simulation includes the sulfate-nitrate-ammonium system (Park et al., 2006), primary (Park et al., 2003) and secondary (Liao et al., 2007) carbonaceous aerosols, mineral dust (Fairlie et al., 2007) and sea-salt (Alexander et al., 2005). Formation of sulfate and nitrate (Park et al., 2004), heterogeneous chemistry (Jacob, 2000) and photolysis rates (Martin et al., 2003b) are all coupled with oxidant simulation. Dry and wet deposition are described in Liu et al. (2001), and include both washout and rainout. The emission inventory has been recently updated to 2005, following van Donkelaar et al. (2008). We use the eight day Global

Table 3-3: Additional $PM_{2.5}$ surface measurements used for comparison and their combined values. Source indicates all sources used to determine location value.

City/Site	Country	In-situ $PM_{2.5}$ ($\mu g/m^3$)	Sat-derived $PM_{2.5}$ ($\mu g/m^3$)	Lat	Lon	Study Period	Num. of Station	Source
LIVERPOOL	AUSTRALIA	8.2	5	-33.9°	150.9°	2002-2005;2005;2005	1;1;1	(Hopke et al., 2008);Environment Protection and Heritage Council;Environment Protection and Heritage Council
LUCAS HEIGHTS	AUSTRALIA	5.7	3.1	-34°	151°	2002-2005;2005	1;1	(Hopke et al., 2008);Environment Protection and Heritage Council
DHAKA	BANGLADESH	33.7	23.9	23.8°	90.4°	2000-2003;2005	1;1;1	(Begum et al., 2006); (Begum et al., 2008)
DHAKA	BANGLADESH	28.7	26.2	23.7°	90.4°	2002-2005		(Hopke et al., 2008)
CUIABA	BRAZIL	10.5	10.7	-15.6°	-56.1°	Jul 1991 - Feb 1993	1	(Artaxo et al., 1994)
RIO DE JANEIRO	BRAZIL	17	7.1	-22.9°	-43.1°	Oct 1998 - Sep 1999	1	(Mariani and de Mello, 2007)
RIO DE JANEIRO	BRAZIL	10	5	-22.9°	-43.4°	Sept 2003 - Sept 2004	10	(Soluri et al., 2007)
SAO PAULO	BRAZIL	22.6	8.8	-23.5°	-46.5°	Jul 1997-March 1998	2	(Castanho and Artaxo, 2001)
SERRA DO NAVIO	BRAZIL	9.9	6.4	1°	-52°	Nov 1991 - Apr 1993	1	(Artaxo et al., 1994)
BANGKOK	CHINA	36.6	23.6	13. 8°	100.5°	2001-2004;Feb 2002 - Jan 2003	1;3	(Oanh et al., 2006);(Chuersuwan et al., 2008)
BEIJING	CHINA	114.1	97.3	39.9°	116.4°	Aug 2001-Sep 2002;2000;2001-2004	2;5;1	(Duan et al., 2006);(Zheng et al., 2005); (Oanh et al., 2006)
BEIJING	CHINA	121	99.6	39.8°	116.5°	Jul 1999- Sep 2000	2	(He et al., 2001)
BEIJING	CHINA	35.6	96.1	39.9°	116.3°	2002-2004	1	(Hopke et al., 2008)
BEIJING	CHINA	127.5	97	39.9°	116.5°	unknown	8	(Zhang et al., 2010)
BEIJING	CHINA	87.7	90.4	39.9°	116.3°	2005-2007	1	(Zhao et al., 2009)
BEIJING	CHINA	54.2	29.6	40.6°	117.1°	2005-2007	1	(Zhao et al., 2009)
BEIJING-SUBURBAN	CHINA	42.1	87.2	39.7°	116°	2003-2004	1	(Hopke et al., 2008)

City/Site	Country	In-situ $PM_{2.5}$ ($\mu g/m^3$)	Sat-derived $PM_{2.5}$ ($\mu g/m^3$)	Lat	Lon	Study Period	Num. of Station	Source
GUANGZHOU	CHINA	97.3	79.3	23.1°	113.1°	unknown	2	(Zhang et al., 2010)
HONG KONG	CHINA	42.8	45.4	22.3°	114.2°	Nov 2000-Feb 2001; Jun-Aug 2001	2	(Ho et al., 2006)
HONG KONG	CHINA	47.4	44.5	25.2°	115.1°	unknown	2	(Zhang et al., 2010)
SHANGHAI	CHINA	92.9	95.8	31.3°	121.3°	2005-2006	2	(Feng et al., 2009)
SHANGHAI	CHINA	59.6	65.9	31.2°	121.5°	1999	2	(Ye et al., 2003)
SHANGHAI	CHINA	78.6	98.1	31.1°	121.3°	unknown	3	(Zhang et al., 2010)
CAIRO	EGYPT	67.4	51.8	30°	31.4°	Fall/Winter 1999 Summer 2002	3	(Abu-Allaban et al., 2007)
CAIRO	EGYPT	79.3	41.6	30°	31.3°	2001-2002	14	(Zakey et al., 2008)
CHENNAI	INDIA	42.2	18	13.1°	80.3°	2001-2004;2002-2003	1;1	(Oanh et al., 2006);(Kumar and Joseph, 2006)
DELHI	INDIA	97	56.8	28.4°	77.1°	Mar 2001 - Jan 2002;Jul-Dec 2003	1;1;113	(The World Bank 2004); (Chowdhury, 2004);(Kumar et al. 2007)
KOLKATA	INDIA	107.8	26.2	18.7°	72.8°	Mar 2001 - Jan 2002	1;1	(The World Bank 2004); (Chowdhury, 2004)
MUMBAI	INDIA	43	26.2	19°	72.8°	Apr 2003- Mar 2004	1	(Kumar et al. 2007)
MUMBAI	INDIA	40.5	23	19.1°	72.9°	2002-2005	1	(Hopke et al., 2008)
MUMBAI	INDIA	52.5	38.8	22.6°	88.3°	Mar 2001 - Jan 2002	1;1	(The World Bank 2004); (Chowdhury, 2004)
NAVI MUMBAI (VASHI)	INDIA	44	26.2	18.8°	73°	Annual	1	(Kothai et al., 2008)
BANDUNG	INDONESIA	29.2	16.8	-6.5°	107.4°	2001-2004;2002-2005	1;1	(Oanh et al., 2006); (Hopke et al., 2008)
LEMBANG	INDONESIA	12.9	19.6	-6.2°	107.2°	2002-2005;	1	(Hopke et al., 2008)
TOKYO	JAPAN	23	23.2	35.7°	139.7°	2001-2004	1	(Minoura et al., 2006)
DAEJEON	KOREA	10.8	20.3	36.4°	127.4°	2002-2005	1	(Hopke et al., 2008)
SEOUL	KOREA	44.3	30	37.4°	126.8°	2002-2004	2	(Kim et al., 2006)
SEOUL	KOREA	37.2	39.5	37.6°	126°	2005-2006	1	(Park et al., 2008)

City/Site	Country	In-situ $PM_{2.5}$ ($\mu g/m^3$)	Sat-derived $PM_{2.5}$ ($\mu g/m^3$)	Lat	Lon	Study Period	Num. of Station	Source
KUWAIT	KUWAIT	38	37.5	29.3°	48°	Feb 2004 - Jul 2005	3	(Brown et al., 2008)
BEIRUT	LEBANON	35.5	24	33.9°	35.5°	Feb-May 2003;2004;Feb 2004-Jan 2005	1;1;1	(Sheehan and Bowman, 2001);(Kouyoumdjian and Saliba, 2006);(Saliba et al., 2007)
KUALA LUMPUR	MALAYSIA	29.3	17.1	3.2°	101.7°	2005	1	(Hopke et al., 2008)
KATHMANDU VALLEY	NEPAL	30.7	22.8	27.7°	85.5°	Dec 1998-Oct 2000	2	(Carrico et al., 2003)
CABAUW	NETHERLANDS	18.2	19.1	52°	4.9°	Aug 2006 - May 2007	1	(Schaap et al., 2008)
ISLAMABAD	PAKISTAN	14.4	30.8	33.7°	73.3°	2002-2004	1	(Hopke et al., 2008)
ATENEO DE MANILLA	PHILIPPINES	35.3	15.9	14.6°	121.1°	2002-2005;2001-2004;Apr - Dec 2001	1;1;1	(Hopke et al., 2008); (Oanh et al., 2006); (Cohen et al., 2002)
SINGAPORE	SINGAPORE	27.2	25.7	1.3°	104°	Jan-Dec 2000	1	(Balasubramanian et al., 2003)
BOTSALANAO	SOUTH AFRICA	10.5	4.9	-25.5°	25.8°	July 2006-July2007	1	(Laakso et al., 2008)
AEA	SRI LANKA	28.4	12.1	6.9°	79.9°	2002-2005	1	(Hopke et al., 2008)
KAOHSIUNG	TAIWAN	68	32.6	22.6°	120.3°	Nov 1998-Apr 1999	6	(Lin, 2002)
BANGKOK	THAILAND	23.8	24.1	13.8°	100.5°	2002-2005	1	(Hopke et al., 2008)
PATHUM THANI	THAILAND	20	19.4	14°	100.5°	2003-2005	1	(Hopke et al., 2008)
ISTANBUL	TURKEY	20.8	17.6	41°	28.6°	Jul 2002 - Jul 2003	1	(Karaca et al., 2005; Karaca et al., 2008)
HANOI	VIETNAM	53.3	49.5	21°	105.8°	Jan - Dec 2001;2001-2004;2002-2005	1;1;1	(Cohen et al., 2002); (Oanh et al., 2006); (Hopke et al., 2008)

Fire Emission Database version 2 (GFEDv2) biomass burning emissions (van der Werf et al., 2006), as implemented by Nassar et al. (2009).

The GEOS-Chem aerosol simulation has been extensively evaluated with ground-based measurements (e.g. Fairlie et al., 2007; Park et al., 2006; Pye et al., 2009) and aircraft measurements (e.g. Dunlea et al., 2009; Heald et al., 2005; van Donkelaar et al., 2008).

3.10.3 Description of Satellite Retrievals

The MODIS instrument provides near-daily global AOD coverage in the absence of clouds. The MODIS AOD retrieval algorithm over land (Levy et al., 2007) applies three spectral bands at 0.47 μm, 0.66 μm and 2.1 μm plus those used for cloud masking, and requires that surface-reflected radiation makes little contribution to total radiation leaving the top of the atmosphere. Dark surfaces are first detected using the infrared (2.1 μm) spectral band, where atmospheric absorption and scattering from aerosols is generally weak. Surface reflection at visible wavelengths (0.47 μm and 0.66 μm) is then estimated through specified relationships with the 2.1 μm reflectivity. Pre-computed seasonally and spatially varying lookup tables (LUT) that combine likely aerosol scenarios with surface reflectivities are then matched with top-of-atmosphere observations to determine AOD values representing 10 km × 10 km retrieval regions. Quality assured collection (version) 5 MODIS AOD over land has been validated such that at least two-thirds of retrievals are within ±(0.05 + 15%) using Aerosol Robotic Network (AERONET, Holben et al., 1998) measurements of AOD (Remer et al., 2008). The ratio of two spectral bands is used estimate the contribution of non-dust (fine) aerosol to total AOD, but this product is highly uncertain (Remer et al., 2005), especially over land, where it is considered an algorithm diagnostic rather than a retrieval quantity (Anderson et al., 2005; Levy et al., 2009).

The MODIS BRDF/Albedo product (MOD43 V5, Lucht et al., 2000) estimates 16-day average land surface albedo through an algorithm that is separate from the surface reflectivity estimate used by the MODIS AOD retrieval. Albedo, the hemispheric integration of directional surface reflectance, is separated into black-sky and white-sky albedo, where these refer to the albedo under purely direct and diffuse conditions, respectively. The true albedo varies between these two extremes.

The MISR instrument observes radiation leaving the top of the atmosphere in four spectral bands (0.446, 0.558, 0.672 and 0.866 μm), each at nine viewing angles (±70.5°, ±60.0°, ±45.6°, ±25.1° and nadir). MISR takes 9 days for complete global coverage at the equator, and two days near the poles, in the absence of clouds. The MISR AOD retrieval algorithm (Diner et al., 2005; Martonchik et al., 2002; Martonchik et al., 2009) uses same-scene, multi-angle, multi-spectral observations to infer AOD and aerosol microphysical property information over 18 km × 18 km retrieval regions, assuming only approximate spectral invariance of the surface angular reflectance, via pre-calculated LUTs. MISR AOD has been validated such that two-thirds of retrievals fall within the maximum of ±(0.05 or 20%) of ground truth observations (Kahn et al., 2005). The MISR aerosol product also provides estimates of AOD contribution according to aerosol size, dividing AOD into the fraction of particles of radius < 0.35 μm, between 0.35-0.7 μm and > 0.7 μm. The aerosol-size retrieval is most reliable when AOD is greater than 0.2 (Kahn et al., 2009a).

We explored using satellite retrievals of aerosol fine mode fraction (FMF) in lieu of the GEOS-Chem simulation of this quantity in the calculation of η, but found that simulated FMF was more accurate for our application due to retrieval uncertainties, temporal coverage and consistency of fine mode definition. We determine FMF from the GEOS-Chem simulation as the

ratio of fine AOD (sulfate, organic carbon, black carbon, and fine dust and fine sea salt) to total AOD (fine AOD + coarse dust and coarse sea salt).

3.10.4 Combining MODIS and MISR observations

Here we describe our approach to combine AOD retrievals from both MODIS and MISR. We translate daily AOD measurements between Jan. 1 2001 and Dec. 31 2006 from MODIS level 2, version 5, best quality and MISR level 2 (F09_0017-F11_0021, best estimate) onto a global 0.1° × 0.1° grid. MODIS AOD retrievals exhibit a high bias over deserts and coastal sites due to surface brightness and subpixel water contamination (Abdou et al., 2005) partially explaining the poor agreement between MODIS AOD and surface $PM_{2.5}$ observed the western United States (Engel-Cox et al., 2004b; Hu, 2009; Liu et al., 2007b). Systematic regional differences between MODIS

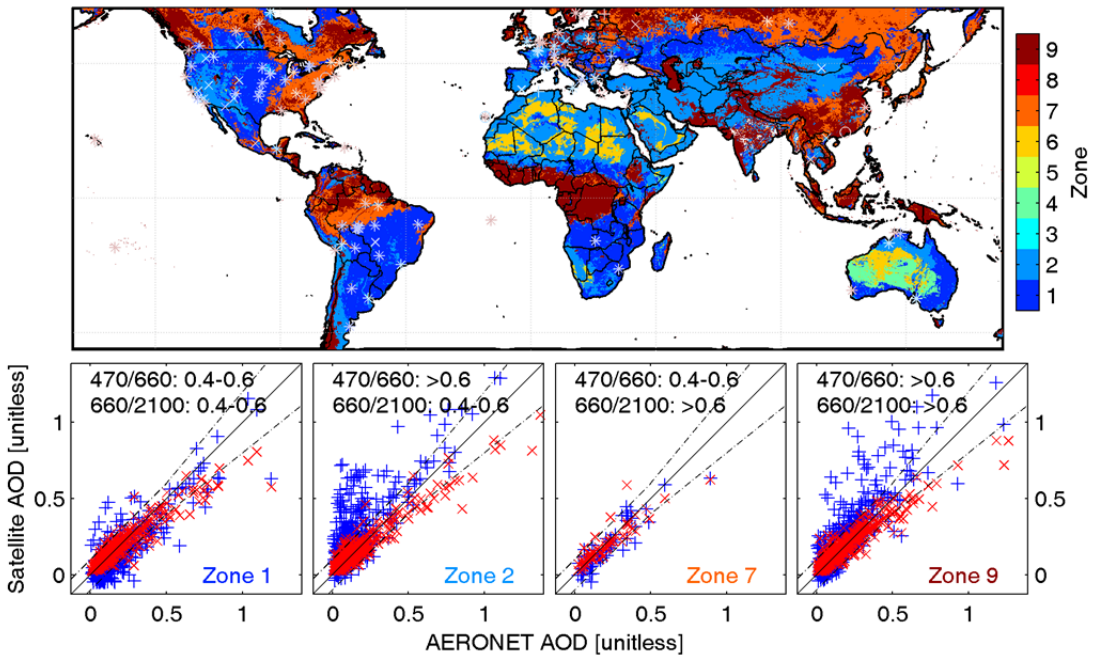

Figure 3-9: Sample of albedo ratio zones, or surface types, used for AOD filtration. The top panel shows zone definitions for July. Marker positions and colors indicate AERONET locations and zones. Acceptable agreement (within 0.1 or 20%) of AERONET and MODIS (+), MISR (×) or both (*) AOD retrievals is shown at each site. An 'o' indicates neither satellite retrieval meets this criteria. The bottom row compares AERONET and unfiltered satellite AOD for all months within the predominant zones. MODIS AOD are denoted by blue '+' and MISR AOD by red '×'. Agreement of 0.1 or 20% lie within the black dotted lines.

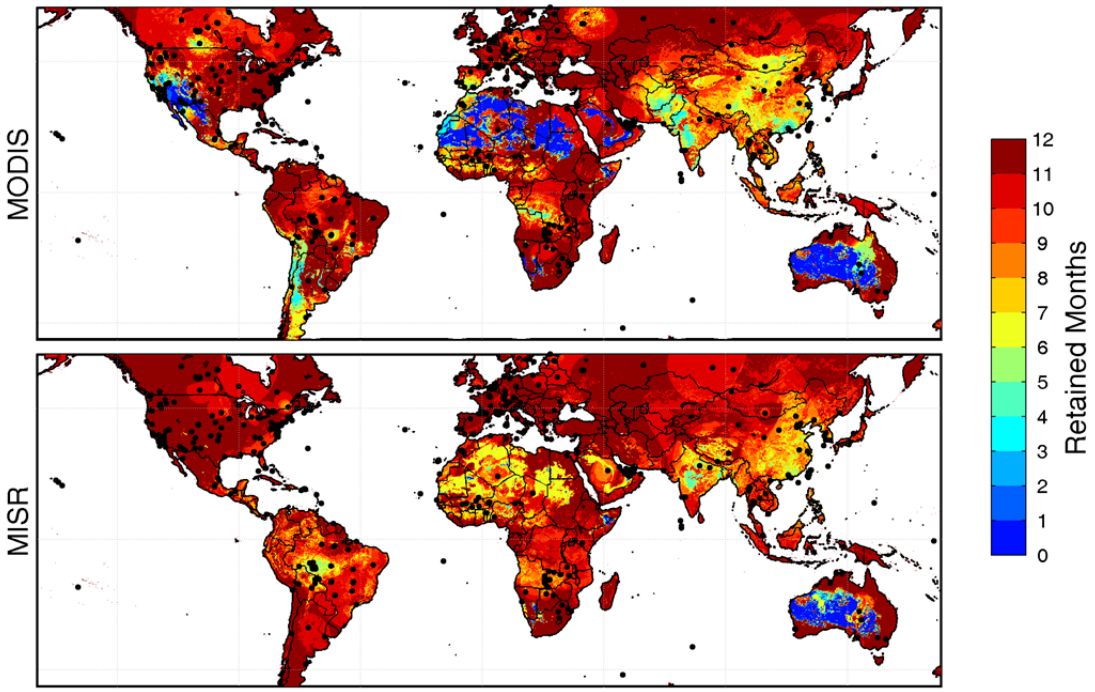

Figure 3-10: Number of months of MODIS and MISR AOD included in satellite-derived $PM_{2.5}$ estimate. Points denote AERONET stations used for bias identification.

and MISR AOD are also found over north-central Africa, northern India and Bangladesh, and the Patagonia Desert region of South America (Kahn et al., 2009a).

We use the MODIS BRDF/Albedo product to distinguish surface types and identify regional error in AOD retrieval. Two ratios of six-year monthly mean black-sky albedo (0.47 µm / 0.66 µm and 0.66 µm / 2.1 µm) are used to divide the Earth's surface into nine albedo-based domains, as defined by the combinations of each ratio being < 0.4, 0.4 - 0.6, and > 0.6. Four surface types dominate, as shown for July in the top panel of Figure 3-9. MODIS and MISR AOD are then compared against ground-based retrievals of AOD from the AERONET to calculate an average monthly bias for each instrument within each domain. Local AERONET comparisons are combined according to surface type. We reject all satellite AOD retrievals with a local estimated monthly bias in excess of the maximum of ±(0.1 or 20%). Data from regions that cannot be

confirmed to be within these bounds are rejected. Nearby AERONET sites are weighted more heavily in the comparison to allow more representative measurements to dominate the filtration process. The bottom row of Figure 3-9 compares unfiltered satellite and AERONET AOD by zone for all months. MODIS AOD over zone 2 (470/660: >0.6; 660/2100: 0.4-0.6) and zone 9 (470/660: >0.6; 660/2100: >0.6) show more scatter than other zones. Figure 3-10 shows the total number of months included from each instrument after this filtration process. MODIS AOD are frequently rejected over bright surfaces, such as deserts, and are more heavily filtered than MISR. Regions with few months are more susceptible to sampling bias as discussed in the main text. Fortunately most of the regions with poor seasonal sampling tend to have low population.

To reduce the influence of large particles, we also exclude individual MODIS and MISR AOD with less than 20% fine mode fraction based upon their respective retrievals of this quantity. The albedo-filtered, fine-mode-filtered AOD from MODIS and MISR are averaged to produce daily of AOD at 0.1° × 0.1°.

3.10.5 Comparison of GEOS-Chem vertical structure with CALIPSO measurements

The Cloud-Aerosol Lidar and Infrared Pathfinder Satellite Observations (CALIPSO) satellite has been providing aerosol backscatter and extinction profiles from orbit since June 2006 (Vaughan et al., 2004). Extinction profiles obtained from CALIPSO are presently unvalidated, beta-quality products. This dataset, however, is the most complete measurement-based representation of global aerosol profiles currently available and a valuable source of information for the validation of simulated vertical profiles and their impact on satellite-derived $PM_{2.5}$. We therefore compare simulated and measured AOD relative vertical profiles from GEOS-Chem and CALIPSO.

Figure 3-11 shows average relative vertical profiles from CALIPSO for various land regions, for June-December 2006, the period of overlap with GEOS-4 meteorological fields. The fraction of AOD within the simulated lower mixed layer ranges from about 30% over Europe to 50% over North Africa. This represents a lower bound for fully sampled mean conditions, as profiles taken during high pollution events are unlikely to reach the ground due to attenuation of the CALIPSO beam. Figure 3-11 also shows the mean of coincidently sampled profiles from the GEOS-Chem

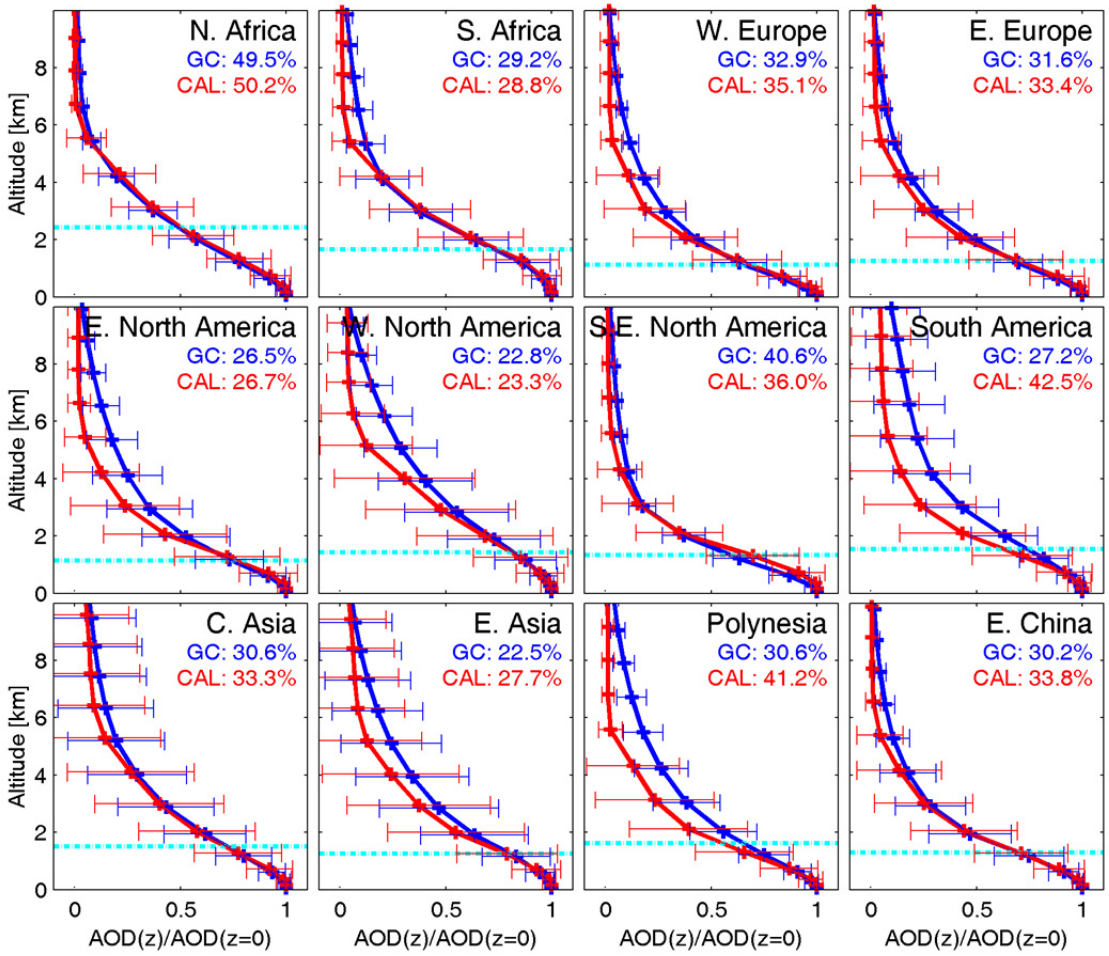

Figure 3-11: Vertically-resolved aerosol optical depth (AOD) from the top of the atmosphere to the given altitude (z). Red lines show values retrieved from the CALIPSO (CAL) satellite instrument over June-December 2006. Blue lines show values simulated with GEOS-Chem (GC) and sampled coincidently with CALIPSO. Cyan lines denote simulated mixed layer height. Percentages give fraction of AOD within the mixed layer. Regions are defined in Figure 3-6 of the main article. Error bars give one standard deviation.

Table 3-4: Comparison of simulated and satellite-derived $PM_{2.5}$ with ground-based measurements.[a]

Region	Data Source	Sampling Resolution	slope	bias [μg/m^3]	r	n
North America[b,e]	Satellite	0.1° × 0.1°	1.07	-1.75	0.77	1057
		2° × 2.5°	0.94	0.38	0.82	190
	Simulation	2° × 2.5°	1.26	-3.14	0.87	190
E. North America[b,e]	Satellite	0.1° × 0.1°	1.20	-3.40	0.74	798
		2° × 2.5°	1.04	-1.54	0.83	117
	Simulation	2° × 2.5°	1.34	-3.80	0.92	117
W. North America[b,e]	Satellite	0.1° × 0.1°	0.69	1.39	0.67	259
		2° × 2.5°	0.83	0.76	0.53	73
	Simulation	2° × 2.5°	0.49	2.40	0.40	73
Global[c,e]	Satellite	0.1° × 0.1°	0.86	1.15	0.83	244
		2° × 2.5°	0.59	4.37	0.75	244
	Simulation	2° × 2.5°	0.54	8.89	0.63	244
Global (non-EU)[d,e]	Satellite	0.1° × 0.1°	0.91	-2.64	0.83	84
		2° × 2.5°	0.64	0.78	0.76	84
	Simulation	2° × 2.5°	0.60	2.45	0.72	84

[a] All $PM_{2.5}$ data are averaged within the sampling resolution. A minimum of 50 measurements for each point.
[b] North American ground measurements are coincidently sampled with both satellite and simulated values.
[c] Global excludes North American sites.
[d] Global (non-EU) additionally excludes European sites.
[e] NA and Global comparisons are conducted at 35% and 50% relative humidity, respectively, for appropriate comparison with ground measurements.

simulation. Simulated and retrieved profiles are consistent. The largest regional differences occur at approximately 5 km. The fraction of AOD in the mixed layer typically differ by less than 5%, with the exception of South America and Polynesia, where this difference is within 15%.

There are concerns about an error in the CALIPSO data below 800 m (Ray Hoff, personal communication). Differences in the mixed layer fraction of simulated and observed AOD remain within the above percentages when excluding these values.

3.10.6 COMPARISON OF SIMULATED AND SATELLITE-DERIVED $PM_{2.5}$

Of interest is whether the satellite-derived $PM_{2.5}$ improves over the GEOS-Chem simulation of $PM_{2.5}$. Table 3-4 compares satellite-derived and simulated $PM_{2.5}$ with ground-based $PM_{2.5}$ over North America and the rest of the world. $PM_{2.5}$ data are sampled coincidently over North America. Annual average measurements are used for the rest of the world. The slope between ground-based measurements and satellite-derived $PM_{2.5}$ at 0.1° × 0.1° is consistently nearer to unity as compared to the simulation. The bias is also smaller between the satellite-data and ground-based measurements. Much of the global improvement in slope is driven by the finer resolution of satellite-derived $PM_{2.5}$ (0.86 for 0.1° × 0.1° versus 0.59 for 2° × 2.5°), but correlation is higher with the satellite product than for the simulation regardless (satellite-derived: 0.75-0.83 versus simulated: 0.63). By contrast, coarse resolution comparisons over western North America have an improved slope relative to simulation (0.83 versus 0.49), but a poorer

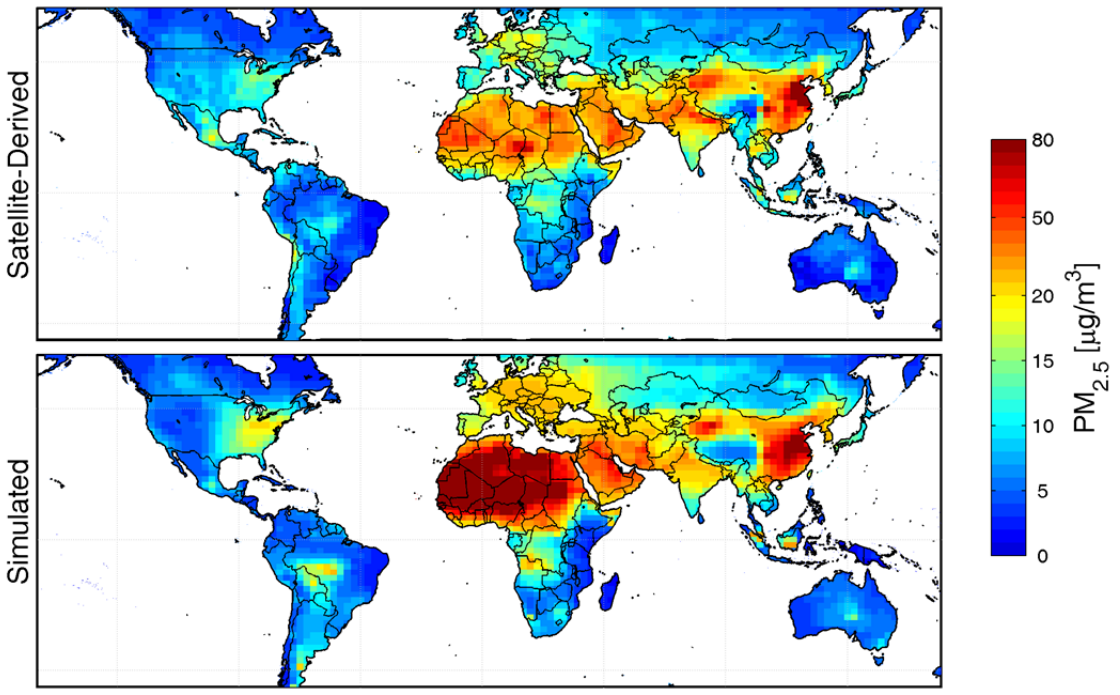

Figure 3-12: Comparison of coincidently sampled satellite-estimated and simulated $PM_{2.5}$. Satellite-estimated $PM_{2.5}$ has been degraded to a resolution of 2° × 2.5°.

correlation than at 0.1° × 0.1° (0.67 versus 0.53).

Figure 3-12 shows global coincidently sampled satellite-derived and simulated $PM_{2.5}$ at the simulation resolution of 2° × 2.5°. Both $PM_{2.5}$ estimates agree with each other (r = 0.77), with major enhancements associated with dust, biomass burning and industrial activities. The magnitude of the concentrations, however, have pronounced differences. Simulated values of $PM_{2.5}$ over the Sahara exceed satellite-derived estimates by 20-150 μg/m^3. Satellite-derived $PM_{2.5}$ deviate from simulated concentrations over east Asia and northern India by as much as 30 μg/m^3. Satellite-derived $PM_{2.5}$ over Mexico has an enhancement of 5-10 μg/m^3 relative to simulation The large population present in the latter three regions make differences of particular epidemiological significance and may indicate regional bias in current emission inventories.

Chapter 4. SATELLITE-BASED ESTIMATES OF GROUND-LEVEL FINE PARTICULATE MATTER DURING EXTREME EVENTS: A CASE STUDY OF THE MOSCOW FIRES IN 2010

Authors: Aaron van Donkelaar[1,*], Randall V. Martin[1,2], Rob C. Levy[3], Arlindo M. da Silva[4], Michal Krzyzanowski[5], Natalia E. Chubarova[6], Eugenia Semutnikova[7], and Aaron J. Cohen[8]

[1]Dept. of Physics and Atmospheric Science, Dalhousie University, Halifax, Nova Scotia, Canada (aaron.van.donkelaar@dal.ca, randall.martin@dal.ca)

[2]Harvard-Smithsonian Center for Astrophsyics, Cambridge, Massachusetts, USA

[3]NASA Goddard Space Flight Center, Greenbelt, Maryland, USA (robert.c.levy@nasa.gov)

[4]Global Modeling and Assimilation Office, NASA Goddard Space Flight Center, Greenbelt, Maryland, USA (arlindo.m.dasilva@nasa.gov)

[5]European Centre for Environment and Health, WHO Regional Office for Europe, Bonn, Germany (mkr@ecehbonn.euro.who.int)

[6]Geography Dept., Moscow State University, Moscow, Russia (chubarova@imp.kiae.ru)

[7]State Environmental Organization, Mosecomonitoring, Moscow, Russia (info@mosecom.ru)

[8]Health Effects Institute, Boston, MA, USA (acohen@healtheffects.org)

[*]corresponding author: Aaron van Donkelaar, Dept. of Physics and Atmospheric Science, Dalhousie University, 6300 Coburg Road, Halifax, NS, B3H 3J5, (902) 494-1820, aaron.van.Donkelaar@dal.ca

Article submitted to Atmospheric Environment on April 20, 2011. Relaxed MODIS retrieval run by R. Levy and health impact assessment performed by A. Cohen and M. Krzyzanowski. All text, figures, tables and remaining presented results were contributed by the first author.

4.1 ABSTRACT

We estimate fine particulate matter ($PM_{2.5}$) concentrations daily using satellite observations of a major biomass burning event around Moscow during summer 2010. We increase the coverage of aerosol optical depth (AOD) retrieved from the MODIS satellite instrument by relaxing the operational cloud screening criteria which can mistake extreme aerosol events for cloud. This relaxed product has excellent agreement with coincident operational retrievals (r^2=0.994; slope = 1.010) and increases coverage during the fires by 21.3%. We relate MODIS AOD to $PM_{2.5}$ using a chemical transport model (GEOS-Chem) and find good agreement with $PM_{2.5}$ values estimated from in-situ PM_{10} (r^2=0.85, slope=1.06). We find that the relationship between AOD and $PM_{2.5}$ is insensitive to uncertainties in biomass burning emissions. Both satellite-derived and in-situ values have peak daily mean concentrations of approximately 600 $\mu g/m^3$ on August 7, 2010 in the Moscow region. We estimate that exposure to air pollution from the Moscow wildfires may have caused hundreds of excess deaths.

4.2 INTRODUCTION

Extensive fires occurred in the Moscow region starting in late July 2010. No estimates of the health impacts of the Moscow fires have been published to date, but it is reasonable to assume that these extreme, short-lived excursions in ambient air pollution resulted in serious adverse health effects. Large short-term increases in air pollution, or air pollution episodes, in the mid-twentieth century were associated with rapid and pronounced increases in mortality from respiratory and cardiovascular disease (Anderson, 1999). More recent evidence links massive biomass burning from agricultural burning and forest fires to adverse health effects that range from minor irritation of the eyes and respiratory system to increased rates of hospital admissions for respiratory disease and mortality (Naeher et al., 2007). However, ground-level

monitors are often sparse or unavailable in regions affected by fires. Additional observations are needed to assess pollutant concentrations and possible health impacts.

Satellite remote sensing of atmospheric aerosol provides a rich data source about particulate matter concentrations. Algorithmic developments continue to improve the accuracy with which ground-level fine aerosol mass ($PM_{2.5}$) can be estimated from satellite remote sensing. These estimates use aerosol optical depth (AOD), a measure of the total extinction by aerosol of light passing through the atmospheric column, to estimate $PM_{2.5}$ through physical, statistical or hybrid relationships developed from ground-level $PM_{2.5}$ measurements (e.g. Gupta et al., 2006b; Koelemeijer et al., 2006; Liu et al., 2007b; Liu et al., 2005b; Wang and Christopher, 2003). Local observations of $PM_{2.5}$, vertical structure and relative humidity have all be used to improve the accuracy of remotely sensed $PM_{2.5}$ (e.g. Di Nicolantonio et al., 2009; Engel-Cox et al., 2006; Schaap et al., 2008).

Chemical transport models, which calculate the four-dimensional distribution of atmospheric aerosol mass, can accurately relate AOD to ground-level $PM_{2.5}$, allowing estimates in locations without nearby ground-based observations (Drury et al., 2010; Liu et al., 2004; van Donkelaar et al., 2010; van Donkelaar et al., 2006; Wang et al., 2010). Here we apply this approach to the Moscow wildfires to test its performance during major short-term pollution events.

The next section describes our approach to estimate $PM_{2.5}$ by interpreting AOD retrievals from the Moderate Resolution Imaging Spectroradiometer (MODIS) using the GEOS-Chem chemical transport model. Results are given and compared with in-situ $PM_{2.5}$ estimates. Developments to the operational MODIS aerosol retrieval algorithm for extreme events and the sensitivity of the AOD to $PM_{2.5}$ relationship to local emissions are also discussed. The

subsequent section extends previous studies of extreme $PM_{2.5}$ events to estimate the excess mortality in Moscow during this period.

4.3 Estimating Ground-Level Aerosol Pollution from Satellite Observations

The MODIS instrument obtains near daily global coverage at 32 spectral bands at a resolution of 250-1000 m, depending on the channel. Two MODIS instruments are currently in operation. The first, onboard the NASA Terra satellite, was launched in 1999 with a 10:30 a.m. local equatorial overpass time. The second, onboard the NASA Aqua satellite, was launched in 2002 with a 1:30 p.m. local equatorial overpass time. The wide spectral range and swath width of these versatile instruments has allowed for an AOD retrieval (Levy et al., 2007) at 10 km × 10 km with good accuracy (0.05+0.15×AOD; Remer et al., 2008) that has proven valuable for both daily and long-term observations of aerosol.

Detection and removal of clouds is an important part of the MODIS AOD retrieval, since AOD is not retrieved in the presence of cloud. The operational MODIS AOD product (MOD04 and MYD04) detects cloud-contaminated pixels at 500m resolution using spatial variability and brightness at 0.47 μm and 1.38 μm (Remer et al., 2006). The center pixel of each 3 x 3 group of pixels is designated as cloudy if the standard deviation of the group's reflectance is >0.0025 at 0.47 μm or >0.025 at 1.38 μm. These criteria use the small-scale variability that is typical of clouds but abnormal in aerosol to identify cloudy pixels. The 1.38 μm channel is sensitive to cirrus clouds. Any pixel with a 0.47 μm reflectance >0.4 is also considered cloudy, since clouds are highly reflective at this wavelength. Pixels on the granule perimeter are masked according to their neighbour. In addition to cloud masking, any retrieved AOD greater than 5.0 is removed. These criteria are typically effective, yet during extreme events aerosol plumes may be mistaken for cloud or AOD may exceed 5.0.

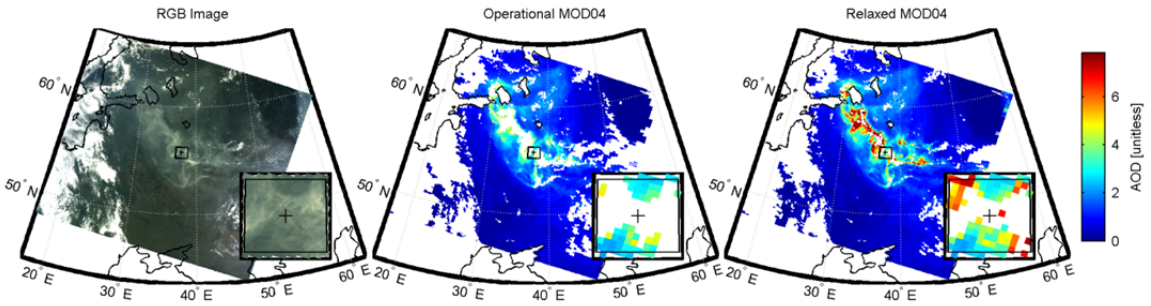

Figure 4-1: The MODIS Terra granule from August 8, 2010 08:50 UTC. From left to right, the RGB image, the operational AOD retrieval and the relaxed criteria AOD retrieval are shown. The black crosshair and box identify Moscow and the Moscow Region, respectively, and are enlarged within the lower right subplot of each panel.

The left panel of Figure 4-1 shows a MODIS Terra RGB image from August 8, 2010 at 08:50 UTC. Dense forest fire smoke is visible as gray plumes over the Moscow region, in contrast with white clouds to the east and west. The operational MODIS AOD retrieval, shown in the middle panel, correctly removes pixels affected by cloud, but also removes much of the dense aerosol plume over Moscow.

We explore the effects of relaxing the cloud screening criteria to increase coverage of the AOD retrieval. The maximum allowed spatial variability at 0.47 µm is doubled to 0.005. Additionally, if this 0.47 µm threshold is exceeded, but the 2.1 µm variability is < 0.025, a pixel is classified as aerosol. The latter criterion reflects the transparency of fine aerosol at long wavelengths relative to cloud or dust (Kaufman et al., 1997). Finally, we increase the maximum allowed AOD to 10.0 to allow for dense smoke.

The result of this relaxed cloud filter is shown in the right panel of Figure 4-1. A pronounced aerosol plume becomes evident, but the cloud screening on the edge of the region remains intact. The coverage is increased over Moscow although some peaks of the plume remain unretrieved. The relaxed filter has significant agreement (r^2=0.995) with the operational product and negligible bias (slope = 1.017; offset = 0.009), yet retains an additional 2275 10 km × 10 km pixels for a range of AOD levels. We reprocess MODIS Aqua and Terra granules using

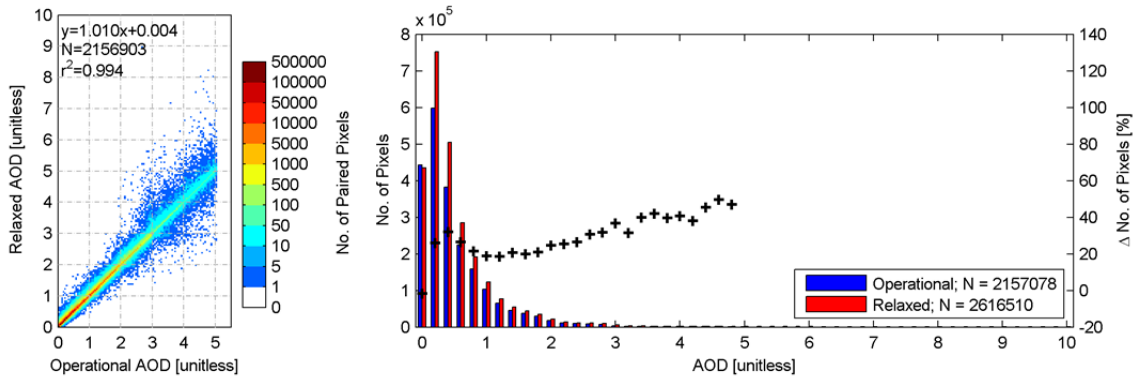

Figure 4-2: Comparison of MODIS AOD from the operational and relaxed criteria. Both panels compare all pixels from the 238 reprocessed granules. The right panel plots both the total number of retrievals (bars) and the percent change in number of AOD retrievals (pluses).

our relaxed criteria between 30°E - 60°E and 50°N - 65°N between July 26, 2010 to August 20, 2010.

Figure 4-2 compares MODIS AOD retrieved using the operational and relaxed criteria. On average the relaxed criteria retained an additional 21.3% of pixels from the 238 granules processed, generally with an increasing amount of additional coverage at higher AOD. The agreement between the relaxed and operational retrievals is high (r^2 = 0.994; slope = 1.010; offset = 0.004), and both show similar distributions.

The accuracy of the MODIS AOD retrieval algorithm can be affected by the local applicability of its assumptions about aerosol scattering and surface reflectivity (e.g. Abdou et al., 2005; Drury et al., 2008; Kahn et al., 2009b). Figure 4-4 compares temporally and spatially coincident summertime AOD from the Moscow Aerosol Robotic Network (AERONET; Holben et al., 1998) sun photometer with operational MODIS AOD retrievals between 2004-2009, prior to this biomass burning event. AERONET provides a more direct measurement of AOD, relying on fewer assumptions than satellite retrievals and accurate to within 0.01 (Holben et al., 1998). The operational MODIS AOD data from both Aqua and Terra are well correlated with AERONET

observations at this site(r = 0.71-0.82), but have a small bias (slope =0.89-1.08). We correct our Aqua and Terra relaxed MODIS AOD retrievals by their respective slopes to reduce the bias.

We use the GEOS-Chem chemical transport model (Bey et al., 2001; v8-03-01; http://geos-chem.org) to relate AOD to ground-level $PM_{2.5}$ concentrations. The GEOS-Chem model solves for the temporal and spatial evolution of aerosol and trace gases using meteorological data sets, emission inventories, and equations that represent the physics and chemistry of atmospheric composition. The GEOS-Chem aerosol simulation includes the sulphate-ammonium-nitrate-water system (Park et al., 2004), primary carbonaceous aerosols (Park et al., 2003), secondary organic aerosols (Henze et al., 2008), sea-salt (Alexander et al., 2005), and mineral dust (Fairlie et al., 2007). Gas-aerosol equilibrium is computed using ISORROPIA II (Pye et al., 2009). The aerosol and oxidant simulations are coupled through formation of sulphate and nitrate (Park et al., 2004), heterogeneous chemistry (Evans and Jacob, 2005; Jacob, 2000; Thornton et al., 2008), and aerosol effects on photolysis rates (Lee et al., 2009; Martin et al., 2003b).

This GEOS-Chem simulation uses assimilated meteorology from the Goddard Earth

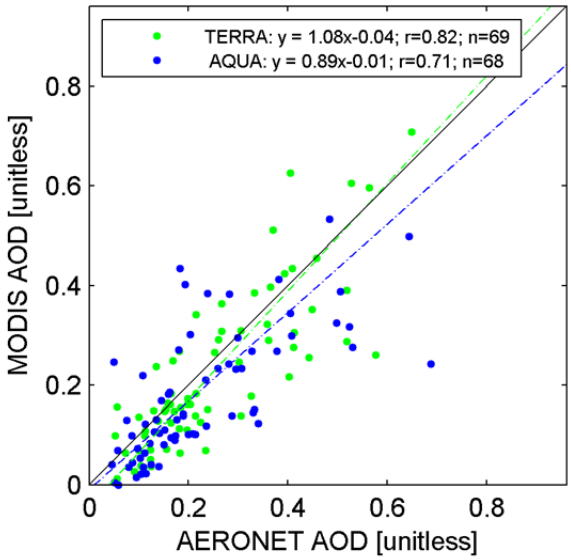

Figure 4-3: Comparison of summertime AOD from AERONET and MODIS over Moscow between 2004-2009. MODIS AOD are shown in blue for Aqua and green for Terra.

Observing System (GEOS-5), degraded to 2° x 2.5° horizontal resolution and 47 vertical levels. Global anthropogenic emissions are based upon EDGAR 3.2FT2000 (Olivier et al., 2002), and scaled to 2006 following the approach of van Donkelaar et al. (2008). Global anthropogenic emissions are overwritten in areas with regional inventories, such as the European Monitoring and Evaluation Programme (EMEP; http://www.emep.int/) over Europe. We use daily Quick Fire Emissions Database version 2 (QFED v2) biomass burning emissions of organic carbon, black carbon and SO_2. QFED v2.1 relates emissions to MODIS retrieved Fire Radiative Power via biome-specific calibration constants and observed area following *Kaiser et al.* (2009). QFED 2.1 is calibrated as to produce global average biomass emissions consistent with the Global Fire Emission Database version 2 (GFED v2; van der Werf et al., 2006). Biomass burning emissions in GEOS-Chem are released into the lowest model level. Smoldering fires, such as from peat, likely emit predominantly into the planetary boundary layer as represented by this simple scheme.

Following van Donkelaar et al. (2010), we estimate $PM_{2.5}$ as

$$PM_{2.5} = \eta \times AOD \qquad 4\text{-}1$$

where η is determined from the ratio of simulated $PM_{2.5}$ to simulated AOD at satellite overpass. η is a function of aerosol size, aerosol type, relative humidity, and the vertical structure of aerosol extinction.

Of concern is the sensitivity of η to error in the biomass burning inventory for this unusual event. We test the robustness of η to this uncertainty by comparing with values calculated using mean monthly average biomass burning emissions from a different inventory. GFED2 v2 calculates biomass burning emissions as a function of time varying precipitation, temperature, solar radiation and fractional-absorbed photosynthetically active radiation (Giglio et al., 2006).

The right panels of Figure 4-4 show the organic carbon emissions from monthly mean 1997-2008 GFED v2 emissions and the average QFED v2 emissions for July 22 – August 20, 2010. Both

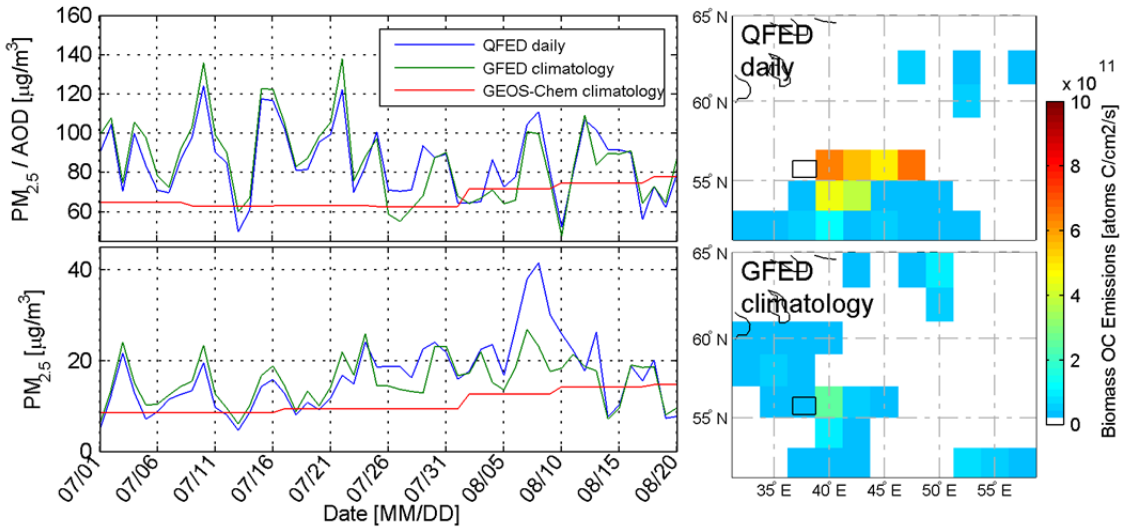

Figure 4-4: Effect of emissions on the AOD to $PM_{2.5}$ relationship (η). The left panels show simulated η and $PM_{2.5}$ values using QFED daily and GFED climatological biomass burning emissions. Also shown are 2004-2008 climatological values of $PM_{2.5}$ and η. The right panels show daily average organic carbon (OC) emissions from July 22, 2010 to August 20, 2010. The black box identifies the Moscow region.

inventories show peak mean organic carbon emissions east of Moscow, but the period-specific QFED v2 emissions show much higher emissions and broader sources extending further east.

The upper left panel of Figure 4-4 shows the time series of η from July 1, 2010 to August 20, 2010. Values of η show little difference (typically < 10%) whether using daily (QFED) or climatological (GFED) biomass burning emissions, despite these large changes in emissions (right panels) and large changes in simulated surface $PM_{2.5}$ (lower left panel). We also compare with climatological η values, calculated as a five-year mean (2004-2008) of the +/-15 surrounding days of each 8th Julian day. Large differences are observed between our previous η estimates and this climatology, highlighting the effect of meteorology on the relationship between AOD and $PM_{2.5}$.

Figure 4-5 shows mean satellite-derived $PM_{2.5}$ concentrations in the Moscow region for the period July 7-21, 2010, leading up to the fire event. Mean satellite-derived $PM_{2.5}$ concentrations range from 13.1-35.7 μg/m^3, and have enhancements in the urban core. Two in-situ TEOM

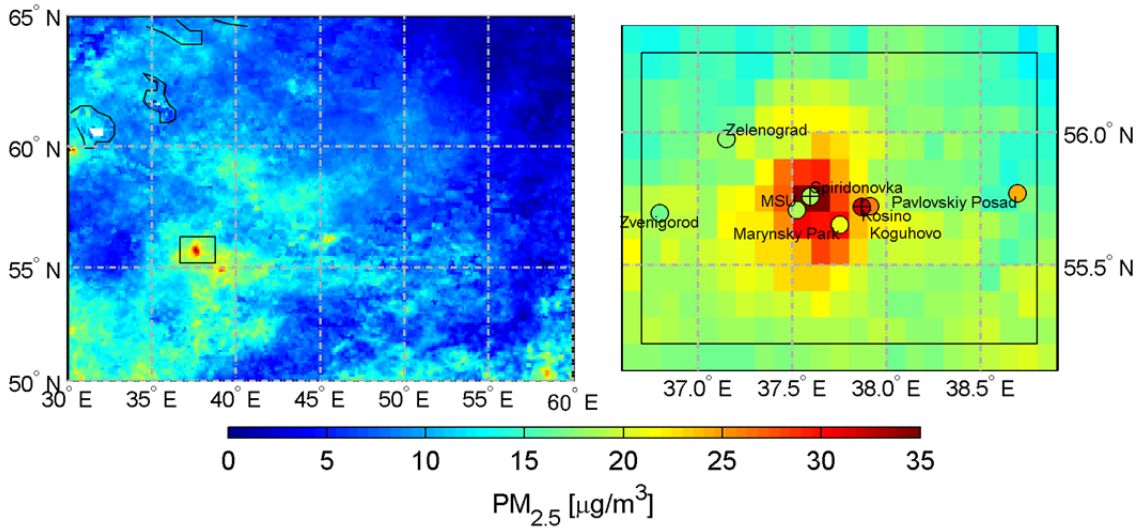

Figure 4-5: Satellite-derived mean $PM_{2.5}$ for July 7-21, 2010. The Moscow region is shown by the black box and enlarged in the right-hand panel. Filled circles give in-situ values, with cross-haired locations denoting direct $PM_{2.5}$ measurements with others estimated from in-situ PM_{10}. Table 4-1 provides details of each station.

$PM_{2.5}$ monitors were operational in Moscow during this period, but $PM_{2.5}$ measurements are not available outside the city center. We find that the aerosol fine fraction ranges from 40-100% during this time using PM_{10} measurements coincident with the two $PM_{2.5}$ monitors. We apply the mean fine fraction (66.8%) to local in-situ PM_{10} measurements to broaden our comparison, also shown in Figure 4-5. Similar to our satellite-derived estimates, daily mean in-situ $PM_{2.5}$ (Table 4-1) ranges from 16.7-32.1 $\mu g/m^3$ during this time. Differences between in-situ and satellite-derived $PM_{2.5}$ spatial patterns possibly reflect differences in spatial representativeness between these metrics or daily/spatial deviations in the fine fraction applied to PM_{10}, as well as errors the in-situ and satellite-derived value themselves.

The $PM_{2.5}$ TEOM monitors were not in operation during the wildfire event due to the abnormally hot conditions. We continue to estimate in-situ $PM_{2.5}$ from the PM_{10} monitors that did remain in operation throughout the event by assuming an 80% fine fraction from biomass burning (Martin et al., 2010). Figure 4-6 compares in-situ and satellite-derived $PM_{2.5}$ between July 14, 2010 and August 18, 2010. Both metrics show good agreement (r^2=0.85, slope=1.06),

with in-situ values in the range of satellite-derived $PM_{2.5}$. A peak value of approximately 600 $\mu g/m^3$ is given by both metrics on August 7, 2010. A sensitivity study in which $PM_{2.5}$ was derived using the operational MODIS AOD product lowered the daily median peak concentration to less than 400 $\mu g/m^3$ due to filtration of aerosol by the operational cloud filter.

Figure 4-7 shows regional mean daily overpass $PM_{2.5}$ estimates from MODIS Aqua and Terra for August 3-10, 2010. Extremely high levels of $PM_{2.5}$ span hundreds of thousands of square kilometers. The largest plumes intercept Moscow on August 6-9, 2010.

4.4 Health Impacts of the Moscow Fires

Although direct estimates of health impacts of the Moscow fires are not currently available, some insight into the possible magnitude of the health impacts caused by the fires can come

Table 4-1: Aerosol monitoring stations in the Moscow region.

Station	Type	Class	Coordinates	In-situ $PM_{2.5}$[a] July 7-21, 2010[b] Mean (Range) $\mu g/m^3$	No. of obs.	In-situ $PM_{2.5}$[a] August 3-10, 2010[c] Mean (Range) $\mu g/m^3$	No. of obs.
Marymsky Park	PM_{10}	Urban	55°39'8.45"N, 37°45'4.92"E	21.0 (12.7-34.1)	15	261.8 (73.6-608.0)	8
Zelenograd	PM_{10}	Suburban	55°58'38.69"N, 37°09'1.49"E	18.0 (10.7-27.4)	15	275.2 (108.8-518.4)	8
MSU	PM_{10}	Suburban	55°42'26.45"N, 37°31'20.60"E	18.7 (18.7-18.7)	1	264.4 (51.2-611.2)	8
Kosino	$PM_{2.5}$, PM_{10}	Urban	55°43'13.40"N, 37°52'2.96"E	32.1 (21.0-41.0)	8	332.6 (113.6-724.8)	8
Spiridonovka	$PM_{2.5}$, PM_{10}	Urban	55°45'33.55"N, 37°35'43.84"E	18.6 (13.0-25.0)	8	270.1 (107.2-382.4)	3
Pavlovsky Posad	PM_{10}	Rural Background	55°46'16.45"N, 38°41'34.02"E	24.3 (12.7-42.8)	10	236.2 (55.2-564.0)	8
Zvenigorod	PM_{10}	Rural Background	55°41'49.44"N, 36°47'44.14"E	16.7 (15.4-17.4)	4	223.4 (84.0-447.2)	5
Kozhuhovo	PM_{10}	Suburban	55°43'21.66"N; 37°54'37.69"E	26.1 (14.7-39.4)	13	325.7 (113.6-672.8)	8

[a] $PM_{2.5}$ is estimated from PM_{10} with the exception of Kosino and Spirionovka for July 7-21, 2010.
[b] a fine fraction of 66.8% is used, based upon coincident $PM_{2.5}$ and PM_{10} measurements at Kosino and Spirionovka between July 7-21, 2010.
[c] a fine fraction of 80% is used during the biomass burning event (Martin et al., 2010).

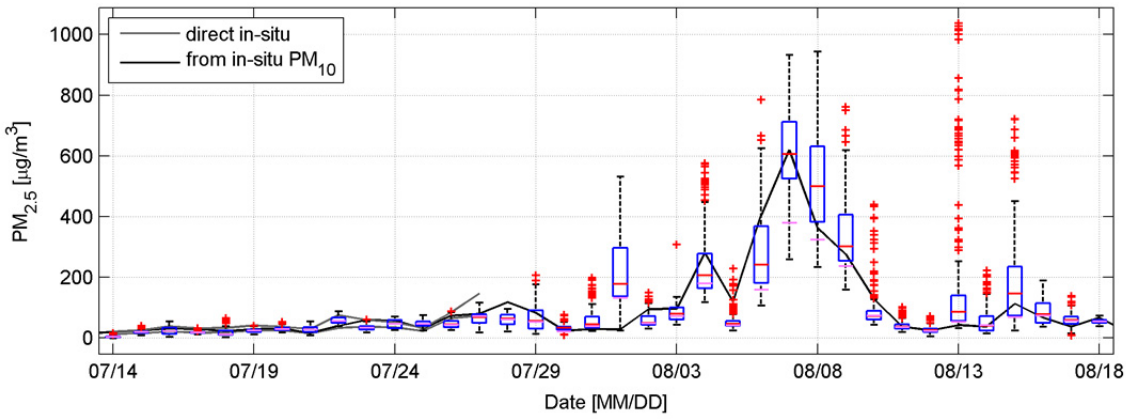

Figure 4-6: Comparison of in-situ and satellite-derived $PM_{2.5}$ during the summer 2010 fire event. The box and whisker plot presents satellite-derived $PM_{2.5}$ within the boxed region of Figures 4-1, 4-4, 4-5 and 4-7. Blue boxes surround the 25th and 75th percentiles of the satellite-derived $PM_{2.5}$. Medians and full ranges are given by the red lines and error bars, respectively. Outliers are denoted by red pluses. All satellite-derived $PM_{2.5}$ values given here use the relaxed cloud screening product from MODIS, except for the magenta line which indicate median $PM_{2.5}$ derived from the operational MODIS AOD product. The black line denotes mean $PM_{2.5}$ estimated from in-situ PM_{10} monitors. Dark grey lines correspond to direct in-situ $PM_{2.5}$ measurements.

from considering the quantitative impacts that have been observed in time series studies associating the daily changes in population mortality with daily average concentration of particulate matter.

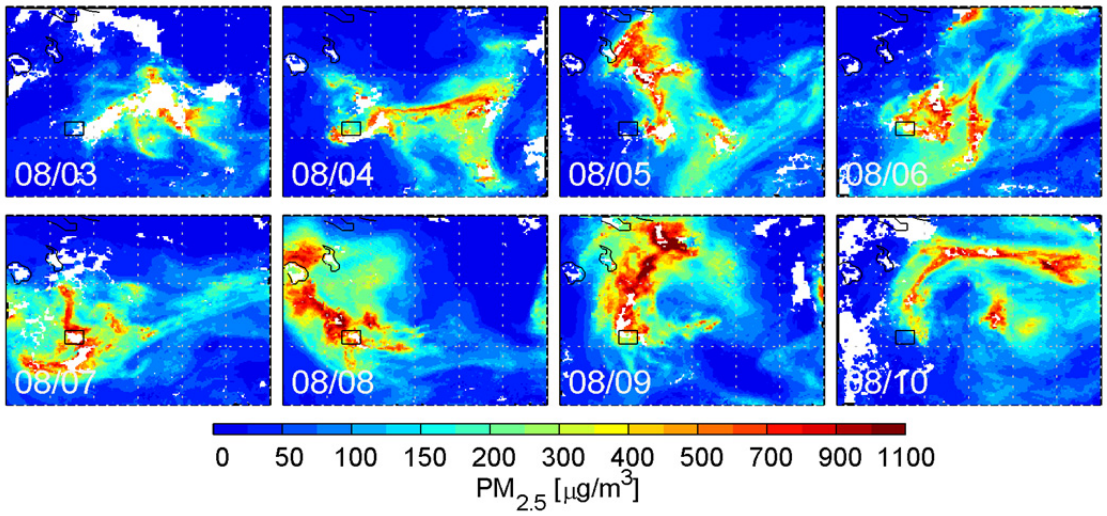

Figure 4-7: Daily satellite-derived $PM_{2.5}$ from August 3-10, 2010. The black box identifies the Moscow region.

We estimate the increased relative risk of death (ΔRR_d) on a day with PM_{10} concentration C_d based on the relative risk estimate of RR (per 10 μg/m^3 PM_{10}) inferred from the meta-analysis of time-series studies according to the form

$$\Delta RR_d = (RR-1)(C_d - C_r)/10 \qquad 4\text{-}2$$

where C_r is the reference concentration of PM_{10} (in the absence of the fires).

The excess of mortality on day d was calculated as

$$\Delta M_d = M \cdot \Delta RR_d / (\Delta RR_d + 1) \qquad 4\text{-}3$$

where M is the expected number of deaths per day in the absence of fires.

The meta-analysis of European studies, conducted in 33 cities, indicated a 10 μg/m^3 increase in daily PM_{10} levels is associated with 0.6% (95% Confident Interval (CI) 0.4%-0.8%) increase in total daily number of deaths (WHO, 2005). Similar risks were estimated by studies conducted in Asia (Wong et al., 2008). Assuming a similar association of daily mortality with PM_{10} levels in Moscow during the fires, enhancement of PM_{10} above the pre-fire level (29 μg/m^3 for 7-21 July 2010, using an 66.8% fine fraction as above), would lead to an average 17.1% (95% CI 11.4%-22.8%, based on CI of the risk increase per 10 μg/m^3) increase in the risk of death during the fires (2-10 August). With the approximate average daily number of deaths in Moscow estimated to be 400, this would lead to an excess of about 482 deaths during this 9 day period (95% CI 346-600) (Figure 4-8).

An additional source of information on the link between mortality and air pollution from forest fires is the analysis of impacts of fires that occurred in Indonesia in 1997 (Sastry, 2002). This study estimated an increase of all cause mortality in Kuala Lumpur, Malaysia, by 19% (SE 10.9%) on high air pollution days (PM_{10} > 210 μg/m^3), with the most pronounced effect among people 65-74 years of age (56%, SE 32.8%, Sastry, 2002, Table 4). Mortality increased by 21.8%

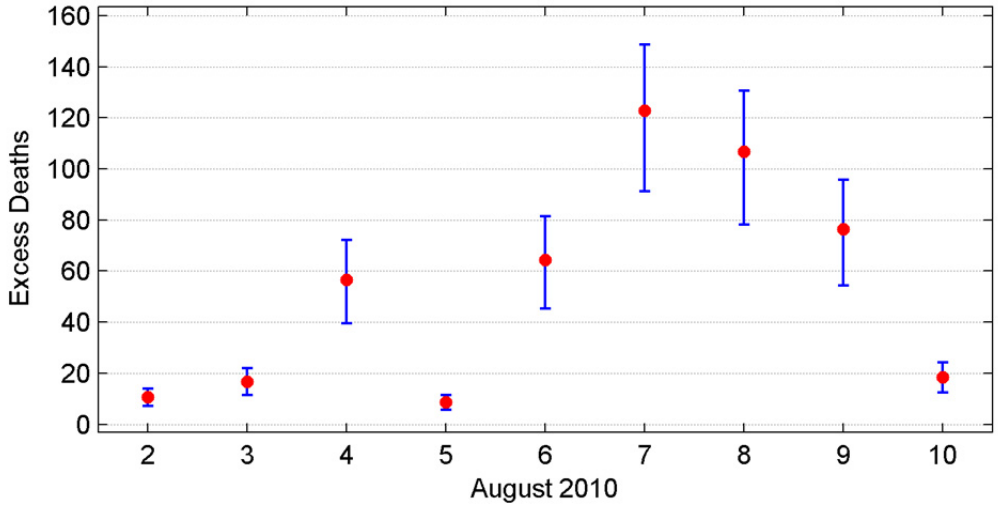

Figure 4-8: Estimated number of daily deaths in Moscow due to smoke from the wildfires, August 2-10, 2010. Error bar denote the 95% confidence interval.

(SE 8.6%), especially among infants and the 65-74 age group, on days of low visibility (<0.91 km) which is indicative of high air pollution from forest fires (Sastry, 2002, Table 8). Using this risk coefficient for days with high PM_{10} levels from this study, we can estimate an excess of about 64 deaths in each of the 5 days in which PM_{10} exceeded 210 µg/m3 in Moscow. This approach would suggest a total excess of 320 deaths (95 CI ranging from no effect to 575 deaths).

Although these estimates suggest that air pollution from the fires may have caused serious adverse health effects, they entail many assumptions and are highly uncertain. When high levels of biomass smoke are accompanied by extreme heat, as was the case in the Moscow fires, both air pollution and heat may cause serious adverse health effects, and the independent effect of increased exposure to air pollution may be difficult to quantify. Moreover, exposure to particulate air pollution and extreme heat may interact, resulting in effects that are more than additive (Qian et al., 2008). In addition, both estimates given above assume a linear relation between short-term exposure to PM and the excess relative risk of mortality across a broad range of PM levels. However, Sastry (2002, Table 3) suggests that the relationship may be

supra-linear at levels in excess of 200 μg/m^3 PM_{10}, while others argue that there may be a marked decrease in the excess relative risk at very high levels of exposure (Pope et al., 2011). Furthermore, we estimate only the effects of exposure on the days of the episode. Health impacts over the longer term may be affected by both reduced mortality in the aftermath of the episode, so-called "harvesting" or "mortality displacement" (due to the depletion of frail or otherwise susceptible individuals), or by chronic effects caused by the extreme exposures (e.g. the long-term sequalae of acute myocardial infarctions brought on by the episode). More definitive estimates of the health impacts of the fires would require a careful analysis of local data on morbidity and mortality for the relevant time periods.

4.5 CONCLUSIONS

We estimated daily mean ground-level $PM_{2.5}$ concentrations during satellite overpass by using the GEOS-Chem model to relate MODIS AOD to $PM_{2.5}$ during the major biomass burning event around Moscow in summer 2010. We found that these satellite-derived estimates well represent ground-level $PM_{2.5}$ estimated from PM_{10} measurements (r^2=0.85, slope=1.06). Peak daily mean satellite-derived $PM_{2.5}$ exceed 600 μg/m^3 in the Moscow area on August 7, 2010, with similar $PM_{2.5}$ values estimated from in-situ measurements of PM_{10}. High levels of $PM_{2.5}$ were estimated to affect hundreds of thousands of square kilometers surrounding Moscow.

To obtain these results, we presented a relaxed cloud screening criteria for the MODIS AOD retrieval algorithm that increases coverage during extreme aerosol events without apparent misclassification of clouds. The relaxed criteria allows retrieval of an additional 21.3% of pixels during this period in the Moscow region. It has strong agreement with the operational retrieval algorithm for coincident pixels (r^2 = 0.994; slope = 1.010), with the recovered pixels spread across a range of AOD values.

We found that the relationship between AOD and $PM_{2.5}$ is robust against changes to emissions, but is strongly affected by changes in meteorology. These results suggest that satellite observations can be used to monitor daily ground-level $PM_{2.5}$ during major events without direct calibration to in-situ $PM_{2.5}$.

Using separate relationships determined from two other major biomass burning events, we estimated that exposure to air pollution from the Moscow wildfires may have caused hundreds of excess deaths.

4.6 Disclaimer

The views expressed in this paper are those of the authors and do not necessarily reflect the views of the Health Effects Institute or its sponsors.

4.7 Acknowledgements

This work was supported by the Natural Science and Engineering Research Council of Canada (NSERC) and the Killam Trust.

Chapter 5. CONCLUSION

5.1 SUMMARY OF THIS PRESENT WORK

In the first part of this work, we combine aircraft and surface observations from the Intercontinental Chemical Transport Experiment (INTEX-B) with satellite retrievals and simulated values to better understand Asian aerosol emissions and the impact of long range aerosol transport on Canadian air quality. We estimate an increase in east Asian SO_x emissions between 2000 to 2006 of 6.2-9.6% interpreting Aerosol Optical Depth (AOD) trends retrieved by the Multiangle Imaging Spectroradiometer (MISR) and the Moderate Resolution Imaging Spectroradiometer (MODIS) with the GEOS-Chem chemical transport model, in agreement with bottom-up estimates of 9.9% (Streets et al., 2003). By further interpreting INTEX-B with GEOS-Chem, we find that the outflow of Asian SO_x is strongest in the lower troposphere, with enhanced $SO_4^=$concentrations of 1-1.5 μg/m^3 observed by the DC-8 between 700-800 hPa over the Pacific Ocean. Closer to North America, mean C-130 and Cessna aircraft $SO_4^=$ measurements of 1-1.5 μg/m^3 over 600-800 hPa suggest that Asian plumes are often elevated by orographic effects nearer to the coast.

Using historic aircraft measurements from 1985, we find an increase of free tropospheric SO_x of 60-90% from 1985 to 2006. Sensitivity simulations for 1985 and without East Asian emissions indicate that their relative contribution to $SO_4^=$ concentrations during April and May between 500-900 hPa increased by 72-85% due to emission changes as compared to 1985 depending on the specific region.

Campaign-mean simulations show that 50% of the $SO_4^=$ burden between 1 and 5 km over Whistler is of anthropogenic Asian origin. These emissions increase surface concentrations along the western Canadian coast by an average 0.31 μg/m^3 (~30%) in spring. This effect is

corroborated with surface measurements, where we find an increase of 0.32 μg/m^3 with each 10% increase in simulated fraction of Asian $SO_4^=$ during INTEX-B, with episodic enhancements of more than 1.5 μg/m^3.

In the second part of this work, we produce a global climatology of surface fine aerosol concentrations ($PM_{2.5}$) by interpreting satellite retrievals of AOD from MODIS and MISR with the GEOS-Chem chemical transport model. We found significant spatial agreement between mean coincident satellite-derived and ground-based $PM_{2.5}$ for North America (slope = 1.07, r = 0.77, n = 1057), as well as evidence of global agreement with non-coincident measurements from published and unpublished data (slope = 0.86, r = 0.83, n = 244). This level of agreement is globally better than is found by simulation alone (slope = 0.54, r = 0.63, n=244), in part due to the higher resolution of the satellite retrievals. We estimate a 1-sigma error of 25% by evaluating the accuracy of the simulated aerosol vertical structure with measurements from the Cloud-Aerosol Lidar and Infrared Pathfinder Satellite Observations (CALIPSO) satellite and testing the impact of sampling frequency using GEOS-Chem. In agreement with this estimate, we find that one standard deviation of mean coincidently sampled $PM_{2.5}$ measurements are within ±(1 μg/m^3 + 15%) of our satellite-derived value.

These satellite-derived $PM_{2.5}$ estimates suggest the global population-weighted geometric mean $PM_{2.5}$ concentration is 20 μg/m^3 and that 80% of the global population resides in locations where ambient concentrations exceed the WHO Air Quality Guideline of 10 μg/m^3. Application of the satellite-derived $PM_{2.5}$ dataset also identifies global regions and areas of specific concern; half (50%) of the eastern Asian population lives in regions that exceed the WHO Air Quality Interim Target 3 of 35 μg/m^3, and are therefore at increased risk from air pollution-related health impacts. These results highlight the potential of satellite aerosol observations to contribute to chronic effects studies at regional and global scales.

The final section of this work tests the ability of satellite-derived $PM_{2.5}$ estimates to capture daily $PM_{2.5}$ in Moscow during the major biomass burning event that occurred there in summer 2010 using MODIS. We found that satellite-derived estimates well represented ground-level $PM_{2.5}$ estimated from PM_{10} measurements (r^2=0.85, slope=1.06) during the event and estimate a peak concentration of 600 μg/m^3 in Moscow on August 7, 2010, in agreement with in-situ estimates. The operational cloud screening algorithm used by the MODIS AOD retrieval can confuse dense aerosol plume for cloud during extreme events. We suggest relaxed cloud screening criteria which provide an additional 21.3% coverage during the Moscow wildfires while maintaining significant agreement with the standard operational product (r^2 = 0.994; slope = 1.010). The additional coverage provided by the relaxed criteria improves agreement between satellite-derived and in-situ $PM_{2.5}$ estimates, with the operational cloud screening reducing peak on August 7, 2010 to 400 μg/m^3. Using a meta-analysis of previous studies investigating the health impact of major biomass burning events, we estimate that the Moscow wildfires may have caused hundreds of excess deaths.

5.2 PRESENT AND FUTURE STUDIES UTILIZING THIS WORK

The production of global long-term mean estimates of $PM_{2.5}$ has generated excitement among some epidemiologists due to the sparseness of global in-situ measurements and the association between ambient $PM_{2.5}$ and increased risk of several chronic diseases. This work has received considerable media attention such as a NASA press release (Voiland, 2010), National Geographic China (Zhang, 2010), the Canadian Broadcasting Corporation (Jones, 2010) and the United Nations Environment Programme (UNEP) Yearbook (Bech and Goverse, 2011).

Canadian in-situ monitoring of $PM_{2.5}$ occurs predominantly near major cities. As a result, several Canadian studies are using our satellite-derived $PM_{2.5}$ estimates. Villeneuve et al. (in

press) directly linked satellite-derived estimates of $PM_{2.5}$ to the health records of 122,548 Canadians to associate factors such as smoking with ambient $PM_{2.5}$. Higher levels of smoking occur in regions of lower $PM_{2.5}$, acting as a confounder against associations between lung cancer and heart disease. Crouse et al. (in prep) assigned satellite-derived $PM_{2.5}$ concentrations to the 2.1 million Canadians who took part in the 1991 detailed census to find a 10% increase in mortality from non-accidental death per 10 $\mu g/m^3$ increase in $PM_{2.5}$ exposure. They found similar associations using in-situ measurements at 11 major Canadian cities. Hystad et al. (submitted) incorporated satellite-derived $PM_{2.5}$ estimates into a landuse regression model and found that these estimate dominated its predictive capabilities of $PM_{2.5}$ variation (r^2 = 41% out of a total r^2 = 46%).

Evans et al. (in prep) and projects such as the World Health Organisation's (WHO) Global Burden of Disease (Brauer et al., in prep.) have begun to incorporate satellite-derived $PM_{2.5}$ estimates to assess the global impact of $PM_{2.5}$ on human health. Evans et al. (in prep) found that adult mortality from 8.0% of cardiopulmonary disease, 12.8% of lung cancer and 9.4% of ischemic heart disease is globally attributable to anthropogenic $PM_{2.5}$. World-wide asthma prevalence is also being investigated (Butland et al., in prep).

5.3 Future Directions

This thesis is a part of a growing body of evidence of the value of remote sensing for the monitoring of air quality. There is, however, much work to do before this field of research reaches its full potential. The major assumptions related to surface reflectivity and aerosol scattering properties that are built into AOD retrievals are a large source of uncertainty. The use of filtration, such as was done in Chapter 3, limits the direct impact on poorly represented areas, but reduces the number of observations. Alternate approaches that either apply corrections to

these areas (Hyer et al., 2011) or address the root causes of their uncertainties (e.g. Castanho et al., 2008; Drury et al., 2010; Lyapustin et al., 2011; Wang et al., 2010) would increase observations and reduce noise. Increased coverage may also be obtained by improvements to cloud screening algorithms, such as presented in Chapter 4, if these changes can be shown to be globally applicable.

Uncertainties in aerosol chemical production mechanisms and both direct and precursor emissions (e.g. Pye and Seinfeld, 2010) limit our ability to represent aerosol distributions and vertical structures (e.g. Heald et al., 2005), and affect our ability to relate AOD to $PM_{2.5}$ at the surface. Model resolution also plays a role, since relatively coarse global models cannot capture small-scale variation, yet many regional models do not include long-range transport which may limit their ability to represent the entire atmospheric column. Nested capabilities in chemical transport models, such as now implemented in GEOS-Chem, or improved boundary conditions for regional models may bridge these qualities and allow column-representative AOD-$PM_{2.5}$ relationships at fine resolution.

REFERENCES

2004. Toward Cleaner Urban Air in South Asia: Tackling Transport Pollution, Understanding Sources. The World Bank.

Abdou, W.A., Diner, D.J., Martonchik, J.V., Bruegge, C.J., Kahn, R.A., Gaitley, B.J., Crean, K.A., Remer, L.A., Holben, B., 2005. Comparison of coincident Multiangle Imaging Spectroradiometer and Moderate Resolution Imaging Spectroradiometer aerosol optical depths over land and ocean scenes containing Aerosol Robotic Network sites. Journal of Geophysical Research-Atmospheres 110.

Abu-Allaban, M., Lowenthal, D.H., Gertler, A.W., Labib, M., 2007. Sources of PM10 and PM2.5 in Cairo's ambient air. Environmental Monitoring and Assessment, 417-425-417-425.

Alexander, B., Park, R.J., Jacob, D.J., Li, Q.B., Yantosca, R.M., Savarino, J., Lee, C.C.W., Thiemens, M.H., 2005. Sulfate formation in sea-salt aerosols: Constraints from oxygen isotopes. Journal of Geophysical Research-Atmospheres 110.

Allen, G., 2010. Evaluation of Transformation Methods for Adjustment of Historial TEOM Data in the NAPS Network. Analysis and Air Quality Section, Environment Canada.

Anderson, H.R., 1999. Health Effects of Air Pollution Episodes, in: S., H., Samet, J., Koen, H., Maynard, R. (Eds.), Air Pollution and Health. Academic Press, London.

Anderson, T.L., Wu, Y.H., Chu, D.A., Schmid, B., Redemann, J., Dubovik, O., 2005. Testing the MODIS satellite retrieval of aerosol fine-mode fraction. Journal of Geophysical Research-Atmospheres 110.

Andreae, M.O., Berresheim, H., Andreae, T.W., Kritz, M.A., Bates, T.S., Merrill, J.T., 1988. VERTICAL-DISTRIBUTION OF DIMETHYLSULFIDE, SULFUR-DIOXIDE, AEROSOL IONS, AND RADON OVER THE NORTHEAST PACIFIC-OCEAN. Journal of Atmospheric Chemistry 6, 149-173.

Andres, R.J., Kasgnoc, A.D., 1998. A time-averaged inventory of subaerial volcanic sulfur emissions. Journal of Geophysical Research-Atmospheres 103, 25251-25261.

Arellano, A.F., Kasibhatla, P.S., Giglio, L., van der Werf, G.R., Randerson, J.T., 2004. Top-down estimates of global CO sources using MOPITT measurements. Geophysical Research Letters 31.

Artaxo, P., Gerab, F., Yamasoe, M.A., Martins, J.V., 1994. FINE MODE AEROSOL COMPOSITION AT 3 LONG-TERM ATMOSPHERIC MONITORING SITES IN THE AMAZON BASIN. Journal of Geophysical Research-Atmospheres 99, 22857-22868.

Bailey, R., Barrie, L.A., Halsall, C.J., Fellin, P., Muir, D.C.G., 2000. Atmospheric organochlorine pesticides in the western Canadian Arctic: Evidence of transpacific transport. Journal of Geophysical Research-Atmospheres 105, 11805-11811.

Balasubramanian, R., Qian, W.B., Decesari, S., Facchini, M.C., Fuzzi, S., 2003. Comprehensive characterization of PM2.5 aerosols in Singapore. Journal of Geophysical Research-Atmospheres 108.

Barrie, L.A., Li, S.M., Toom, D.L., Landsberger, S., Sturges, W., 1994. Lower Tropospheric Measurements of Halogens, Nitrates, and Sulfur-Oxides during Polar Sunrise Experiment 1992. Journal of Geophysical Research-Atmospheres 99, 25453-25467.

Bech, S., Goverse, T., 2011. UNEP Yearbook 2011: Emerging Issues in Our Global Environment, pp. 10-11.

Beelen, R., Hoek, G., van den Brandt, P.A., Goldbohm, R.A., Fishcer, P., Schouten, L.J., Jerrett, M., Hughes, E., Armstrong, B., Brunekreef, B., 2008. Long-Term Effects of Traffic-Related Air Pollution on Mortality in a Dutch Cohort (NLCS-AIR Study). Environmental Health Perspectives 116, 196-202.

Begum, B.A., Biswas, S.K., Hopke, P.K., 2006. Temporal variations and spatial distribution of ambient PM2.2 and PM10 concentrations in Dhaka, Bangladesh. The Science of the total environment 358, 36-45.

Begum, B.A., Biswas, S.K., Hopke, P.K., 2008. Assessment of trends and present ambient concentrations of PM2.2 and PM10 in Dhaka, Bangladesh. Air Quality, Atmosphere and Health 1, 125-133.

Benkovitz, C.M., Scholtz, M.T., Pacyna, J., Tarrason, L., Dignon, J., Voldner, E.C., Spiro, P.A., Logan, J.A., Graedel, T.E., 1996. Global gridded inventories of anthropogenic emissions of sulfur and nitrogen. Journal of Geophysical Research-Atmospheres 101, 29239-29253.

Bertschi, I.T., Jaffe, D.A., Jaegle, L., Price, H.U., Dennison, J.B., 2004. PHOBEA/ITCT 2002 airborne observations of transpacific transport of ozone, CO, volatile organic compounds, and aerosols to the northeast Pacific: Impacts of Asian anthropogenic and Siberian boreal fire emissions. Journal of Geophysical Research-Atmospheres 109.

Bey, I., Jacob, D.J., Yantosca, R.M., Logan, J.A., Field, B.D., Fiore, A.M., Li, Q.B., Liu, H.G.Y., Mickley, L.J., Schultz, M.G., 2001. Global modeling of tropospheric chemistry with assimilated meteorology: Model description and evaluation. Journal of Geophysical Research-Atmospheres 106, 23073-23095.

Bond, T.C., Streets, D.G., Yarber, K.F., Nelson, S.M., Woo, J.H., Klimont, Z., 2004. A technology-based global inventory of black and organic carbon emissions from combustion. Journal of Geophysical Research-Atmospheres 109.

Brauer, M., Amman, M., Burnett, R.T., Cohen, A., Dentener, F.J., Ezzatti, M., Henderson, S., Krzyzanowski, M., Martin, R.V., Pandey, K.D., van Dingenen, R., van Donkelaar, A., Thurston, G., in prep. Exposure assessment for the estimation of the global burden of disease attributable to outdoor air pollution Environmental Science and Technology.

Brock, C.A., Hudson, P.K., Lovejoy, E.R., Sullivan, A., Nowak, J.B., Huey, L.G., Cooper, O.R., Cziczo, D.J., de Gouw, J., Fehsenfeld, F.C., Holloway, J.S., Hubler, G., Lafleur, B.G., Murphy, D.M., Neuman, J.A., Nicks, D.K., Orsini, D.A., Parrish, D.D., Ryerson, T.B., Tanner, D.J., Warneke, C., Weber, R.J., Wilson, J.C., 2004. Particle characteristics following cloud-modified transport from Asia to North America. Journal of Geophysical Research-Atmospheres 109.

Brown, K.W., Bouhamra, W., Lamoureux, D.P., Evans, J.S., Koutrakis, P., 2008. Characterization of particulate matter for three sites in Kuwait. Journal of the Air & Waste Management Association 58, 994-1003.

Butland, B.K., Strachan, D.P., Anderson, H.R., Brauer, M., Brunekreef, B., Clayton, T., Cohen, A., van Donkelaar, A., Lai, C., Martin, R.V., in prep. World-wide asthma prevalence and outdoor PM2.5 estimated by satellite observations.

Canagaratna, M.R., Jayne, J.T., Jimenez, J.L., Allan, J.D., Alfarra, M.R., Zhang, Q., Onasch, T.B., Drewnick, F., Coe, H., Middlebrook, A., Delia, A., Williams, L.R., Trimborn, A.M., Northway, M.J., DeCarlo, P.F., Kolb, C.E., Davidovits, P., Worsnop, D.R., 2007. Chemical and microphysical characterization of ambient aerosols with the aerodyne aerosol mass spectrometer. Mass Spectrometry Reviews 26, 185-222.

Carn, S.A., Krueger, A.J., Krotkov, N.A., Yang, K., Levelt, P.F., 2007. Sulfur dioxide emissions from Peruvian copper smelters detected by the Ozone Monitoring Instrument. Geophysical Research Letters 34.

Carrico, C.M., Bergin, M.H., Shrestha, A.B., Dibb, J.E., Gomes, L., Harris, J.M., 2003. The importance of carbon and mineral dust to seasonal aerosol properties in the Nepal Himalaya. Atmospheric Environment 37, 2811-2824.

Castanho, A., Martins, J.V., Artaxo, P., 2008. MODIS aerosol optical depth Retrievals with high spatial resolution over an urban area using the critical reflectance. Journal of Geophysical Research-Atmospheres 113.

Castanho, A.D.A., Artaxo, P., 2001. Wintertime and summertime Sao Paulo aerosol source apportionment study. Atmospheric Environment 35, 4889-4902.

Chen, C.-H., Liu, W.-L., Chen, C.-H., 2006. Development of a multiple objective planning theory and system for sustainable air quality monitoring networks. Science of the Total Environment 354, 1-19.

Chowdhury, M., 2004. Characterization of fine particle air pollution in the indian subcontinent. PhD. Dissertation, Georgia Institute of Technology.

Chuersuwan, N., Nimrat, S., Lekphet, S., Kerdkumrai, T., 2008. Levels and major sources of PM2.5 and PM10 in Bangkok Metropolitan Region. Environment International 34, 671-677.

Cofer, W.R., Collins, V.G., Talbot, R.W., 1985. IMPROVED AQUEOUS SCRUBBER FOR COLLECTION OF SOLUBLE ATMOSPHERIC TRACE GASES. Environmental Science & Technology 19, 557-560.

Cohen, A.J., Anderson, H.R., Ostro, B., Dev Pandey, K., Krzyzanowski, M., Kunzli, N., Gutschmidt, K., Pope, C.A., Romieu, I., Samet, J.M., Smith, K.R., 2003. Global and Regional Burden of Diseases Attributable to Selected Major Risk Factors - Chapter 17: Urban air pollution. World Health Organization 1, 1353-1433.

Cohen, D.D., Garton, D., Stelcer, E., Wang, T., Poon, S., Kim, J., Oh, S.N., Shin, H.-J., Ko, M.Y., Santos, F., Esquerra, L., thu Bac, V., Hien, P.D., Uematsu, M., 2002. Characterisation of PM2.5 and PM10 Fine Particle Pollution in Several Asian Regions. 16th Int. Clean Air Conf.

Corbett, J.J., Wang, C., Winebrake, J.J., Green, E., 2007. Allocation and forecasting of global ship emissions. Clean Air Task Force Report.

Crouse, D.L., Peters, P.A., van Donkelaar, A., Goldberg, M.S., Villeneuve, P.J., Brion, O., Khan, S., Atari, D.O., Jerret, M., Pope, C.A., Brauer, M., Brook, R.D., Martin, R.V., Stieb, D., Burnett, R.T., in prep. Risk of Mortality in Relation to Long-term Exposure to Low Concentrations of Fine Particulate Matter: A Canadian National-level Cohort Study. Environmental Health Perspectives.

DeCarlo, P.F., Kimmel, J.R., Trimborn, A., Northway, M.J., Jayne, J.T., Aiken, A.C., Gonin, M., Fuhrer, K., Horvath, T., Docherty, K.S., Worsnop, D.R., Jimenez, J.L., 2006. Field-deployable, high-resolution, time-of-flight aerosol mass spectrometer. Analytical Chemistry 78, 8281-8289.

Di Girolamo, L., Bond, T.C., Bramer, D., Diner, D.J., Fettinger, F., Kahn, R.A., Martonchik, J.V., Ramana, M.V., Ramanathan, V., Rasch, P.J., 2004. Analysis of Multi-angle Imaging SpectroRadiometer (MISR) aerosol optical depths over greater India during winter 2001-2004. Geophysical Research Letters 31.

Di Nicolantonio, W., Cacciari, A., Tomasi, C., 2009. Particulate Matter at Surface: Northern Italy Monitoring Based on Satellite Remote Sensing, Meteorological Fields, and in-situ Sampling. IEEE Journal of Selected Topics in Applied Earth Observations and Remote Sensing 2, 284-292.

Diner, D.D., Braswell, B.H., Davies, R., Gobron, N., Hu, J., Jin, Y., Kahn, R.A., Knyazikhin, Y., Loeb, N., J.-P., M., Nolin, A.W., Pinty, B., Schaaf, C.B., Seiz, G., Stroeve, J., 2005. The value of multiangle measurements for retrieving structurally and radiatively consistent properties of clouds, aerosols, and surfaces. Remote Sensing of Environment 97, 495-518.

Dockery, D.W., Pope, C.A., Xu, X.P., Spengler, J.D., Ware, J.H., Fay, M.E., Ferris, B.G., Speizer, F.E., 1993. AN ASSOCIATION BETWEEN AIR-POLLUTION AND MORTALITY IN 6 UNITED-STATES CITIES. New England Journal of Medicine 329, 1753-1759.

Drury, E., Jacob, D.J., Spurr, R.J.D., Wang, J., Shinozuka, Y., Anderson, B.E., Clarke, A.D., Dibb, J., McNaughton, C., Weber, R., 2010. Synthesis of satellite (MODIS), aircraft (ICARTT), and surface (IMPROVE, EPA-AQS, AERONET) aerosol observations over eastern North America to improve MODIS aerosol retrievals and constrain surface aerosol concentrations and sources. Journal of Geophysical Research-Atmospheres 115.

Drury, E., Jacob, D.J., Wang, J., Spurr, R.J.D., Chance, K., 2008. Improved algorithm for MODIS satellite retrievals of aerosol optical depths over western North America. Journal of Geophysical Research-Atmospheres 113.

Duan, F.K., He, K.B., Ma, Y.L., Yang, F.M., Yu, X.C., Cadle, S.H., Chan, T., Mulawa, P.A., 2006. Concentration and chemical characteristics of PM2.5 in Beijing, China: 2001-2002. Science of the Total Environment 355, 264-275.

Dubovik, O., Lapyonok, T., Kaufman, Y.J., Chin, M., Ginoux, P., Kahn, R.A., Sinyuk, A., 2008. Retrieving global aerosol sources from satellites using inverse modeling. Atmospheric Chemistry and Physics 8, 209-250.

Dubovik, O., Lapyonok, T., Kaufman, Y.J., Chin, M., Ginoux, P., Sinyuk, A., 2007. Retrieving global sources of aerosols from MODIS observations by Inverting GOCART model. Atmospheric Chemistry and Physics Discussions 7, 38-29-3718.

Dunlea, E.J., DeCarlo, P.F., Aiken, A.C., Kimmel, J.R., Peltier, R.E., Weber, R.J., Tomlinson, J., Collins, D.R., Shinozuka, Y., McNaughton, C.S., Howell, S.G., Clarke, A.D., Emmons, L.K., Apel, E.C., Pfister, G.G., van Donkelaar, A., Martin, R.V., Millet, D.B., Heald, C.L., Jimenez, J.L., 2009. Evolution of Asian aerosols during transpacific transport in INTEX-B. Atmospheric Chemistry and Physics 9, 7257-7287.

Eisinger, M., Burrows, J.P., 1998. Tropospheric sulfur dioxide observed by the ERS-2 GOME instrument. Geophysical Research Letters 25, 4177-4180.

Engel-Cox, J.A., Hoff, R.M., Haymet, A.D.J., 2004a. Recommendations on the use of satellite remote-sensing data for urban air quality. Journal of the Air & Waste Management Association 54, 1360-1371.

Engel-Cox, J.A., Hoff, R.M., Rogers, R., Dimmick, F., Rush, A.C., Szykman, J.J., Al-Saadi, J., Chu, D.A., Zell, E.R., 2006. Integrating lidar and satellite optical depth with ambient monitoring for 3-dimensional particulate characterization. Atmospheric Environment 40, 8056-8067.

Engel-Cox, J.A., Holloman, C.H., Coutant, B.W., Hoff, R.M., 2004b. Qualitative and quantitative evaluation of MODIS satellite sensor data for regional and urban scale air quality. Atmospheric Environment 38, 2495-2509.

Evans, J.A., van Donkelaar, A., Martin, R.V., Burnett, R.T., Rainham, D.G., Birkett, N.J., Krewski, D., in prep. Estimates of global mortality attributable to particulate air pollution using satellite imagery.

Evans, M.J., Jacob, D.J., 2005. Impact of new laboratory studies of N2O5 hydrolysis on global model budgets of tropospheric nitrogen oxides, ozone, and OH. Geophysical Research Letters 32.

Fairlie, T.D., Jacob, D.J., Park, R.J., 2007. The impact of transpacific transport of mineral dust in the United States. Atmospheric Environment 41, 1251-1266.

Feng, Y., Chen, Y., Guo, H., Zhi, G., Xiong, S., Li, J., Sheng, G., Fu, J., 2009. Characteristics of organic and elemental carbon in PM2.5 samples in Shanghai, China. Atmospheric Research 92, 434-442.

Giglio, L., van der Werf, G.R., Randerson, J.T., J., C.G., Kasibhatla, P., 2006. Global estimation of burned area using MODIS active fire observations. Atmospheric Chemistry and Physics 6, 957-974.

Gouveia, N., Junger, W., Ponce de Leon, A., Miranda, R., Hurtado, M., Rojas, L., Carbajal, L., Tzintzun, G., Cifuentes, L., Strappa, V., Romieu, I., 2008. Air Pollution and Mortality in Latin America: Results from the ESCALA Project (Multi-City Study of Air Pollution and Health Effects in Latin America), in: Adams, K., van Erp, A. (Eds.), Health Effects Institute Annual Conference.

Gupta, A.K., Nag, S., Mukhopadhyay, U.K., 2006a. Characterisation of PM10, PM2.5 and benzene soluble organic fraction of particulate matter in an urban area of Kolkata, India. Environmental monitoring and assessment 115, 205-222-205-222.

Gupta, P., Christopher, S.A., Wang, J., Gehrig, R., Lee, Y., Kumar, N., 2006b. Satellite remote sensing of particulate matter and air quality assessment over global cities. Atmospheric Environment 40, 5880-5892.

Harner, T., Shoeib, M., Kozma, M., Gobas, F., Li, S.M., 2005. Hexachlorocyclohexanes and endosulfans in urban, rural, and high altitude air samples in the Fraser Valley, British Columbia: Evidence for trans-Pacific transport. Environmental Science & Technology 39, 724-731.

He, K., Yang, F., Ma, Y., Zhang, Q., Yao, X., Chan, C.K., Cadle, S., Chan, T., Mulawa, P., 2001. The characteristics of PM2.5 in Beijing, China. Atmospheric Environment 35, 4959-4970.

Heald, C.L., Jacob, D.J., Jones, D.B.A., Palmer, P.I., Logan, J.A., Streets, D.G., Sachse, G.W., Gille, J.C., Hoffman, R.N., Nehrkorn, T., 2004. Comparative inverse analysis of satellite (MOPITT) and aircraft (TRACE-P) observations to estimate Asian sources of carbon monoxide. Journal of Geophysical Research-Atmospheres 109.

Heald, C.L., Jacob, D.J., Park, R.J., Alexander, B., Fairlie, T.D., Yantosca, R.M., Chu, D.A., 2006. Transpacific transport of Asian anthropogenic aerosols and its impact on surface air quality in the United States. Journal of Geophysical Research-Atmospheres 111.

Heald, C.L., Jacob, D.J., Park, R.J., Russell, L.M., Huebert, B.J., Seinfeld, J.H., Liao, H., Weber, R.J., 2005. A large organic aerosol source in the free troposphere missing from current models. Geophysical Research Letters 32.

Heald, C.L., Ridley, D.A., Kreidenweis, S.M., Drury, E., 2010. Satellite observations cap the atmospheric organic aerosol budget. Geophysical Research Letters 37.

Henze, D.K., Seinfeld, J.H., Ng, N.L., Kroll, J.H., Fu, T.M., Jacob, D.J., Heald, C.L., 2008. Global modeling of secondary organic aerosol formation from aromatic hydrocarbons: high- vs. low-yield pathways. Atmospheric Chemistry and Physics 8, 2405-2421.

Herrmann, L., Jahn, R., Maurer, T., 2010. Mineral dust around the Sahara-from source to sink A review with emphasis on contributions of the German soil science community in the last twenty years. Journal of Plant Nutrition and Soil Science 173, 811-821.

Hirsh, R.M., Gilroy, E.J., 1984. Methods of fitting a straight line to data: examples in water resoureces. Journal of the American Water Resources Association 20, 705-711.

Ho, K.F., Cao, J.J., Lee, S.C., Chan, C.K., 2006. Source apportionment of PM2.5 in urban area of Hong Kong. Journal of Hazardous Materials 138, 73-85.

Hoff, R.M., Christopher, S.A., 2009. Remote Sensing of Particulate Pollution from Space: Have We Reached the Promised Land? Journal of Air & Waste Management Association 59, 645-675.

Holben, B.N., Eck, T.F., Slutsker, I., Tanre, D., Buis, J.P., Setzer, A., Vermote, E., Reagan, J.A., Kaufman, Y.J., Nakajima, T., Lavenu, F., Jankowiak, I., Smirnov, A., 1998. AERONET - A federated instrument network and data archive for aerosol characterization. Remote Sensing of Environment 66, 1-16.

Hopke, P.K., Cohen, D.D., Begum, B.A., Biswas, S.K., Ni, B.F., Pandit, G.G., Santoso, M., Chung, Y.S., Davy, P., Markwitz, A., Waheed, S., Siddique, N., Santos, F.L., Pabroa, P.C.B., Seneviratne,

M.C.S., Wimolwattanapun, W., Bunprapob, S., Vuong, T.B., Hien, P.D., Markowicz, A., 2008. Urban air quality in the Asian region. Science of the Total Environment 404, 103-112.

Hu, Z., 2009. Spatial anaylsis of MODIS aerosol optical depth, PM2.5 and chronic coronary heart disease. International Journal of Health Geographics 8:27.

Huey, L.G., Tanner, D.J., Slusher, D.L., Dibb, J.E., Arimoto, R., Chen, G., Davis, D., Buhr, M.P., Nowak, J.B., Mauldin, R.L., Eisele, F.L., Kosciuch, E., 2004. CIMS measurements of HNO3 and SO2 at the South Pole during ISCAT 2000. Atmospheric Environment 38, 5411-5421.

Huo, M.Q., Sun, Q.A., Bai, Y.H., Xie, P., Liu, Z.R., Wang, X.S., Li, J.L., 2011. Acidic and basic properties and buffer capacity of airborne particulate matter in an urban area of Beijing. Environmental Monitoring and Assessment 176, 355-364.

Hyer, E.J., Reid, J.S., Zhang, J., 2011. An over-land aerosol optical depth data set for data assimilation by filtering, correction, and aggregation of MODIS Collection 5 optical depth retrievals. Atmospheric Measurement Techniques 4, 379-408.

Hystad, P., Setton, E., Cervantes, A., Poplawski, K., Deschenes, S., Brauer, M., Martin, R.V., van Donkelaar, A., Lamsal, L.N., Jerret, M., Demers, P., submitted. Creating National Air Pollution Models for Population Exposure Assessment in Canada. Environmental Health Perspectives.

IPCC, 2008. IPCC Fourth Assessment Report.

Jacob, D.J., 2000. Heterogeneous chemistry and tropospheric ozone. Atmospheric Environment 34, 2131-2159.

Jacob, D.J., Crawford, J.H., Kleb, M.M., Connors, V.S., Bendura, R.J., Raper, J.L., Sachse, G.W., Gille, J.C., Emmons, L., Heald, C.L., 2003. Transport and Chemical Evolution over the Pacific (TRACE-P) aircraft mission: Design, execution, and first results. Journal of Geophysical Research-Atmospheres 108, 1-19.

Jaegle, L., Steinberger, L., Martin, R.V., Chance, K., 2005. Global partitioning of NOx sources using satellite observations: Relative roles of fossil fuel combustion, biomass burning and soil emissions. Faraday Discussions 130, 407-423.

Jaffe, D., Anderson, T., Covert, D., Kotchenruther, R., Trost, B., Danielson, J., Simpson, W., Berntsen, T., Karlsdottir, S., Blake, D., Harris, J., Carmichael, G., Uno, I., 1999. Transport of Asian air pollution to North America. Geophysical Research Letters 26, 711-714.

Jayne, J.T., Leard, D.C., Zhang, X.F., Davidovits, P., Smith, K.A., Kolb, C.E., Worsnop, D.R., 2000. Development of an aerosol mass spectrometer for size and composition analysis of submicron particles. Aerosol Science and Technology 33, 49-70.

Jimenez, J.L., Jayne, J.T., Shi, Q., Kolb, C.E., Worsnop, D.R., Yourshaw, I., Seinfeld, J.H., Flagan, R.C., Zhang, X.F., Smith, K.A., Morris, J.W., Davidovits, P., 2003. Ambient aerosol sampling using the Aerodyne Aerosol Mass Spectrometer. Journal of Geophysical Research-Atmospheres 108.

Jones, A.J., Christopher, S.A., 2007. MODIS derived fine mode fraction characteristics of marine, dust, and anthropogenic aerosols over the ocean, constrained by GOCART, MOPITT, and TOMS. Journal of geophysical research 112.

Jones, C., 2010. CBC news: Mapping pollution.

Jordan, C.E., Dibb, J.E., Anderson, B.E., Fuelberg, H.E., 2003. Uptake of nitrate and sulfate on dust aerosols during TRACE-P. Journal of Geophysical Research-Atmospheres 108, 1-10.

Kahn, R., Nelson, D., Garay, M., Levy, R., Bull, M., Diner, D.D., Martinchik, J., Paradise, S., Hansen, E., Remer, L.A., 2009a. MISR aerosol product attributes, and statistical comparisons with MODIS. Transactions on Geoscience and Remote Sensing.

Kahn, R.A., Gaitley, B.J., Martonchik, J.V., Diner, D.J., Crean, K.A., Holben, B., 2005. Multiangle Imaging Spectroradiometer (MISR) global aerosol optical depth validation based on 2 years of coincident Aerosol Robotic Network (AERONET) observations. Journal of Geophysical Research-Atmospheres 110.

Kahn, R.A., Li, W.-H., Moroney, C., Diner, D.J., Martonchik, J.V., Fishbein, E., 2007. Aerosol source plume physical characteristics from space-based multiangle imaging. Journal of geophysical research 112.

Kahn, R.A., Nelson, D.L., Garay, M.J., Levy, R.C., Bull, M.A., Diner, D.J., Martonchik, J.V., Paradise, S.R., Hansen, E.G., Remer, L.A., 2009b. MISR Aerosol Product Attributes and Statistical Comparisons with MODIS. IEEE TRANSACTIONS ON GEOSCIENCE AND REMOTE SENSING 47.

Kaiser, J.W., Flemming, J., Schultz, M.G., Suttie, M., Wooster, M.J., 2009. The MACC Global Fire Assimilation System: First Emission Products (GFASv0). ECMWF Tech. Memo No. 596.

Karaca, F., Alagha, O., Erturk, F., 2005. Statistical characterization of atmospheric PM10 and PM2.5 concentrations at a non-impacted suburban site of Istanbul, Turkey. Chemosphere 59, 1183-1183-1190.

Karaca, F., Alagha, O., Erturk, F., Yilmaz, Y.Z., Ozkara, T., 2008. Seasonal variation of source contributions to atmospheric fine and coarse particles at suburban area in Istanbul, Turkey. Environmental Engineering Science 25, 767-781.

Karanasiou, A., Moreno, T., Amato, F., Lumbreras, J., Narros, A., Borge, R., Tobias, A., Boldo, E., Linares, C., Pey, J., Reche, C., Alastuey, A., Querol, X., 2011. Road dust contribution to PM levels -

Evaluation of the effectiveness of street washing activities by means of Positive Matrix Factorization. Atmospheric Environment 45, 2193-2201.

Kaufman, Y.J., Tanre, D., Remer, L.A., Vermote, E.F., Chu, A., Holben, B.N., 1997. Operational remote sensing of tropospheric aerosol over land from EOS moderate resolution imaging spectroradiometer. Journal of Geophysical Research-Atmospheres 102, 17051-17067.

Khokhar, M.F., Frankenberg, C., Van Roozendael, M., Beirle, S., Kuhl, S., Richter, A., Platt, U., Wagner, T., 2005. Satellite observations of atmospheric SO2 from volcanic eruptions during the time-period of 1996-2002, Atmospheric Remote Sensing: Earth's Surface, Troposphere, Stratosphere and Mesosphere - I, pp. 879-887.

Kim, S., Huey, L.G., Stickel, R.E., Tanner, D.J., Crawford, J.H., Olson, J.R., Chen, G., Brune, W.H., Ren, X., Lesher, R., Wooldridge, P.J., Bertram, T.H., Perring, A., Cohen, R.C., Lefer, B.L., Shetter, R.E., Avery, M., Diskin, G., Sokolik, I., 2007. Measurement of HO2NO2 in the free troposphere during the intercontinental chemical transport experiment - North America 2004. Journal of Geophysical Research-Atmospheres 112.

Kim, Y.J., Kim, K.W., Kim, S.D., Lee, B.K., Han, J.S., 2006. Fine particulate matter characteristics and its impact on visibility impairment at two urban sites in Korea: Seoul and Incheon, Atmospheric Environment. Pergamon, Oxford, p. 593.

Koelemeijer, R.B.A., Homan, C.D., Matthijsen, J., 2006. Comparison of spatial and temporal variations of aerosol optical thickness and particulate matter over Europe. Atmospheric Environment 40, 5304-5315.

Kothai, P., Saradhi, I.V., Prathibha, P., Hopke, P.K., Pandit, G.G., Puranik, V.D., 2008. Source Apportionment of Coarse and Fine Particulate Matter at Navi Mumbai, India. Aerosol and air quality research 8, 423-436.

Kouyoumdjian, H., Saliba, N.A., 2006. Mass concentration and ion composition of coarse and fine particles in an urban area in Beirut: effect of calcium carbonate on the absorption of nitric and sulfuric acids and the depletion of chloride. Atmospheric Chemistry and Physics 6, 1865-1877.

Krotkov, N.A., Carn, S.A., Krueger, A.J., Bhartia, P.K., Yang, K., 2006. Band residual difference algorithm for retrieval of SO2 from the aura Ozone Monitoring Instrument (OMI). Ieee Transactions on Geoscience and Remote Sensing 44, 1259-1266.

Kuhns, H., Knipping, E.M., Vukovich, J.M., 2005. Development of a United States-Mexico emissions inventory for the Big Bend Regional Aerosol and Visibility Observational (BRAVO) Study. Journal of the Air & Waste Management Association 55, 677-692.

Kumar, R., Joseph, A.E., 2006. Air pollution concentrations of PM2.5, PM10 and NO2 at ambient and kerbsite and their correlation in Metro City - Mumbai. Environmental monitoring and assessment 119, 191-199.

Kunzli, N., Medina, S., Kaiser, R., Quenel, P., Horak, F.J., Studnicka, M., 2001. Assessment of Deaths Attributable to Air Pollution: Should We Use Risk Estimates based on Time Series or on Cohort Studies? American Journal of Epidemiology 153, 1050-1055.

Laakso, L., Laakso, H., Aalto, P.P., Keronen, P., Petaja, T., Nieminen, T., Pohja, T., Siivola, E., Kulmala, M., Kgabi, N., Molefe, M., Mabaso, D., Phalatse, D., Pienaar, K., Kerminen, V.M., 2008. Basic characteristics of atmospheric particles, trace gases and meteorology in a relatively clean Southern African Savannah environment. Atmospheric Chemistry and Physics 8, 4823-4839.

Lamsal, L.N., Martin, R.V., van Donkelaar, A., Steinbacher, M., Celarier, E.A., Bucsela, E., Dunlea, E.J., Pinto, J.P., 2008. Ground-level nitrogen dioxide concentrations inferred from the satellite-borne Ozone Monitoring Instrument. Journal of Geophysical Research-Atmospheres 113, doi:10.1029/2007JD009235.

Leaitch, W.R., Macdonald, A.M., Anlauf, K.G., Liu, P.S.K., Toom-Sauntry, D., Li, S.M., Liggio, J., Hayden, K., Wasey, M.A., Russell, L.M., Takahama, S., Liu, S., van Donkelaar, A., Duck, T., Martin, R.V., Zhang, Q., Sun, Y., McKendry, I., Shantz, N.C., Cubison, M., 2009. Evidence for Asian dust effects from aerosol plume measurements during INTEX-B 2006 near Whistler, BC. Atmospheric Chemistry and Physics 9, 3523-3546.

Lee, C., Martin, R.V., van Donkelaar, A., O'Byrne, G., Krotkov, N., Richter, A., Huey, L.G., Holloway, J.S., 2009. Retrieval of vertical columns of sulfur dioxide from SCIAMACHY and OMI: Air mass factor algorithm development, validation, and error analysis. Journal of Geophysical Research-Atmospheres 114.

Leue, C., Wenig, M., Wagner, T., Klimm, O., Platt, U., Jahne, B., 2001. Quantitative analysis of NOx emissions from Global Ozone Monitoring Experiment satellite image sequences. Journal of Geophysical Research-Atmospheres 106, 5493-5505.

Levy, R., Leptoukh, G., Kahn, R., Zubko, V., Gopalan, A., Remer, L., 2009. A Critical Look at Deriving Monthly Aerosol Optical Depth From Satellite Data. IEEE Transactions on Geoscience and Remote Sensing in press.

Levy, R.C., Remer, L.A., Mattoo, S., Vermote, E.F., Kaufman, Y.J., 2007. Second-generation operational algorithm: Retrieval of aerosol properties over land from inversion of Moderate Resolution Imaging Spectroradiometer spectral reflectance. Journal of Geophysical Research-Atmospheres 112.

Liang, Q., Jaegle, L., Jaffe, D.A., Weiss-Penzias, P., Heckman, A., Snow, J.A., 2004. Long-range transport of Asian pollution to the northeast Pacific: Seasonal variations and transport pathways of carbon monoxide. Journal of Geophysical Research-Atmospheres 109.

Liao, H., Henze, D.K., Seinfeld, J.H., Wu, S.L., Mickley, L.J., 2007. Biogenic secondary organic aerosol over the United States: Comparison of climatological simulations with observations. Journal of Geophysical Research-Atmospheres 112.

Lin, J.J., 2002. Characterization of the major chemical species in PM2.5 in the Kaohsiung City, Taiwan. Atmospheric Environment 36, 1911-1920.

Liu, H.Y., Jacob, D.J., Bey, I., Yantosca, R.M., 2001. Constraints from Pb-210 and Be-7 on wet deposition and transport in a global three-dimensional chemical tracer model driven by assimilated meteorological fields. Journal of Geophysical Research-Atmospheres 106, 12109-12128.

Liu, J., Mauzerall, D.L., Horowitz, L.W., 2008. Source-receptor relationships between East Asian sulfur dioxide emissions and Northern Hemisphere sulfate concentrations. Atmospheric Chemistry and Physics 8, 3721-3733.

Liu, J.F., Mauzerall, D.L., Horowitz, L.W., 2005a. Analysis of seasonal and interannual variability in transpacific transport. Journal of Geophysical Research-Atmospheres 110.

Liu, P.S.K., Deng, R., Smith, K.A., Williams, L.R., Jayne, J.T., Canagaratna, M.R., Moore, K., Onasch, T.B., Worsnop, D.R., Deshler, T., 2007a. Transmission efficiency of an aerodynamic focusing lens system: Comparison of model calculations and laboratory measurements for the Aerodyne Aerosol Mass Spectrometer. Aerosol Science and Technology 41, 721-733.

Liu, Y., Koutrakis, P., Kahn, R., 2007b. Estimating fine particulate matter component concentrations and size distribution using satellite-retrieved fractional aerosol optical depth: Part 1 - Method Deleopment. Journal of Air & Waste Management Association 57, 1351-1359.

Liu, Y., Park, R.J., Jacob, D.J., Li, Q.B., Kilaru, V., Sarnat, J.A., 2004. Mapping annual mean ground-level PM2.5 concentrations using Multiangle Imaging Spectroradiometer aerosol optical thickness over the contiguous United States. Journal of Geophysical Research-Atmospheres 109.

Liu, Y., Sarnat, J.A., Kilaru, A., Jacob, D.J., Koutrakis, P., 2005b. Estimating ground-level PM2.5 in the eastern united states using satellite remote sensing. Environmental Science & Technology 39, 3269-3278.

Lohmann, U., Feichter, J., 2005. Global indirect aerosol effects: a review. Atmospheric Chemistry and Physics 5, 715-737.

Lucht, W., Schaaf, C.B., Strahler, A.H., 2000. An algorithm for the retrieval of albedo from space using semiempirical BRDF models. Ieee Transactions on Geoscience and Remote Sensing 38, 977-998.

Lyapustin, A., Wang, Y., Laszlo, I., Kahn, R., Korkin, S., Remer, L., Levy, R., Reid, J.S., 2011. Multiangle implementation of atmospheric correction (MAIAC): 2. Aerosol algorithm. Journal of Geophysical Research-Atmospheres 116.

Macdonald, A.M., Anlauf, K.G., Leaitch, W.R., Liu, P.S.K., 2006. Multi-year chemistry of particles and selected trace gases at the Whistler High Elevation Site. EOS Trans. 87, AEB-0719.

Mariani, R.L., de Mello, W.Z., 2007. PM2.5-10, PM2.5 and associated water-soluble inorganic species at a coastal urban site in the metropolitan region of Rio de Janeiro. Atmospheric Environment 41, 2887-2892.

Martin, R.V., 2008. Satellite remote sensing of surface air quality. Atmospheric Environment 42, 7823-7843.

Martin, R.V., Jacob, D.J., Chance, K., Kurosu, T.P., Palmer, P.I., Evans, M.J., 2003a. Global inventory of nitrogen oxide emissions constrained by space-based observations of NO2 columns. Journal of Geophysical Research-Atmospheres 108.

Martin, R.V., Jacob, D.J., Yantosca, R.M., Chin, M., Ginoux, P., 2003b. Global and regional decreases in tropospheric oxidants from photochemical effects of aerosols. Journal of Geophysical Research-Atmospheres 108.

Martin, S.T., Andreae, M.O., Artaxo, P., Baumgardner, D., Chen, Q., Goldstein, A.H., Guenther, A., Heald, C.L., Mayol-Bracero, O.L., McMurry, P.H., Pauliquevis, T., Poschl, U., Prather, K.A., Roberts, G.C., Saleska, S.R., Dias, M.A.S., Spracklen, D.V., Swietlicki, E., Trebs, I., 2010. Sources and properties of Amazonian aerosol particles. Reviews of Geophysics 48.

Martonchik, J.V., Diner, D.J., Crean, K.A., Bull, M.A., 2002. Regional aerosol retrieval results from MISR. Ieee Transactions on Geoscience and Remote Sensing 40, 1520-1531.

Martonchik, J.V., Kahn, R.A., Diner, D.J., 2009. Retrieval of Aerosol Properties over Land Using MISR Observations, in: Kokhanovsky, A.A., Leeuw, G.d. (Eds.), Satellite Aerosol Remote Sensing Over Land. Springer, Berlin.

Massie, S.T., Torres, O., Smith, S.J., 2004. Total Ozone Mapping Spectrometer (TOMS) observations of increases in Asian aerosol in winter from 1979 to 2000. Journal of Geophysical Research-Atmospheres 109.

McDonnell, W.F., Nishino-Ishikawa, N., Petersen, F.F., Chen, L.H., Abbey, D.E., 2000. Relationships of mortality with the fine and coarse fractions of long-term ambient PM10 concentrations in nonsmokers. Journal of Exposure Analysis and Environmental Epidemiology 10, 427-436.

McKendry, I.G., Hacker, J.P., Stull, R., Sakiyama, S., Mignacca, D., Reid, K., 2001. Long-range transport of Asian dust to the Lower Fraser Valley, British Columbia, Canada. Journal of Geophysical Research-Atmospheres 106, 18361-18370.

McKendry, I.G., Macdonald, A.M., Leaitch, W.R., van Donkelaar, A., Zhang, Q., Duck, T., Martin, R.V., 2008. Trans-Pacific dust events observed at Whistler, British Columbia during INTEX-B. Atmospheric Chemistry and Physics 8, 6297-6307.

McKendry, I.G., Strawbridge, K.B., O'Neill, N.T., Macdonald, A.M., Liu, P.S.K., Leaitch, W.R., Anlauf, K.G., Jaegle, L., Fairlie, T.D., Westphal, D.L., 2007. Trans-Pacific transport of Saharan dust to western North America: A case study. Journal of Geophysical Research-Atmospheres 112.

McNaughton, C.S., Clarke, A.D., Howell, S.G., Pinkerton, M., Anderson, B., Thornhill, L., Hudgins, C., Winstead, E., Dibb, J.E., Scheuer, E., Maring, H., 2007. Results from the DC-8 Inlet Characterization Experiment (DICE): Airborne versus surface sampling of mineral dust and sea salt aerosols. Aerosol Science and Technology 41, 136-159.

Minoura, H., Takahashib, K., Chow, J.C., Watson, J.G., 2006. Multi-year trend in fine and coarse particle mass, carbon, and ions in downtown Tokyo, Japan. Atmospheric Environment 40, 2478-2487.

Mishchenko, M.I., Geogdzhayev, I.V., 2007. Satellite remote sensing reveals regional tropospheric aerosol trends. Optics Express 15, 7423-7438.

Muller, J.F., Stavrakou, T., 2005. Inversion of CO and NOx emissions using the adjoint of the IMAGES model. Atmospheric Chemistry and Physics 5, 1157-1186.

Naeher, L.P., Brauer, M., Lipsett, M., Zelikoff, J.T., Simpson, C.D., Koenig, J.Q., Smith, K.R., 2007. Woodsmoke Health Effects: A Review. Inhalation Toxicology 19, 67-106.

Nassar, R., Logon, J.A., Megretskaia, I.A., Murray, L.T., Zhang, L., Jones, D.B.A., 2009. Analysis of tropical tropospheric ozone, carbon monoxide and water vapor during the 2006 El Niño using TES observations and the GEOS-Chem model. Journal of Geophysical Research-Atmospheres in press.

Oanh, N.T.K., Upadhyaya, N., Zhuang, Y.H., Hao, Z.P., Murthy, D.V.S., Lestari, P., Villarin, J.T., Chengchua, K., Co, H.X., Dung, N.T., Lindgren, E.S., 2006. Particulate air pollution in six Asian cities: Spatial and temporal distributions, and associated sources. Atmospheric Environment 40, 3367-3380.

Olivier, J.G.J., Berdowski, J.J.M., Peters, J.A.H.W., Bakker, J., Visschedijk, A.J.H., Bloos, J.J., 2002. Applications of EDGAR Including a description of EDGAR 3.2 reference database with trend data for 1970-1995. Document.

Paciorek, C.J., Liu, Y., 2009. Limitations of Remotely-sensed Aerosol as a Spatial Proxy for Fine Particulate Matter. Environmental Health Perspectives 117.

Park, E.-j., Kim, D.-s., Park, K., 2008. Monitoring of ambient particles and heavy metals in a residential area of Seoul, Korea. Environmental monitoring and assessment 137, 441-449.

Park, R.J., Jacob, D.J., Chin, M., Martin, R.V., 2003. Sources of carbonaceous aerosols over the United States and implications for natural visibility. Journal of Geophysical Research-Atmospheres 108.

Park, R.J., Jacob, D.J., Field, B.D., Yantosca, R.M., Chin, M., 2004. Natural and transboundary pollution influences on sulfate-nitrate-ammonium aerosols in the United States: Implications for policy. Journal of Geophysical Research-Atmospheres 109.

Park, R.J., Jacob, D.J., Kumar, N., Yantosca, R.M., 2006. Regional visibility statistics in the United States: Natural and transboundary pollution influences, and implications for the Regional Haze Rule. Atmospheric Environment 40, 5405-5423.

Park, R.J., Jacob, D.J., Palmer, P.I., Clarke, A.D., Weber, R.J., Zondlo, M.A., Eisele, F.L., Bandy, A.R., Thornton, D.C., Sachse, G.W., Bond, T.C., 2005. Export efficiency of black carbon aerosol in continental outflow: Global implications. Journal of Geophysical Research-Atmospheres 110.

Parrish, D.D., Hahn, C.J., Williams, E.J., Norton, R.B., Fehsenfeld, F.C., Singh, H.B., Shetter, J.D., Gandrud, B.W., Ridley, B.A., 1992. Indications of photochemical histories of Pacific air masses from measurements of atmospheric tracer species at Pt. Arena, California. Journal of Geophysical Research 97, 15883-15901.

Peltier, R.E., Hecobian, A.H., Weber, R.J., Stohl, A., Atlas, E.L., Riemer, D.D., Blake, D.R., Apel, E., Campos, T., Karl, T., 2008. Investigating the sources and atmospheric processing of fine particles from Asia and the Northwestern United States measured during INTEX B. Atmospheric Chemistry and Physics 8, 1835-1853.

Petron, G., Granier, C., Khattatov, B., Yudin, V., Lamarque, J.F., Emmons, L., Gille, J., Edwards, D.P., 2004. Monthly CO surface sources inventory based on the 2000-2001 MOPITT satellite data. Geophysical Research Letters 31.

Pope, C.A., Burnett, R.T., Thun, M.J., Calle, E.E., Krewski, D., Ito, K., Thurston, G.D., 2002. Lung cancer, cardiopulmonary mortality, and long-term exposure to fine particulate air pollution. Jama-Journal of the American Medical Association 287, 1132-1141.

Pope, C.A., Ezzati, M., Dockery, D.W., 2009. Fine-Particulate Air Pollution and Life Expectancy in the United States. New England Journal of Medicine 360, 376-386.

Pope, C.A.I., Brook, R.D., Burnett, R.T., Dockery, D.W., 2011. How is cardiovascular disease mortality risk affected by duration and intensity of fine particulate matter exposure? An integration of the epidemiologic evidence. Air Quality, Atmospheric and Health 4, 5-14.

Price, P.B., Rohde, R.A., Bay, R.C., 2009. Fluxes of microbes, organic aerosols, dust, sea-salt Na ions, non-sea-salt Ca ions, and methanesulfonate onto Greenland and Antarctic ice. Biogeosciences 6, 479-486.

Prospero, J.M., Ginoux, P., Torres, O., Nicholson, S.E., Gill, T.E., 2002. Environmental characterization of global sources of atmospheric soil dust identified with the Nimbus 7 Total Ozone Mapping Spectrometer (TOMS) absorbing aerosol product. Reviews of Geophysics 40.

Pye, H.O.T., Liao, H., Wu, S., Mickley, L.J., Jacob, D.J., Henze, D.K., Seinfeld, J.H., 2009. Effect of changes in climate and emissions on future sulfate-nitrate-ammonium aerosol levels in the United States. Journal of Geophysical Research 114(D01205).

Pye, H.O.T., Seinfeld, J.H., 2010. A global perspective on aerosol from low-volatility organic compounds. Atmospheric Chemistry and Physics 10, 4377-4401.

Qian, Z., He, Q., Lin, H.-M., Kong, L., Bentley, C.M., Liu, W., Dinjin, Z., 2008. High temperatures enhanced acute mortality effects of ambient particle pollution in the "oven" city of Wuhan, China. Environmental Health Perspectives 116, 1172-1178.

Quinn, P.K., Bates, T.S., Coffman, D., Onasch, T.B., Worsnop, D., Baynard, T., de Gouw, J.A., Goldan, P.D., Kuster, W.C., Williams, E., Roberts, J.M., Lerner, B., Stohl, A., Pettersson, A., Lovejoy, E.R., 2006. Impacts of sources and aging on submicrometer aerosol properties in the marine boundary layer across the Gulf of Maine. Journal of Geophysical Research-Atmospheres 111.

Remer, L.A., Kaufman, Y.J., Tanre, D., Mattoo, S., Chu, D.A., Martins, J.V., Li, R.R., Ichoku, C., Levy, R.C., Kleidman, R.G., Eck, T.F., Vermote, E., Holben, B.N., 2005. The MODIS aerosol algorithm, products, and validation. Journal of the Atmospheric Sciences 62, 947-973.

Remer, L.A., Kleidman, R.G., Levy, R.C., Kaufman, Y.J., Tanre, D., Mattoo, S., Martins, J.V., Ichoku, C., Koren, I., Yu, H.B., Holben, B.N., 2008. Global aerosol climatology from the MODIS satellite sensors. Journal of Geophysical Research-Atmospheres 113.

Remer, L.A., Tanré, D., Kaufman, Y.J., Levy, R.C., Mattoo, S., 2006. Algorithm for Remote Sensing of Tropospheric Aerosol from MODIS: Collection 005. Algorithm Theoretical Basis Document.

Richter, A., Burrows, J.P., Nuss, H., Granier, C., Niemeier, U., 2005. Increase in tropospheric nitrogen dioxide over China observed from space. Nature 437, 129-132.

Romieu, I., Gouveia, N., Cifuentes, L., Ponce de Leon, A., Junger, W., Miranda, V., Hurtado-Diaz, M., Rojas, L., Tzintzun, G., 2009. Mortality Effects of Air Pollution in Latin American Cities: Results from the ESCALA Study, in: Adams, K., Cohen, A.J. (Eds.), Health Effects Institutde Annual Conference.

Rupakheti, M., Leaitch, W.R., Lohmann, U., Hayden, K., Brickell, P., Lu, G., Li, S.M., Toom-Sauntry, D., Bottenheim, J.W., Brook, J.R., Vet, R., Jayne, J.T., Worsnop, D.R., 2005. An intensive study of the size and composition of submicron atmospheric aerosols at a rural site in Ontario, Canada. Aerosol Science and Technology 39, 722-736.

Saliba, N.A., Kouyoumdjian, H., Roumié, M., 2007. Effect of local and long-range transport emissions on the elemental composition of PM10-2.5 and PM2.5 in Beirut. Atmospheric Environment 41, 6497-6509.

Sastry, N., 2002. Forest fires, air pollution, and mortality in Southeast Asia. Demography 29, 1-23.

Schaap, M., Apituley, A., Timmermans, R.M.A., Koelemeijer, R.B.A., de Leeuw, G., 2008. Exploring the relation between aerosol optical depth and PM2.5 at Cabauw, the Netherlands. Atmospheric Chemistry and Physics Discussions 8, 17939-17986.

Seinfeld, J.H., Pandis, S.N., 2006. Atmospheric Chemistry and Physics, Second Edition. John Wiley & Sons, Inc.

Sheehan, P.E., Bowman, F.M., 2001. Estimated effects of temperature on secondary organic aerosol concentrations. Environmental Science & Technology 35, 2129-2135.

Singh, H.B., Brune, W.H., Crawford, J.H., Flocke, F., Jacob, D.J., 2009. Chemistry and transport of pollution over the Gulf of Mexico and the Pacific: spring 2006 INTEX-B campaign overview and first results. Atmospheric Chemistry and Physics 9, 2301-2318.

Sirois, A., Barrie, L.A., 1999. Arctic lower tropospheric aerosol trends and composition at Alert, Canada: 1980-1995. Journal of Geophysical Research-Atmospheres 104, 11599-11618.

Soluri, D.S., Godoy, M.L.D.P., Godoy, J.M., Roldao, L.A., 2007. Multi-site PM2.5 and PM2.5-10 aerosol source apportionment in Rio de Janeiro, Brazil. Journal of the Brazilian Chemical Society 18, 838-845.

Song, C.H., Kim, C.M., Lee, Y.J., Carmichael, G.R., Lee, B.K., Lee, D.S., 2007. An evaluation of reaction probabilities of sulfate and nitrate precursors onto East Asian dust particles. Journal of Geophysical Research-Atmospheres 112.

Streets, D.G., Bond, T.C., Carmichael, G.R., Fernandes, S.D., Fu, Q., He, D., Klimont, Z., Nelson, S.M., Tsai, N.Y., Wang, M.Q., Woo, J.H., Yarber, K.F., 2003. An inventory of gaseous and primary aerosol emissions in Asia in the year 2000. Journal of Geophysical Research-Atmospheres 108.

Streets, D.G., Tsai, N.Y., Akimoto, H., Oka, K., 2000. Sulfur dioxide emissions in Asia in the period 1985-1997. Atmospheric Environment 34, 4413-4424.

Streets, D.G., Waldhoff, S.T., 2000. Present and future emissions of air pollutants in China: SO2, NOx, and CO. Atmospheric Environment 34, 363-374.

Streets, D.G., Yan, F., Chin, M., Diehl, T., Mahowald, N., Schultz, M., Wild, M., Wu, Y., Yu, C., 2009. Anthropogenic and natural contributions to regional trends in aerosol optical depth, 1980-2006. Journal of Geophysical Research-Atmospheres 114.

Streets, D.G., Zhang, Q., Wang, L.T., He, K.B., Hao, J.M., Wu, Y., Tang, Y.H., Carmichael, G.R., 2006. Revisiting China's CO emissions after the Transport and Chemical Evolution over the Pacific (TRACE-P) mission: Synthesis of inventories, atmospheric modeling, and observations. Journal of Geophysical Research-Atmospheres 111.

Sun, Y., Zhang, Q., Macdonald, A.M., Hayden, K., Li, S.M., Liggio, J., Liu, P.S.K., Anlauf, K.G., Leaitch, W.R., Steffen, A., Cubison, M., Worsnop, D.R., van Donkelaar, A., Martin, R.V., 2009. Size-resolved aerosol chemistry on Whistler Mountain, Canada with a high-resolution aerosol mass spectrometer during INTEX-B. Atmospheric Chemistry and Physics 9, 3095-3111.

Thornton, J.A., Jaegle, L., McNeill, V.F., 2008. Assessing known pathways for HO2 loss in aqueous atmospheric aerosols: Regional and global impacts on tropospheric oxidents. Journal of Geophysical Research-Atmospheres 113.

Tobler, W., Deichmann, U., Gottsegen, J., Maloy, K., 1997. World Population in a Grid of Spherical Quadrilaterals. International Journal of Population Geography 3, 203-225.

Tsigaridis, K., Krol, M., Dentener, F.J., Balkanski, Y., Lathiere, J., Metzger, S., Hauglustaine, D.A., Kanakidou, M., 2006. Change in global aerosol composition since preindustrial times. Atmospheric Chemistry and Physics 6, 5143-5162.

van der A, R.J., Peters, D., Eskes, H., Boersma, K.F., Van Roozendael, M., De Smedt, I., Kelder, H.M., 2006. Detection of the trend and seasonal variation in tropospheric NO2 over China. Journal of Geophysical Research-Atmospheres 111.

van der Werf, G.R., Randerson, J.T., Giglio, L., Collatz, G.J., Kasibhatla, P.S., Arellano, A.F.J., 2006. Interannual variability in global biomass burning emissions from 1997 to 2004. Atmospheric Chemistry and Physics 6, 3423-3441.

van Donkelaar, A., Martin, R.V., Brauer, M., Kahn, R.A., Levy, R.C., Verduzco, C., 2010. Global Estimates of Ambient Fine Particulate Matter Concentrations from Satellite-Based Aerosol Optical Depth: Development and Application. Environmental Health Perspectives 118.

van Donkelaar, A., Martin, R.V., Leaitch, W.R., Macdonald, A.M., Walker, T.W., Streets, D.G., Zhang, Q., Dunlea, E.J., Jimenez, J.L., Dibb, J.E., Huey, L.G., Weber, R., Andreae, M.O., 2008. Analysis of aircraft and satellite measurements from the Intercontinental Chemical Transport Experiment (INTEX-B) to quantify long-range transport of East Asian sulfur to Canada. Atmospheric Chemistry and Physics 8, 2999-3014.

van Donkelaar, A., Martin, R.V., Park, R.J., 2006. Estimating ground-level PM2.5 using aerosol optical depth determined from satellite remote sensing. Journal of Geophysical Research-Atmospheres 111.

Vaughan, M., Young, S., Winker, D., Powell, K., Omar, A., Liu, Z., Hu, Y., Hostetler, C., 2004. Fully automated analysis of space-based lidar data: an overview of the CALIPSO retrieval algorithms and data products. Proceedings of SPIE 5575, 16-30.

Vestreng, V., Myhre, G., Fagerli, H., Reis, S., Tarrason, L., 2007. Twenty-five years of continuous sulphur dioxide emission reduction in Europe. Atmospheric Chemistry and Physics 7, 3663-3681.

Villeneuve, P.J., Goldberg, M.S., Burnett, R.T., van Donkelaar, A., Chen, H., Martin, R.V., in press. Associations between sociodemographic characteristics, cigarette smoking, obesity, and remote sensing derived estimates of ambient PM2.5: results from a Canadian population-based survey. Journal of Occupational and Environmental Medicine.

Voiland, A., 2010. New Map Offers a Global View of Health-Sapping Air Pollution. NASA's Earth Science News Team

Waheed, A., Li, X.L., Tan, M.G., Bao, L.M., Liu, J.F., Zhang, Y.X., Zhang, G.L., Li, Y., 2011. Size Distribution and Sources of Trace Metals in Ultrafine/Fine/Coarse Airborne Particles in the Atmosphere of Shanghai. Aerosol Science and Technology 45, 163-171.

Walker, T.W., Martin, R.V., van Donkelaar, A., Leaitch, W.R., MacDonald, A.M., Anlauf, K.G., Cohen, R.C., Bertram, T.H., Huey, L.G., Avery, M.A., Weinheimer, A.J., Flocke, F.M., Tarasick, D.W., Thompson, A.M., Streets, D.G., Liu, X., 2010. Trans-Pacific transport of reactive nitrogen and ozone to Canada during spring. Atmospheric Chemistry and Physics 10, 8353-8372.

Wang, J., Christopher, S.A., 2003. Intercomparison between satellite-derived aerosol optical thickness and PM2.5 mass: Implications for air quality studies. Geophysical Research Letters 30.

Wang, J., Xu, X.G., Spurr, R., Wang, Y.X., Drury, E., 2010. Improved algorithm for MODIS satellite retrievals of aerosol optical thickness over land in dusty atmosphere: Implications for air quality monitoring in China. Remote Sensing of Environment 114, 2575-2583.

Weber, R.J., Orsini, D., Daun, Y., Lee, Y.N., Klotz, P.J., Brechtel, F., 2001. A particle-into-liquid collector for rapid measurement of aerosol bulk chemical composition. Aerosol Science and Technology 35, 718-727.

Weijers, E.P., Schaap, M., Nguyen, L., Matthijsen, J., van der Gon, H., ten Brink, H.M., Hoogerbrugge, R., 2011. Anthropogenic and natural constituents in particulate matter in the Netherlands. Atmospheric Chemistry and Physics 11, 2281-2294.

WHO, 2005. Air Quality Guidelines - Global Update 2005. World Health Organization Europe.

Winberry, W.T., 1999. Sampling of ambient air for PM10 using an anderson dichotomous sampler. Center for Environmental Research Information, Office of Research and Development, U. S. Environmental Protection Agency.

Wong, C.-M., Vichit-Vadakan, N., Kan, H., Qian, Z., Teams, P.P., 2008. Public Health and Air Pollution in Asia (PAPA): A Multicity Study of Short-Term Effects of Air Pollution on Mortality. Environmental Health Perspectives 116, 1195-1202.

Ye, B., Ji, X., Yang, H., Yao, X., Chan, C.K., Cadle, S.H., Chan, T., Mulawa, P.A., 2003. Concentration and chemical composition of PM2.5 in Shanghai for a 1-year period. Atmospheric Environment 37, 499-510.

Ying, Q., Kleeman, M.J., 2006. Source contributions to the regional distribution of secondary particulate matter in California. Atmospheric Environment 40, 736-752.

Yu, H.B., Remer, L.A., Chin, M., Bian, H.S., Kleidman, R.G., Diehl, T., 2008. A satellite-based assessment of transpacific transport of pollution aerosol. Journal of Geophysical Research-Atmospheres 113.

Zakey, A.S., Abdel-Wahab, M.M., Pettersson, J.B.C., Gatari, M., Hallquist, M., 2008. Seasonal and spatial variation of atmospheric particulate matter in a developing megacity, the Greater Cairo, Egypt. Atmosfera 21, 171.

Zhang, L., 2010. Hidden Killers, National Geographic China, p. 30.

Zhang, L., Liao, H., Li, J.P., 2010. Impacts of Asian summer monsoon on seasonal and interannual variations of aerosols over eastern China. Journal of Geophysical Research-Atmospheres 115.

Zhang, Q., Streets, D.G., Carmichael, G.R., He, K.B., Huo, H., Kannari, A., Klimont, Z., Park, I.S., Reddy, S., Fu, J.S., Chen, D., Duan, L., Lei, Y., Wang, L.T., Yao, Z.L., 2009. Asian emissions in 2006 for the NASA INTEX-B mission. Atmospheric Chemistry and Physics 9, 5131-5153.

Zhang, Q., Streets, D.G., He, K., Wang, Y., Richter, A., Burrows, J.P., Uno, I., Jang, C.J., Chen, D., Yao, Z., Lei, Y., 2007. NOx emission trends for China, 1995-2004: The view from the ground and the view from space. Journal of Geophysical Research-Atmospheres 112.

Zhao, X., Zhang, X., Xu, X., Xu, J., Meng, W., Pu, W., 2009. Seasonal and diurnal variations of ambient PM2.5 concentration in urban and rural environments in Beijing. Atmospheric Environment 43, 2893-2900.

Zheng, M., Salmon, L.G., Schauer, J.J., Zeng, L.M., Kiang, C.S., Zhang, Y.H., Cass, G.R., 2005. Seasonal trends in PM2.5 source contributions in Beijing, China. Atmospheric Environment 39, 3967-3976.

APPENDIX A

A.1 COPYRIGHT INFORMATION

Chapter 2 of this thesis contains an article published in the Journal of Atmopsheric Chemistry and Physics and Environmental Health Perspectives. The author retains the copyright for this publications. Further information can be found at http://www.atmospheric-chemistry-and-physics.net/general_information/license_and_copyright.html, which states:

LICENSE AND COPYRIGHT AGREEMENT

The following License and Copyright Agreement is valid for any article published by Copernicus Publications on behalf of the European Geosciences Union (EGU) in the journal Atmospheric Chemistry and Physics and its discussion forum Atmospheric Chemistry and Physics.

AUTHOR'S CERTIFICATION

In submitting the manuscript, the authors certify that:

- They are authorized by their co-authors to enter into these arrangements.
- The work described has not been published before (except in the form of an abstract or proceedings-type publication – including discussion papers – or as part of a published lecture or thesis), that it is not under consideration for publication elsewhere, that its publication has been approved by all the author(s) and by the responsible authorities – tacitly or explicitly – of the institutes where the work has been carried out.
- They secure the right to reproduce any material that has already been published or copyrighted elsewhere.
- They agree to the following license and copyright agreement:

COPYRIGHT

- Copyright on any article is retained by the author(s). Regarding copyright transfers please see below.
- Authors grant Copernicus Publications a license to publish the article and identify itself as the original publisher.
- Authors grant Copernicus Publications commercial rights to produce hardcopy volumes of the journal for sale to libraries and individuals.
- Authors grant any third party the right to use the article freely as long as its original authors and citation details are identified.
- The article and any associated published material is distributed under the Creative Commons Attribution 3.0 License.

COPYRIGHT TRANSFERS

Many authors have strict regulations in their contract of employment regarding their works. A transfer of copyright to the institution or company is usual as well as the reservation of specific usage rights. Please note that in case of Open Access publications in combination with a Creative Commons License a transfer of the **copyright** to the institution is possible as it belongs to the author anyway and is not subject to the publisher.

Any **usage rights** are regulated through the Creative Commons License. As Copernicus Publications is using the Creative Commons Attribution 3.0 License, anyone (the author, his/her institution/company, the publisher, as well as the public) is free to copy, distribute, transmit, and adapt the work as long as the original author is given credit (see above). Therefore, specific usage rights cannot be reserved by the author or his/her institution/company, and the publisher cannot include a statement "all rights reserved" in any published paper.

A copyright transfer from the author to his/her institution/company will be expressed in a special "Copyright Statement" at the end of the publication rather than on the first page in the article citation header. Authors are asked to include the following sentence: "The author's copyright for this publication is transferred to *institution/company*".

Chapter 3 of this thesis contains an article published in Environmental Health Perspectives. Publication of Environmental Health Perspectives lies in the public domain. Further information can be found at http://ehp.niehs.nih.gov/docs/admin/copyright.html, which states:

COPYRIGHT/PERMISSIONS

EHP is a publication of the U.S. government. Publication of *EHP* lies in the public domain and is therefore without copyright.

Research articles from *EHP* may be used freely; however, articles from the Environews section of *EHP* may contain photographs or figures copyrighted by other commercial organizations and individuals that may not be used without obtaining prior approval from both the *EHP* editors and the holder of the copyright.

Use of any materials published in *EHP* should be acknowledged (for example, "Reproduced with permission from *Environmental Health Perspectives*") and provide pertinent reference information for the article from which the material was reproduced.